SANDIA REPORT SAND85—1215 • Unlimited Release • UC—62d
Printed May 1986

Optical Characterization of Solid Particle Solar Central Receiver Materials

K. A. Stahl, J. W. Griffin, B. S. Matson, R. B. Pettit

Prepared by
Sandia National Laboratories
Albuquerque, New Mexico 87185 and Livermore, California 94550
for the United States Department of Energy
under Contract DE-AC04-76DP00789

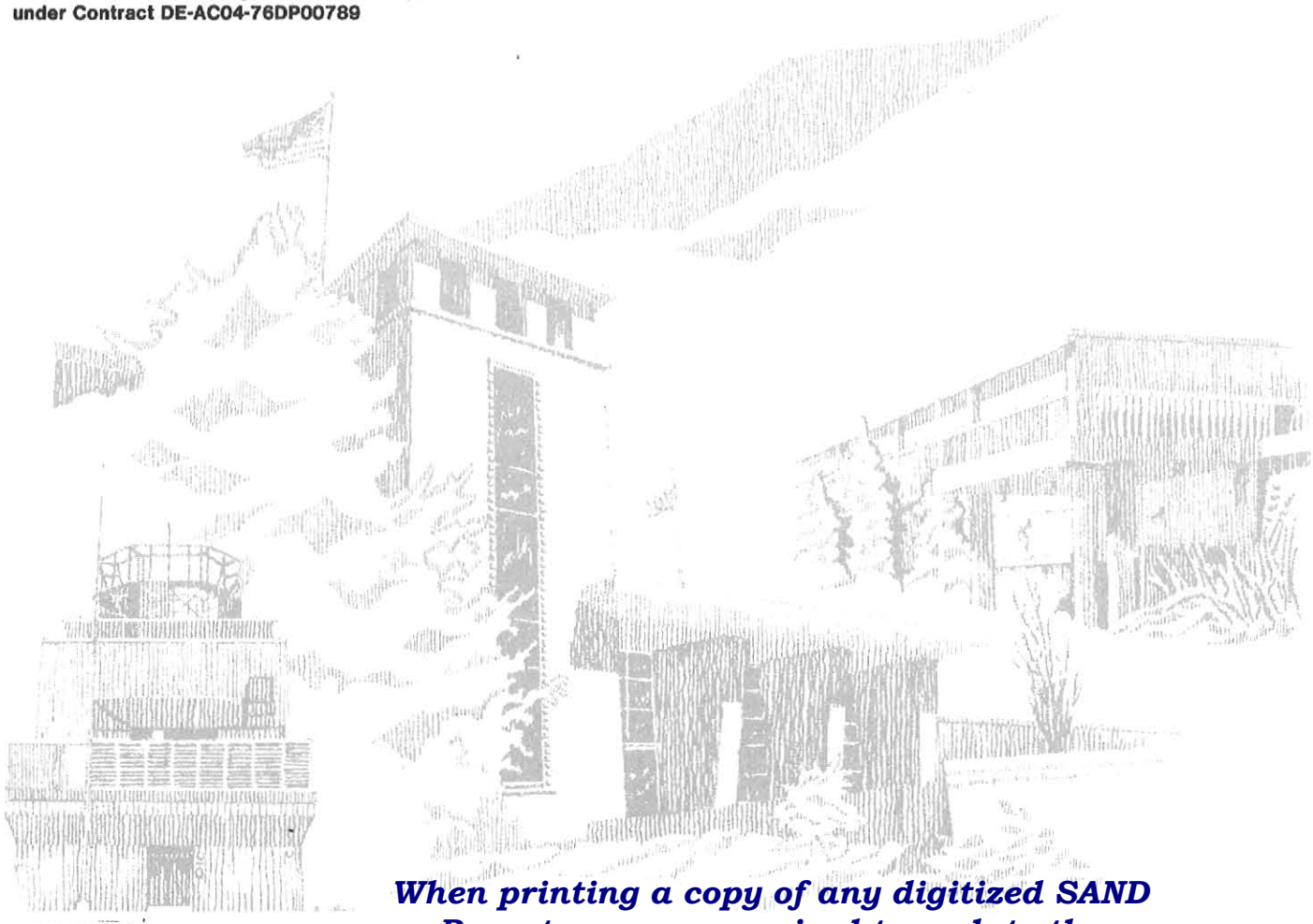

Issued by Sandia National Laboratories, operated for the United States Department of Energy by Sandia Corporation.

Printed in the United States of America
Available from
National Technical Information Service
U.S. Department of Commerce
5285 Port Royal Road
Springfield, VA 22161

NTIS price codes
Printed copy: A06
Microfiche copy: A01

FOREWARD

The research and development described in this document was conducted within the U. S. Department of Energy's (DOE) Solar Thermal Technology Program. The goal of the Solar Thermal Technology Program is to advance the engineering and scientific understanding of solar thermal technology, and to establish the technology base from which private industry can develop solar thermal power production options for introduction into the competitive energy market.

Solar thermal technology concentrates solar radiation by means of tracking mirrors or lenses onto a receiver where the solar energy is absorbed as heat and converted into electricity or incorporated into products as process heat. The two primary solar thermal technologies, central receivers and distributed receivers, employ various point and line-focus optics to concentrate sunlight. Current central receiver systems use fields of heliostats (two-axis tracking mirrors) to focus the sun's radiant energy onto a single tower-mounted receiver. Parabolic dishes up to 17 meters in diameter track the sun in two axes and use mirrors or Fresnel lenses to focus radiant energy onto a receiver. Troughs and bowls are line-focus tracking reflectors that concentrate sunlight onto receiver tubes along their focal lines. Concentrating collector modules can be used alone or in a multi-module system. The concentrated radiant energy absorbed by the solar thermal receiver is transported to the conversion process by a circulating working fluid. Receiver temperatures range from 100°C in low-temperature troughs to over 1500°C in dish and central receiver systems.

The Solar Thermal Technology Program is directing efforts to advance and improve promising system concepts through the research and

development of solar thermal materials, components, and subsystems, and the testing and performance evaluation of subsystems and systems. These efforts are carried out through the technical direction of DOE and its network of national laboratories who work with private industry. Together they have established a comprehensive goal directed program to improve performance and provide technically proven options for eventual incorporation into the Nation's energy supply.

To be successful in contributing to an adequate national energy supply at reasonable cost, solar thermal energy must eventually be economically competitive with a variety of other energy sources. Components and system-level performance targets have been developed as quantitative program goals. The performance targets are used in planning research and development activities, measuring progress, assessing alternative technology options, and making optimal component developments. These targets will be pursued vigorously to insure a successful program.

SAND85-1215
Unlimited Release
UC-62d

OPTICAL CHARACTERIZATION OF SOLID PARTICLE SOLAR CENTRAL RECEIVER MATERIALS

K. A. Stahl

J. W. Griffin

B. S. Matson

R. B. Pettit*

Pacific Northwest Laboratory
Richland, Washington 99352

May 1986

Prepared for Sandia National Laboratory
(Contract No. 300A02554)
under a related services agreement
with the U.S. Department of Energy
under Contract DE-AC06-76RLO 11830.

*Sandia National Laboratories
P. O. Box 5800
Albuquerque, NM 87185

Abstract

The angular scattering properties and scattering and absorption components of the extinction coefficient have been measured for Master Beads^{R}, an iron-doped Al_2O_3 spheroid manufactured by Norton Chemical Co., Worchester, MA. This material, commonly used as a proppant in oil well drilling operations, exhibits good optical absorption properties over the solar insolation spectrum, and favorable thermal and mechanical properties for temperatures up to 1000°C. These characteristics, along with its low cost, make Master Beads^{R} a good candidate as the absorbing medium in the solid particle solar central receiver concept. The objective of the ongoing optical properties measurement program is to obtain information to be used as input to radiation transfer models for prediction of receiver performance. Scattering and extinction measurements were performed at 632.8 nm in a falling curtain geometry of one-particle nominal thickness. Measurements were performed over a range of mass flow rates and particle densities. Photographic documentation of curtain particle density enabled calculation of mean scattering and absorption loss components per particle in the absence of multiple-particle optical interactions. Prediction of optical extinction properties at other wavelengths is anticipated to be straightforward using hemispherical spectral reflectance measurements on bulk samples. Additional scattering and extinction data were acquired on transparent glass microspheres for comparison and as a verification of the measurement apparatus and procedures.

In addition, an experimental system to measure the diffuse reflectance of a particulate sample over the wavelength range of 300 to

2500 nm and at elevated temperatures up to 1000°C was developed and implemented. A description of the experimental apparatus and measurement procedures, as well as optical reflectance data for the Master Beads^{R}, are presented. Using this high temperature measurement system, the diffuse reflectance of Master Beads^{R} changed by less than 1% for sample temperatures from 150°C to 930°C. However, after heating a sample for 3 hours at 1000°C in air, the solar absorptance measured at room temperature decreased from initial values of 0.93 to 0.89.

CONTENTS

FIGURES

TABLE

OPTICAL CHARACTERIZATION OF SOLID PARTICLE SOLAR CENTRAL RECEIVER MATERIALS

I. INTRODUCTION

The following report describes work performed at the Pacific Northwest Laboratory (PNL) in support of optical characterization of materials for the solid particle solar central receiver.[1] This report covers activities over the time period May 1983 through March 1985. Portions of this work have been previously reported.[2,3]

The primary objective of the optical characterization activities at PNL has been to provide optical properties data that could be easily used in a radiative exchange model developed at Sandia National Laboratory Livermore.[4] Since the candidate absorber materials are all particulates, development of modified instrumentation and methods was required for their characterization. This specialized instrumentation and the associated data collection and data processing algorithms are described in this report. Experimental data reported herein includes bulk optical properties (reflectance, transmittance, and absorptance) over the solar insolation wavelength range (300-2500 nm), angular scattering distributions (differential scattering cross section), optical extinction properties (single-particle scattering albedo), and diffuse reflectance at elevated temperatures (150-1000°C). Most of the data reported is for Norton Master Beads^{R}, an iron-doped alumino-silicate material which appears promising for use in the solid particle receiver. Limited bulk optical property data are also presented for materials

evaluated in the early screening phase of the solid particle receiver program.

II. MOTIVATION FOR THE OPTICAL PROPERTIES CHARACTERIZATION TASK

The motivation for the optical properties characterization task was provided by the solid particle receiver radiative performance modeling work performed by Houf, et al.[4] at Sandia National Laboratory Livermore. A brief discussion of this model is appropriate.

Solar central receivers which utilize solid thermal carriers such as sand or small refractory pebbles for direct absorption of concentrated solar radiation are under investigation at Sandia National Laboratories Livermore.[1] In the central receiver concept, a field of tracking mirrors, called heliostats, is used to focus and concentrate solar energy onto a receiver located atop a tower. In the present design, the receiver consists of an open aperture cavity through which a free falling sheet of solid particles is dropped. The particle curtain is directly irradiated by the concentrated solar flux entering the open aperture and the particles are heated to approximately 1000°C before exiting the cavity. The particles are subsequently collected, their heat extracted through a reactor or heat exchanger, and then recycled to the top of the tower to be reheated in the receiver.

A model of the radiation coupling within the falling particle curtain has been developed by Sandia for the purpose of screening candidate solid carriers and for assessing the thermal performance of various particle receiver designs. Processes of importance included in the model are scattering, absorption, and emission of radiant energy.

The model is based on the equation of radiative transfer for a simplified plane parallel particle curtain as depicted in Figure 1. The appropriate equation which governs the radiation field within the particle curtain[4] is

$$\cos\theta \frac{dI_\lambda}{dz}(\theta,\phi,z) = -(\kappa_\lambda + \sigma_\lambda)\, I_\lambda(\theta,\phi,z) + \kappa_\lambda\, I_{B,\lambda}(T) \qquad (1)$$

$$+ \frac{\sigma}{4\pi} \int_0^{2\pi} \int_0^{\pi} I_\lambda(\theta',\phi',z)\, p_\lambda(\theta',\phi' \to \theta,\phi)\, \sin\theta'\, d\theta' d\phi'$$

The quantity $I_\lambda(\theta,\phi,z)$ is the monochromatic intensity at z in the direction (θ,ϕ), where the subscript λ denotes wavelength. It is a representation of the angular distribution of radiant energy at any point z within the particle curtain. The absorption coefficient κ_λ and scattering coefficient σ_λ, as well as the phase function $p_\lambda(\theta',\phi' \to \theta,\phi)$, are monochromatic properties which depend on particle concentration and the optical characteristics of the solid carriers. The absorption and scattering coefficients represent the attenuation per unit distance along a traversing beam of radiation due to the respective effects of absorption and scattering. The phase function, $p_\lambda(\theta',\phi' \to \theta,\phi)$, represents the probability that a beam moving in direction (θ',ϕ'), and confined to a solid angle $d\omega'$, will be scattered into a solid angle $d\omega$ about the (θ,ϕ) direction. The phase function can be written as $p_\lambda(\xi)$, where the angle ξ is the relative scattering angle between the incident and scattered radiation (see Figure 1). The term $I_{B,\lambda}(T)$ is the Planck blackbody distribution and accounts for thermal radiation from the particles at a temperature T.

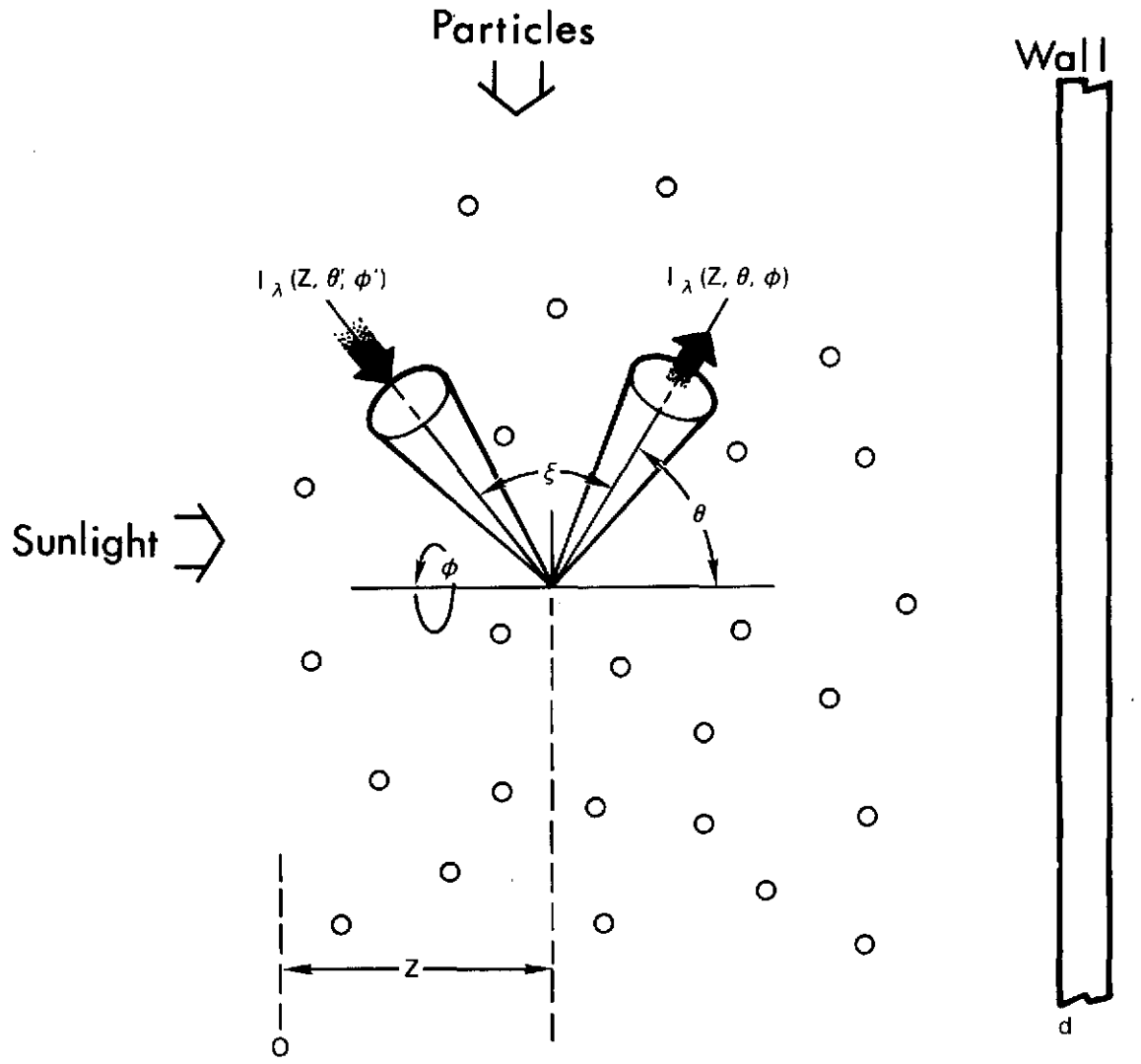

Figure 1. Diagram of the geometry and nomenclature used to define the radiative transfer model showing the falling particle curtain, incident sunlight, and receiver wall.

In the absence of interference between particles, the absorption coefficient, scattering coefficient, and phase function in the particle curtain are simply the sums of the individual particle contributions in a unit volume. If $N(\bar{r})$ is the number of particles per unit volume having a characteristic dimension $\bar{r}$, then the appropriate optical properties are

$$\kappa_\lambda = \int_0^\infty N(\bar{r})\, C_{Abs}(\bar{r})\, d\bar{r} \tag{2}$$

$$\sigma_\lambda = \int_0^\infty N(\bar{r})\, C_{Sca}(\bar{r})\, d\bar{r} \tag{3}$$

and

$$p_\lambda(\xi) = \frac{1}{\sigma_\lambda} \int_0^\infty N(\bar{r})\, C_{Sca}(\bar{r})\, p_\lambda(\xi,\bar{r})\, d\bar{r} \tag{4}$$

where $C_{Abs}(\bar{r})$, $C_{Sca}(\bar{r})$ and $p_\lambda(\xi,\bar{r})$ are the cross sections for absorption, scattering, and the phase function, respectively, for an individual particle of size $\bar{r}$.

A review of the relevant literature shows a lack of data and suitable measurement techniques involving the determination of single-particle scattering and absorption cross sections, and phase functions for the candidate particle materials. Therefore, there is a need to develop experimental techniques to measure these parameters.

Particle diameters are expected to be in the size range between 0.1 to 1.0 mm due to aerodynamic considerations within the solid particle receiver. The particles will be exposed to direct solar radiation as

well as re-radiation from the receiver cavity walls. Hence, the optical properties measurements are desired as a function of wavelength from 300 nm to 10 μm and at temperatures ranging from 20 to 1000°C. Required measurement increments for wavelength and temperature ranges are based on the degree of property variation observed in the data.

III. MEASUREMENT OF BULK REFLECTANCE, TRANSMITTANCE, AND ABSORPTANCE

The first characterization measurements performed on solid particle receiver candidate materials consisted of examination of the optical properties of candidate particulate samples in bulk form over a range of sample areal densities. Using a commercial spectrophotometer with an integrating sphere accessory, the hemispherical reflectance and transmittance of the bulk particulates were measured over the solar insolation band of the optical spectrum, 300 nm to 2500 nm. From the reflectance (R) and transmittance (T) values at each wavelength, one may calculate the material's absorptance (A) by the equation $A = 1 - (R + T)$. The absorptance is then weighted by the solar spectral irradiance to provide a single value for solar absorptance, A_S.

Bulk Measurement Instrumentation

The instrument used for the R, T, and A measurements was a Beckman UV-VIS-NIR 5270 double-beam spectrophotometer. In order to facilitate the detection of the reflected and transmitted light, which was of a highly diffuse nature due to the particulate geometry of the sample, a standard Beckman integrating sphere was installed on the instrument.

Data acquisition and manipulation, as well as control of the instrument, were performed with an HP 1000 computer.

The geometry of the spectrophotometer requires that the sample under test be mounted vertically. Since the candidate samples are loose particles, this constraint necessitated the development of special sample cells. The cells, pictured in Figure 2, are fashioned of white Delrin plastic outer rings which hold and separate two quartz windows, forming a transparent sample chamber. The plastic outer rings are designed to provide for nominal sample chamber thicknesses of 0.51, 1.02, 2.03 and 4.06 mm (0.020, 0.040, 0.080, and 0.160 inches). This range of cell thicknesses allows for investigation of R, T, and A for four different areal densities (grams/cm^2) of each sample material.

The various geometries which are used with the Beckman integrating sphere are shown in the horizontal cross-sectional diagrams of Figures 3 and 4. The integrating sphere accommodates both the reference path and the sample path of the double-beam spectrophotometer. The various ports are labeled in Figures 3a and 4a. The sample and reference entrance ports are stopped down with 13 mm (1/2 inch) square apertures so that any vignetting of incoming light by the outer ring of the sample cell is eliminated. The placement of the sample cell and reference varies according to the type of measurement being made.

Bulk Measurement Technique

To complete a transmittance run, three full spectral scans (300 nm to 2500 nm, with 10 nm increments from 300 nm to 700 nm and 40 nm increments from 700 nm to 2500 nm) are required. First the baseline response of the spectrophotometer must be recorded. To accomplish this,

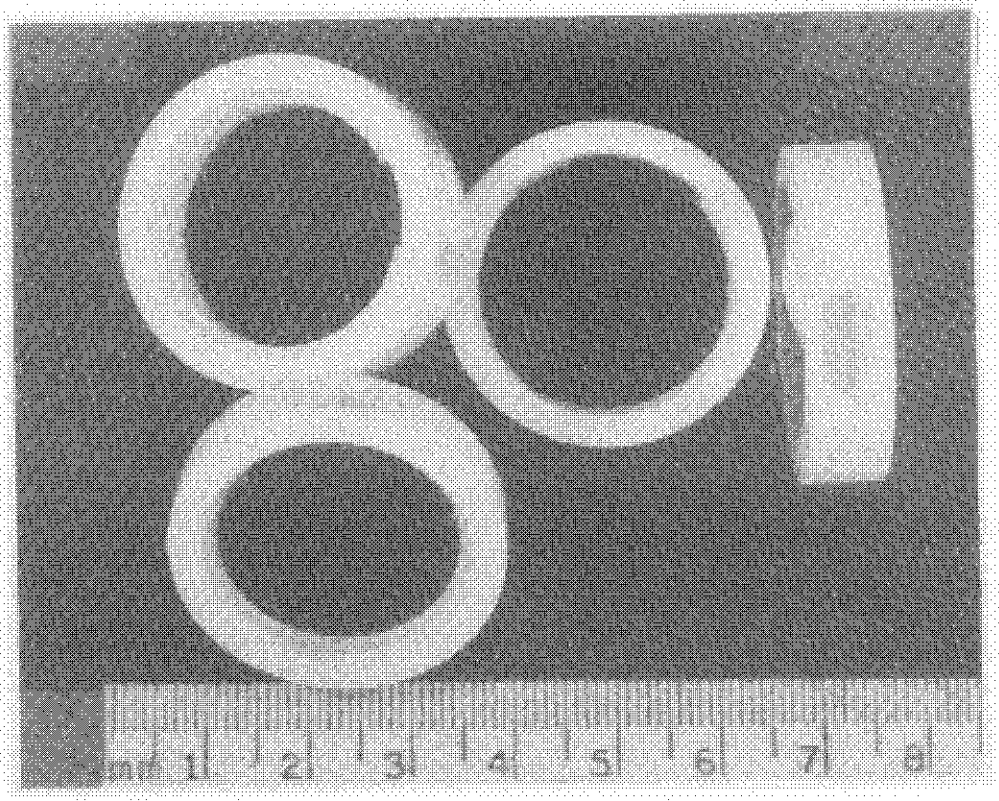

Figure 2. Picture of the quartz sample cells used for the hemispherical transmittance and reflectance measurements.

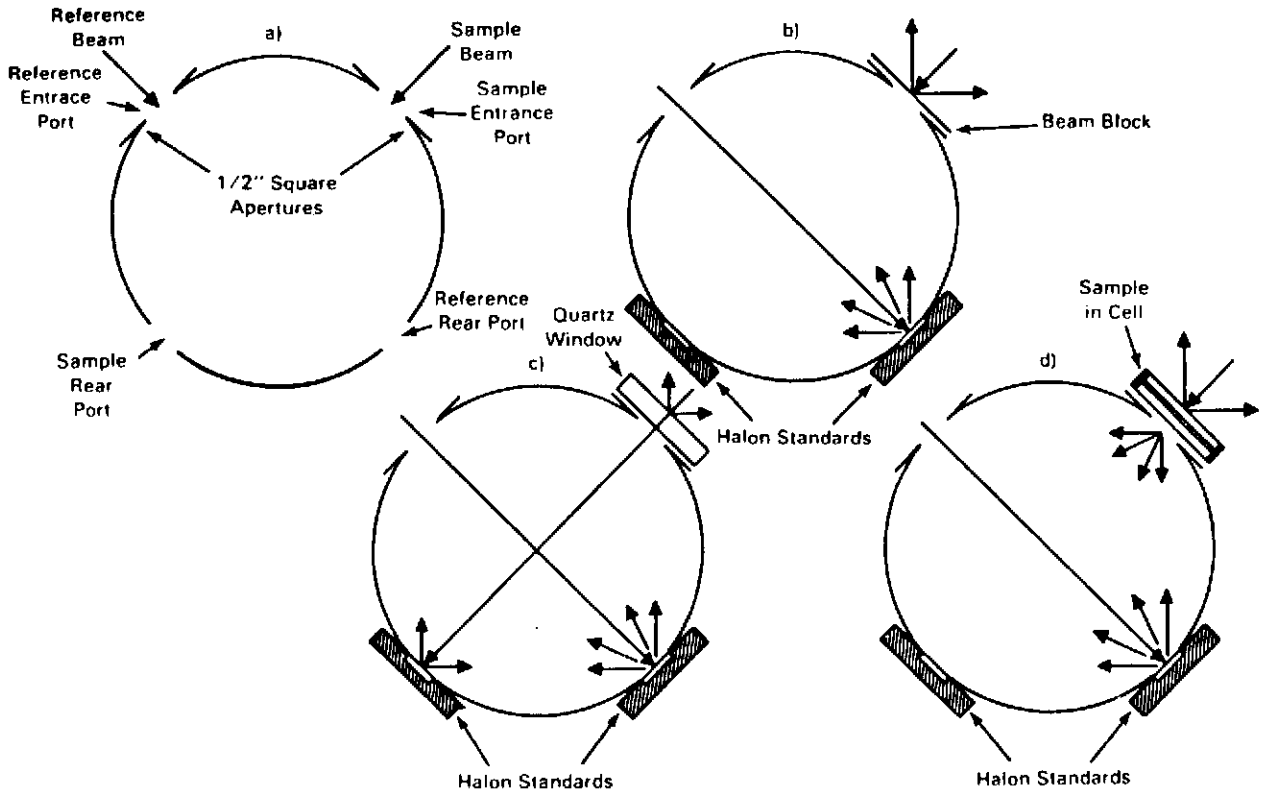

Figure 3. Diagram of Beckman integrating sphere configurations for transmittance measurements: a) sample and reference port locations; b) configuration for baseline measurement; c) configuration for 100% measurement; and d) configuration for sample measurement.

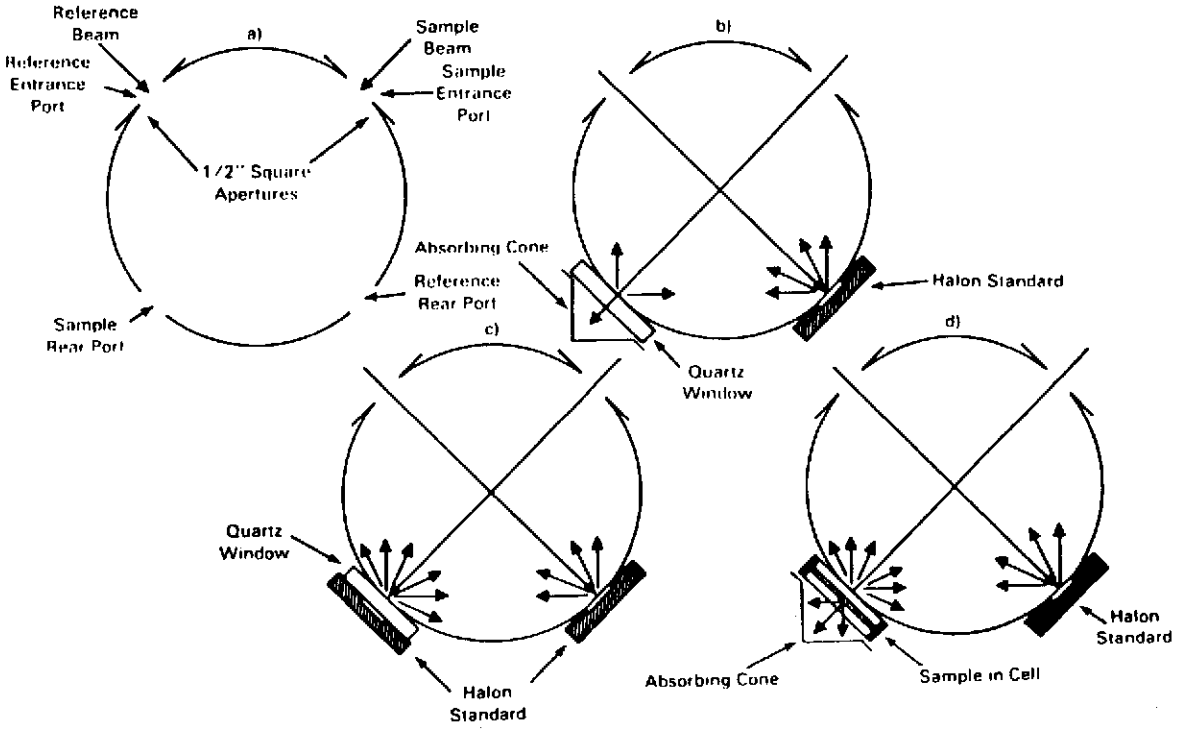

Figure 4. Diagram of Beckman integrating sphere configurations for reflectance measurements: a) sample and reference port locations; b) configuration for baseline measurement; c) configuration for 100% measurement; and d) configuration for sample measurement.

an opaque aluminum beam block is placed in the sample beam entrance port while Halon blocks, packed to a standard density which has been characterized by NBS,[5] are placed in the rear sample and reference ports (Figure 3b). The reference entrance port is open. Halon is well-suited for use as a reference since it is highly diffuse and also very highly reflecting (R = 0.96 to 0.99) over the full solar insolation band. The function of the Halon blocks during the transmission runs is simply to preserve the diffuse surface continuity of the integrating sphere and to prevent the specularly transmitted light from exiting the sphere volume. A full spectral scan with this configuration yields the signal levels, $V_B(\lambda)$, corresponding to zero transmittance. Upon completion and storage of the baseline run, the 100% transmission response of the spectrophotometer must be recorded. For this run, both reference ports (front and rear) and the rear sample port remain unchanged, but the beam block is removed from the sample entrance port and is replaced by a single reference quartz window identical to those used in the sample cells (Figure 3c). Use of this quartz reference enables correction for transmission losses due to reflections at the front and rear surfaces of the cell front window. A full spectral scan with this configuration gives, to a good approximation, the instrument's response, $V_{Max}(\lambda)$, for a 100% transmitting sample contained in the previously described sample cells. The final scan required for calculation of the sample transmittance is the actual sample data run. Again, both of the reference ports remain unchanged as does the rear sample port, but the sample entrance port is now supplied with the particulate sample held in its sample cell (Figure 3d). The full spectral scan with this configuration yields the signal levels, $V_T(\lambda)$, corresponding to the

amount of light transmitted by the sample. The three data runs are then processed to determine the sample transmittance, $T(\lambda)$, using the formula:

$$T(\lambda) = \frac{V_T(\lambda) - V_B(\lambda)}{V_{Max}(\lambda) - V_B(\lambda)} \quad (5)$$

To complete a reflectance measurement, three full spectral scans are again required. First, the instrument baseline signal, $V_B(\lambda)$, is measured and recorded. To accomplish this, both entrance ports are left open and the rear reference port is supplied with a Halon standard. The rear sample port contains a single reference quartz window identical to those used for the sample cells, backed by an absorbing cone (Figure 4b). This configuration provides a close approximation to the case of a totally absorbing sample held in the sample cell. Once again, the quartz window accounts for reflectance enhancements due to reflections at the front and back surfaces of the sample cell front window. Next, the reference reflectance response of the instrument is measured and recorded. To accomplish this, the quartz window and absorbing cone are removed from the rear sample port and replaced with a Halon standard which is covered by another reference quartz window. The entrance reference port remains open and the rear reference port continues to contain a Halon standard (Figure 4c). In this configuration, the signals obtained, $V_r(\lambda)$, represent the response of the instrument for a particulate sample exhibiting a known (NBS calibrated) diffuse reflectance and being held in a quartz-windowed sample cell. Since the reflectance of the Halon is known, all following data may be referenced to the Halon values, $R_H(\lambda)$. Finally, the Halon-window combination is removed and replaced by the

sample, held in its sample cell (Figure 4d). A full spectral scan is completed and the signal levels, $V_R(\lambda)$, corresponding to the amount of light reflected by the sample are recorded. The reflectance of the sample, $R(\lambda)$, is then calculated by the computer according to:

$$R(\lambda) = \frac{V_R(\lambda) - V_B(\lambda)}{V_r(\lambda) - V_B(\lambda)} \cdot R_H(\lambda) \qquad (6)$$

As mentioned earlier, the absorptance of the sample may then be calculated by $A(\lambda) = 1 - [R(\lambda) + T(\lambda)]$.

Bulk Measurement Data

During initial solid particle receiver candidate material screening, many types of particulates were analyzed using this spectrophotometric technique. These materials include mullite, garnet, silicon carbide, aluminum oxide, titanium dioxide, common beach sand, and Master Beads^R, a highly spherical bauxite material manufactured by Norton Company, Worcester, Massachusetts. Master Beads^R are primarily used as a proppant in oil well drilling operations. Figures 5 through 13 show data plots of R, T, and A versus wavelength for each of these materials at the largest areal density available (cell thickness of 4.06 mm). This assures that the transmittance of the sample is as close to zero as possible, and further increases in areal density would have little or no effect upon the transmittance, reflectance, or absorptance of the sample. Stated another way, this assures that the optical properties measured are bulk values. The materials which are light in color, such as mullite and aluminum oxide, exhibit considerably lower absorptance than do dark

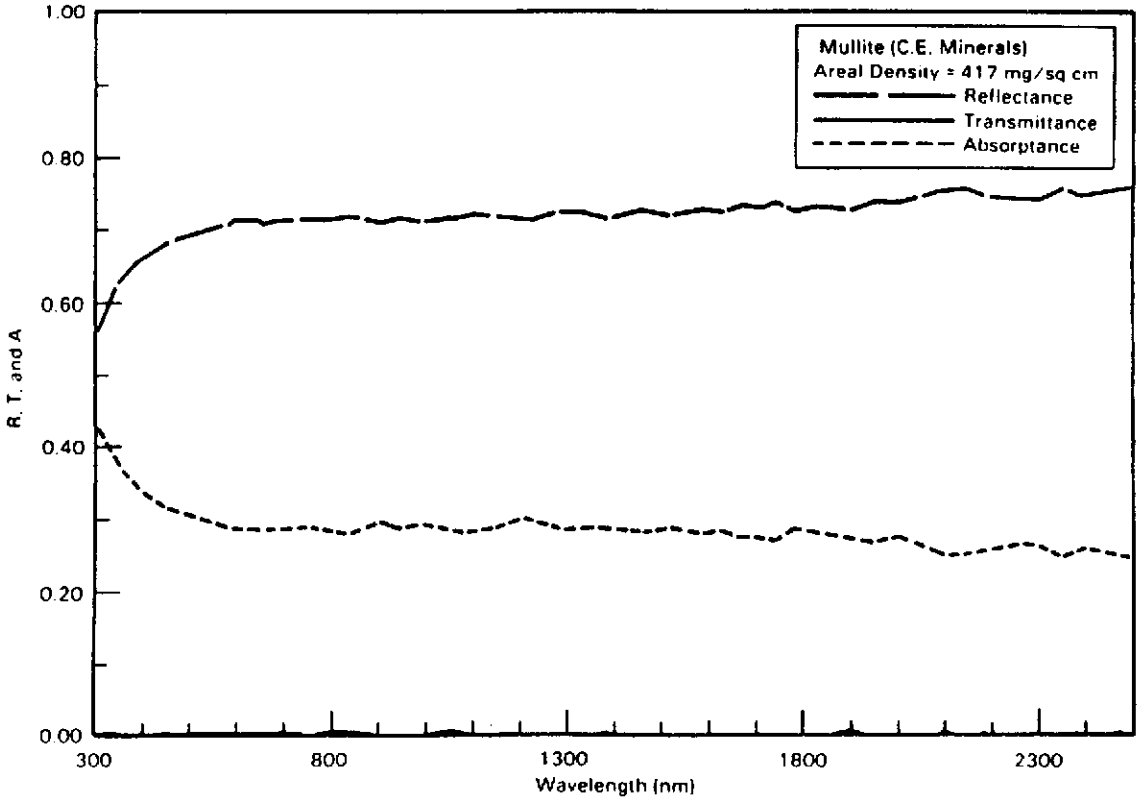

Figure 5. Hemispherical reflectance (R), transmittance (T), and absorptance (A) for Mullite at an areal density of 41 mg/sq.cm.

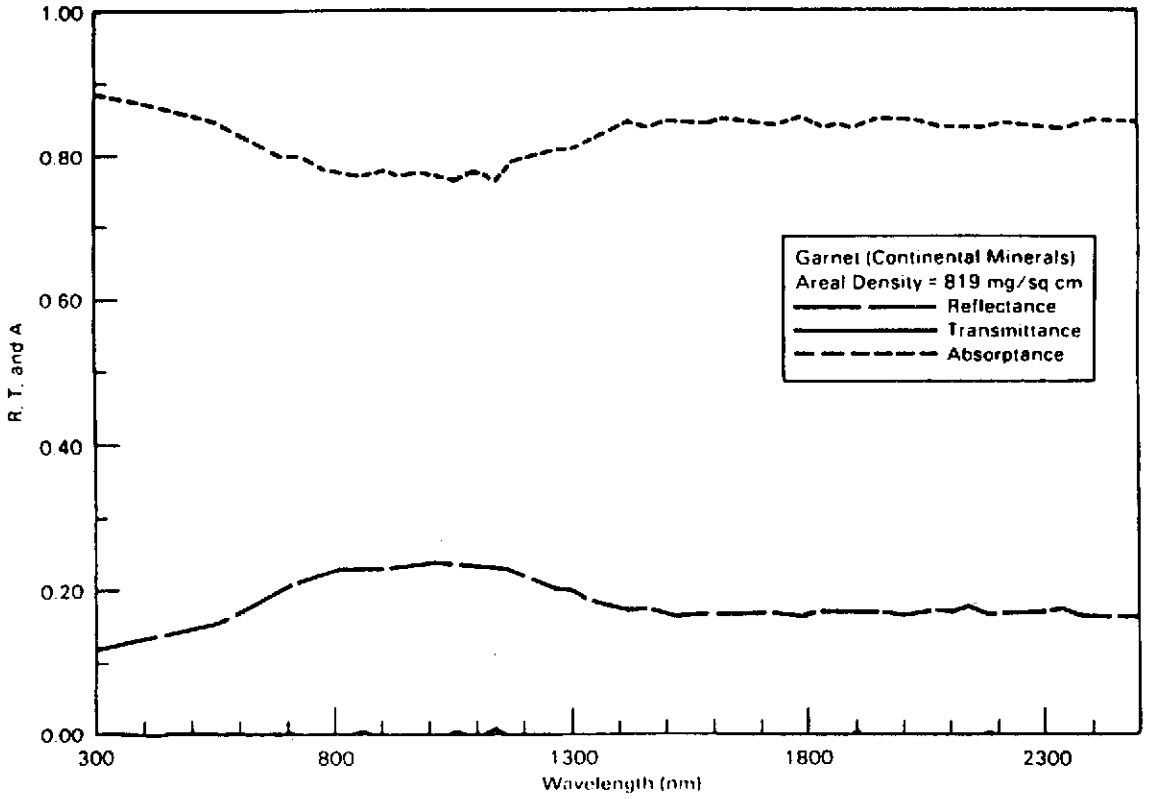

Figure 6. Hemispherical reflectance (R), transmittance (t), and absorptance (A) for Garnet at an areal density of 819 mg/sq.cm.

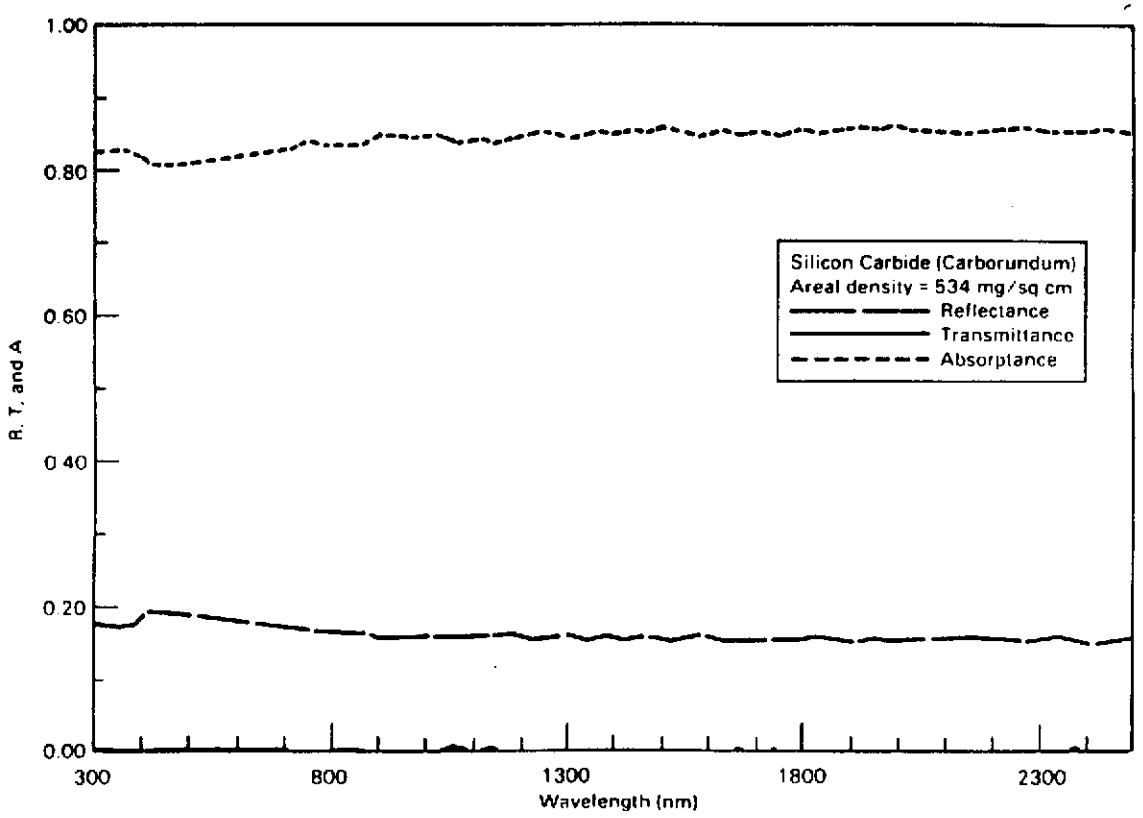

Figure 7. Hemispherical reflectance (R), transmittance (T), and absorptance (A) for SiC at an areal density of 534 mg/sq.cm.

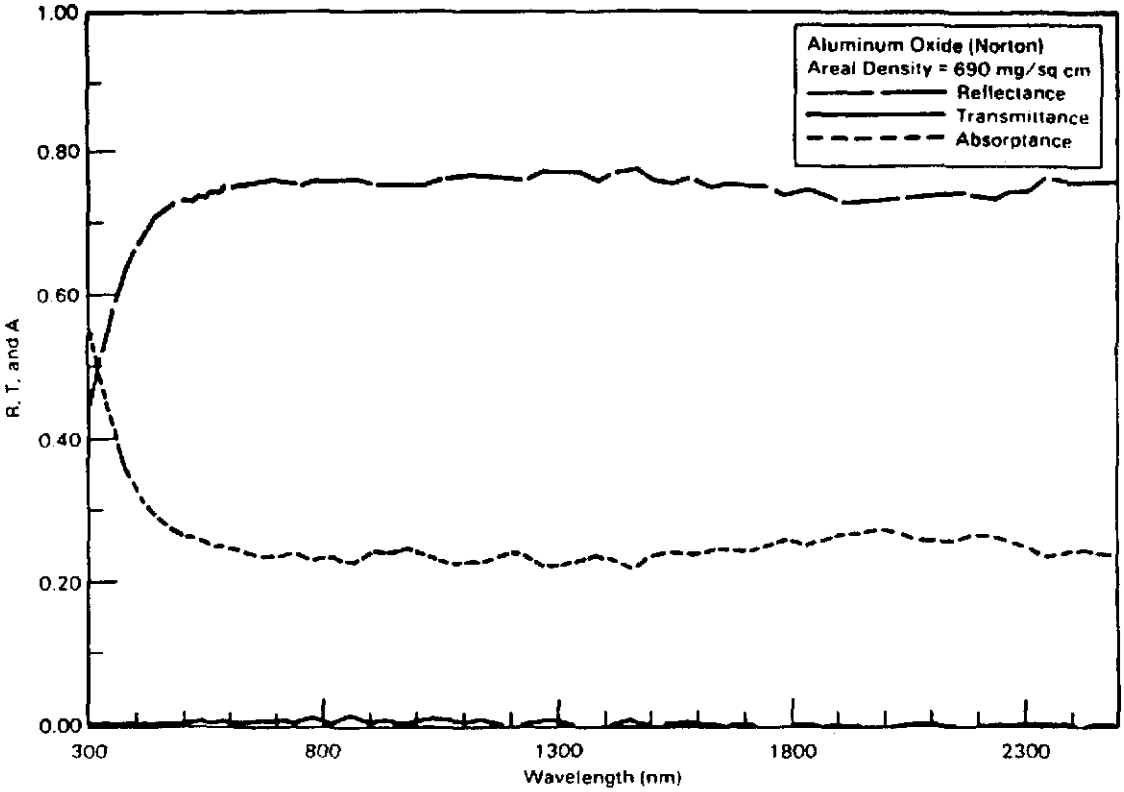

Figure 8. Hemispherical reflectance (R), transmittance (T), and absorptance (A) for Al_2O_3 at an areal density of 690 mg/sq.cm.

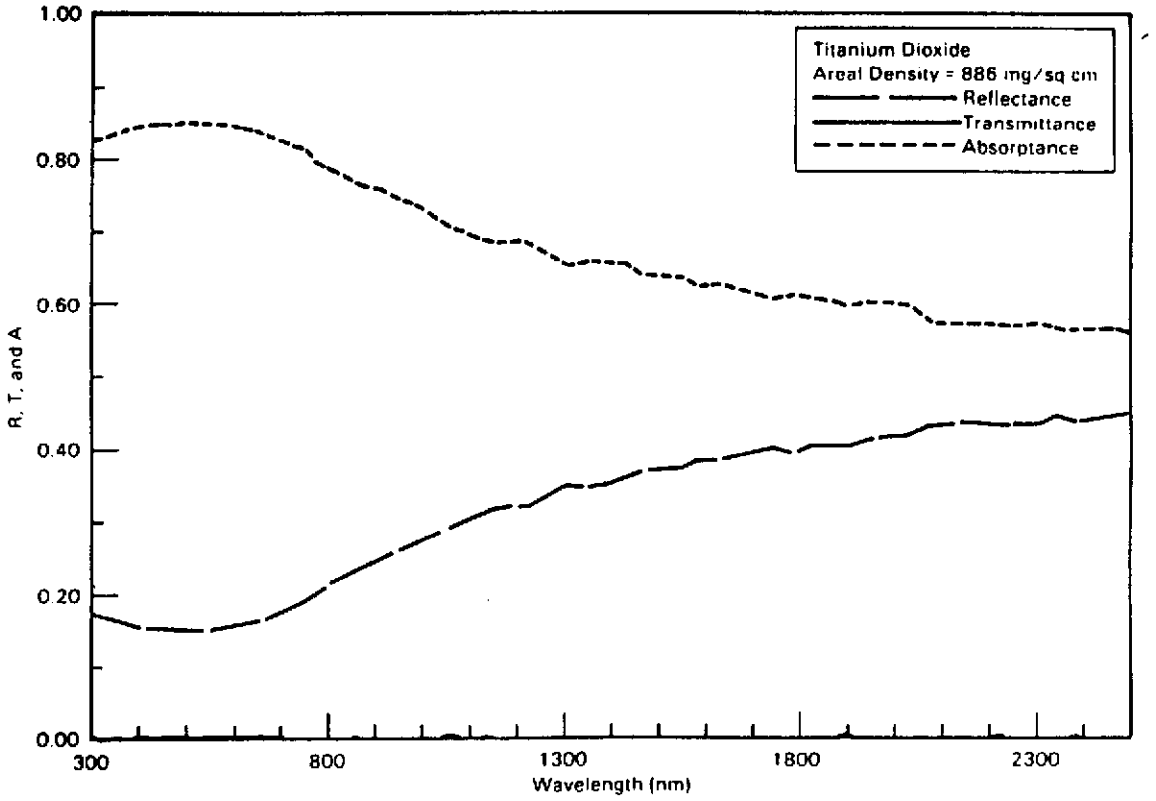

Figure 9. Hemispherical reflectance (R), transmittance (T), and absorptance (A) for TiO_2 at an areal density of 886 mg/sq.cm.

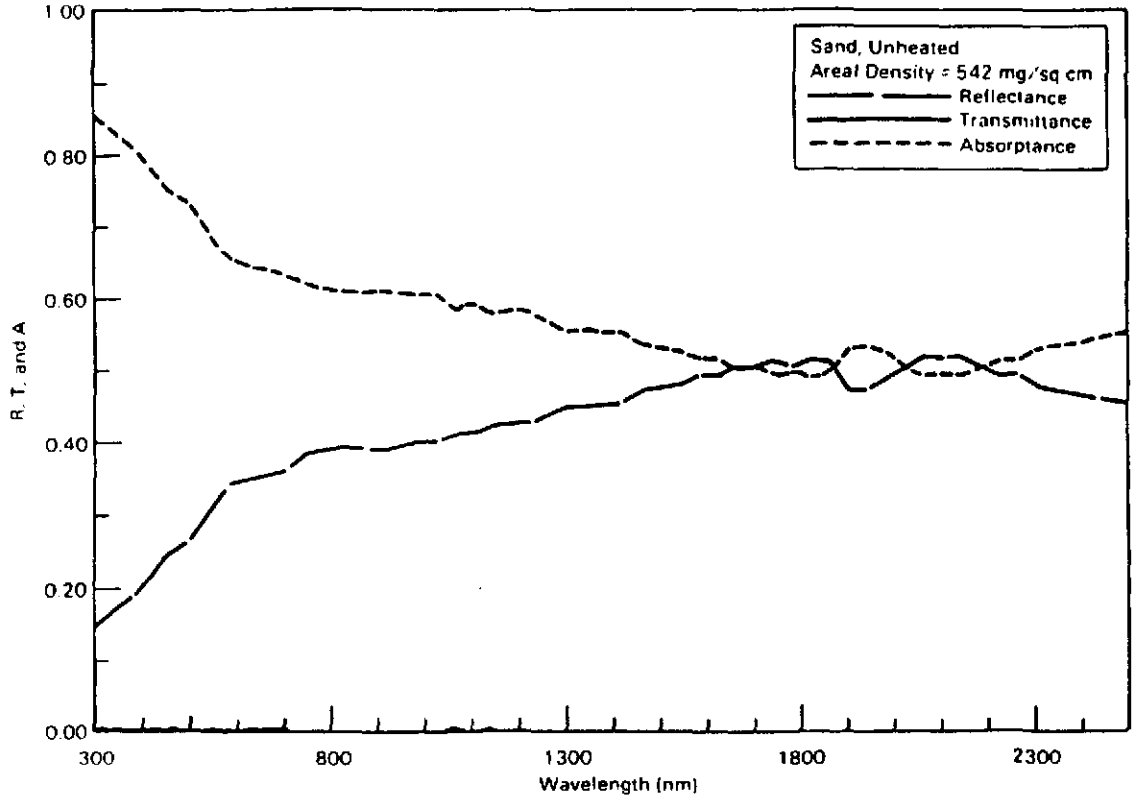

Figure 10. Hemispherical reflectance (R), transmittance (T), and absorptance (A) or sand (unheated) at an areal density of 542 mg/sq.cm.

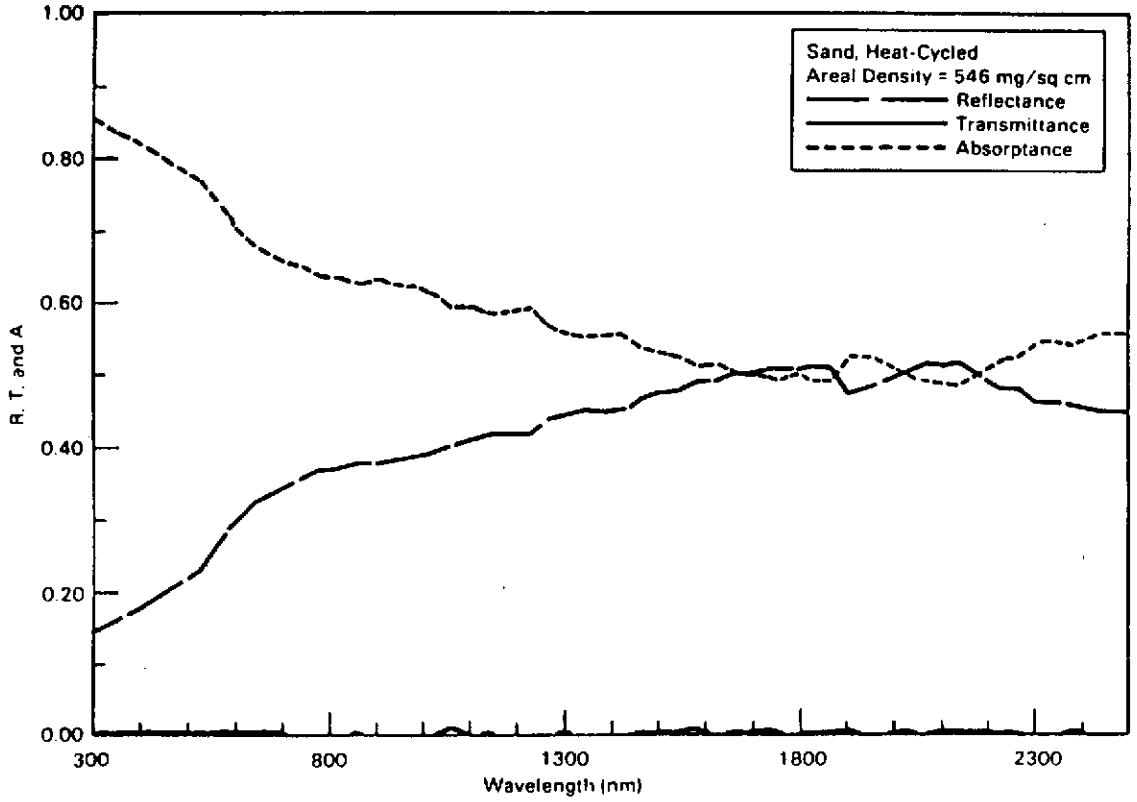

Figure 11. Hemispherical reflectance (R), transmittance (T), and absorptance (A) for sand (heated to 1000°C for 1 hr.) at an areal density of 546 mg/sq.cm.

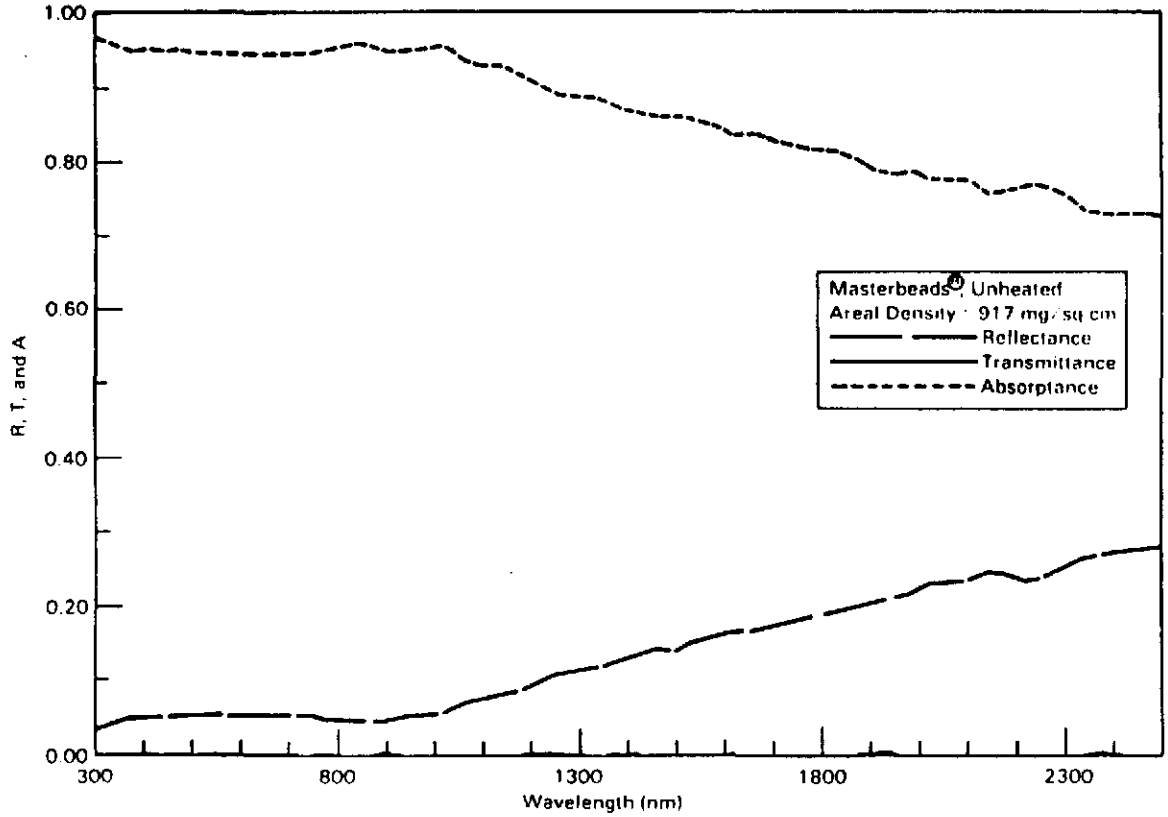

Figure 12. Hemispherical reflectance (R), transmittance (T), and absorptance (A) for Master Beads^{R} (unheated) at an areal density of 917 mg/sq.cm.

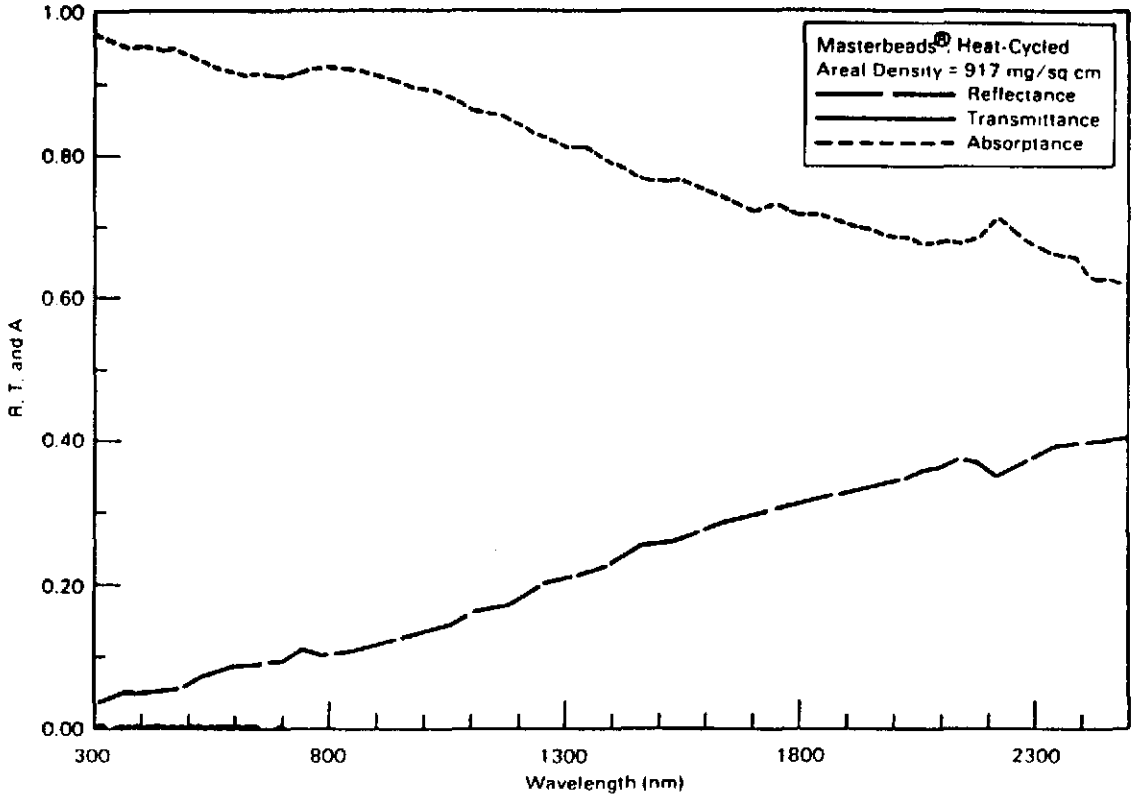

Figure 13. Hemispherical reflectance (R), transmittance (T), and absorptance (A) for Master Beads^{R} (heated to 1000°C for 1 hr.) at an areal density of 917 mg/sq.cm.

materials such as silicon carbide and Master Beads[R]. Examination of these data makes clear the importance of the consideration of optical characteristics as a selection criteria for the heat transfer medium employed in the solid particle receiver. For example, particles showing relatively poor optical absorption in bulk form might be ruled out on this basis alone.

Since the particle curtain in the operating solar receiver will have a finite density, optical absorptance as a function of areal density is of interest. Areal density is defined as the weight of the sample per unit area and is therefore related to the thickness of the sample, e.g., a thicker (along the optic axis) sample gives a larger areal density. To calculate the areal density of a sample, one must first find the weight of the sample being held in the sample cell. Assuming that the dimensions of the sample cell are known, one may use the open aperture of the sample cell to calculate the area that the particulate sample occupies and thus arrive at an areal density for that sample in that particular sample cell. Note that for any sample cell, each sample material will, in general, have a different areal density. Having calculated the areal density of the sample, it is then possible to consider the solar-weighted absorptance of the samples as a function of areal density. The value for solar weighted absorptance is calculated by weighing spectrophotometric absorption values by the solar spectral irradiance[6] over the same wavelength band. The resulting solar weighted curve is then integrated and divided by the integral of the solar spectral irradiance curve to arrive at a single value for solar weighted absorptance. If we denote the solar irradiance by $S(\lambda)$, and the sample

absorptance by $A(\lambda)$, then in mathematical notation the solar weighted absorptance, A_S, is:

$$A_S = \frac{\int_{\lambda_2}^{\lambda_1} S(\lambda)\ A(\lambda)\ d\lambda}{\int_{\lambda_2}^{\lambda_1} S(\lambda)\ d\lambda} \qquad (7)$$

The solar spectral irradiance values used for this procedure are from the NASA air mass 1.5 (AM 1.5) results.[6]

Figure 14 shows an example of the result of the solar weighting procedure. The figure shows the spectrophotometric absorption for Master Beads®, as in Figure 12, with the solar weighted absorptance curve superimposed upon it. The solar absorptance, in this case equaling 0.94, also appears. Figure 15 shows solar absorptance as a function of areal density for each of the nine materials submitted for testing.

While the quartz windows used in the spectrophotometer sample cells possess very good transmittance characteristics over the entire range of interest, their effect upon the measurements described above should not be ignored. The combination of the sample cell and aggregate sample results in an optical "sandwich" consisting of a quartz window, a particulate sample of a known thickness, and another quartz window. Through the use of reference quartz windows in the 100% transmittance and reflectance runs, as previously described, the spectrophotometer measurement procedure provides the means to eliminate the large first order effect, i.e., surface reflection from the initial air-quartz interface. However, the higher order interactions involving quartz-air, air-particle, and particle-quartz interfaces cannot be corrected by

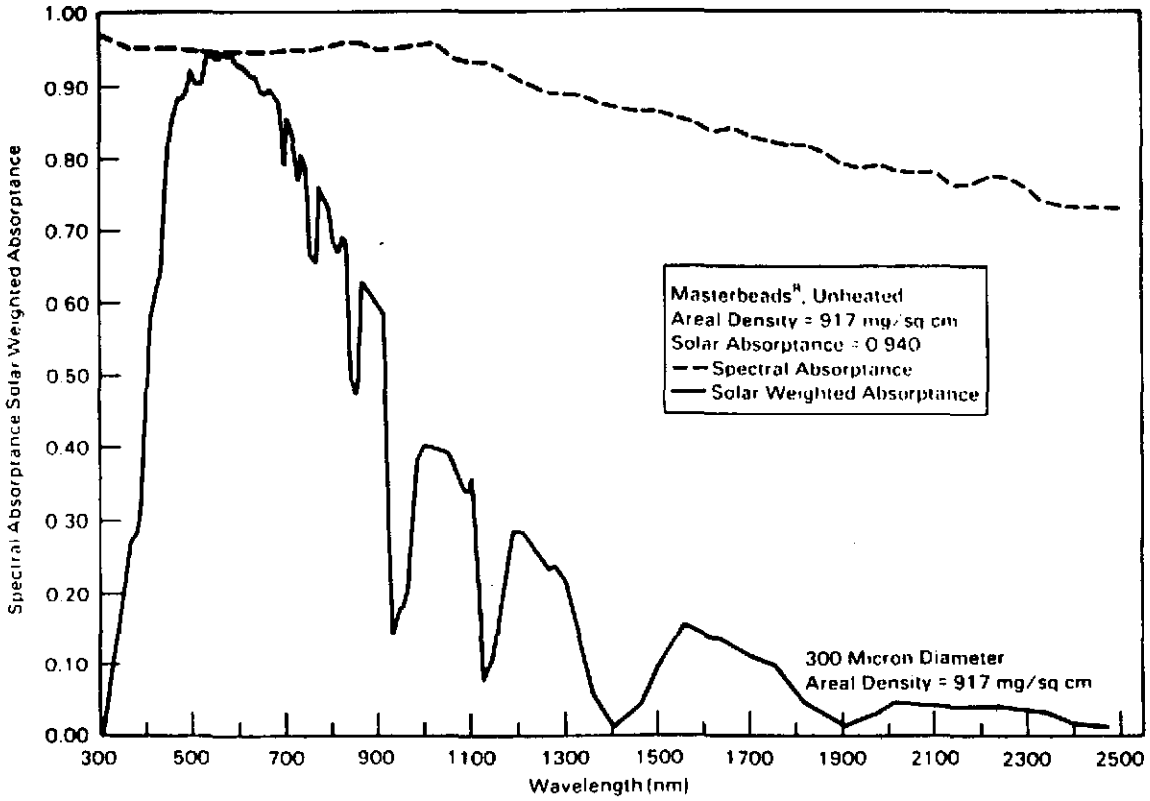

Figure 14. The AM 1.5 solar spectral distribution used to average the spectral absorptance properties of the particles. Also shown is the spectral absorptance of Master Beads^{R} (unheated).

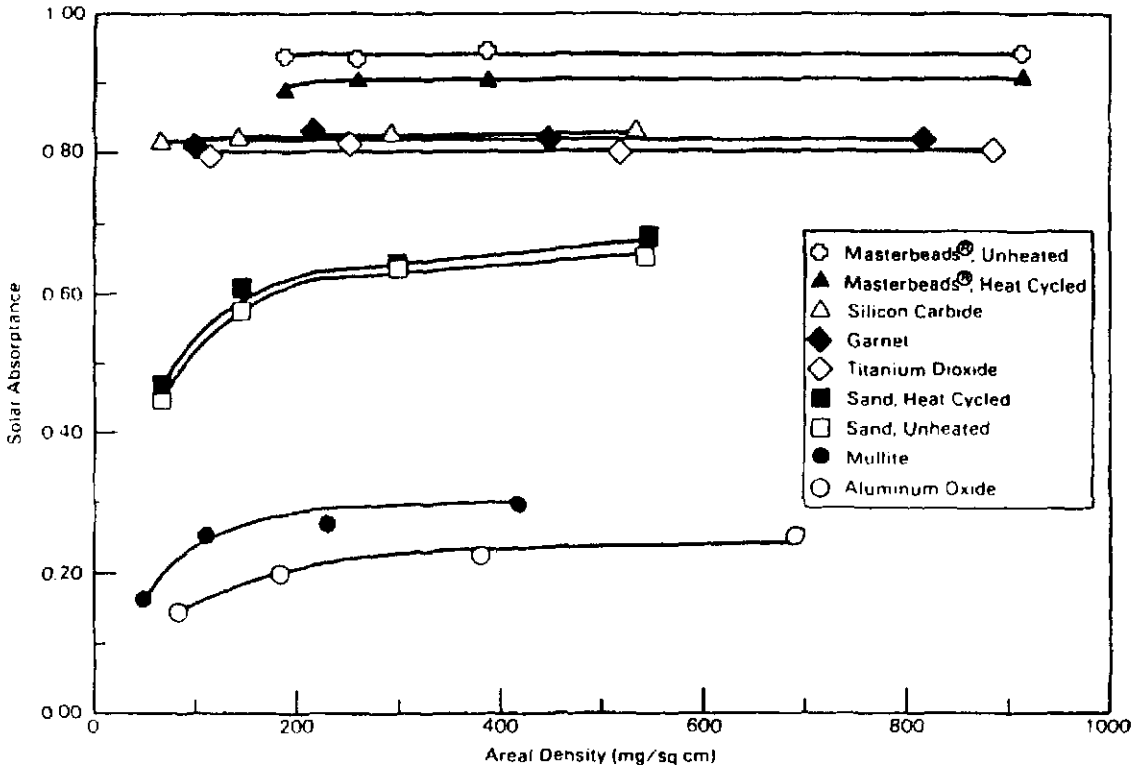

Figure 15. Solar absorptance properties of the various solid particles as a function of areal density.

standard methods and may lead to uncertainties on the order of several percent. Errors of this magnitude are not considered to be critical in the characterization of solid particle receiver materials since trends in the materials' reflectance, transmittance, and absorptance are of primary interest. Should the need arise for R, T, and A data accurate to better than several percent, mathematical techniques for correcting the data will be required.

IV. MEASUREMENT OF ANGULAR SCATTERING DISTRIBUTION

A second area of investigation into the optical properties of solid particle candidates focuses on the angular scattering distribution for a single falling particle. Note that the fact that the particle is falling is incidental. Such a geometry was chosen only to facilitate the measurement of the scattering distribution. Experimental data on angular scattering by the particulates are essential to the use of the radiative transfer model for the solid particle solar central receiver as defined in ref. 4.

To develop the equations for scattering, which are used to suggest experimental measurement procedures and data analysis methods, first consider a spherical particle of diameter D_p and cross sectional area A_p. The optical scattering distribution as a function of scattering angle is described by the differential scattering cross section (DSCS), $\chi(\theta)$. The geometry and nomenclature are summarized in Figure 16. The single-particle DSCS is given by

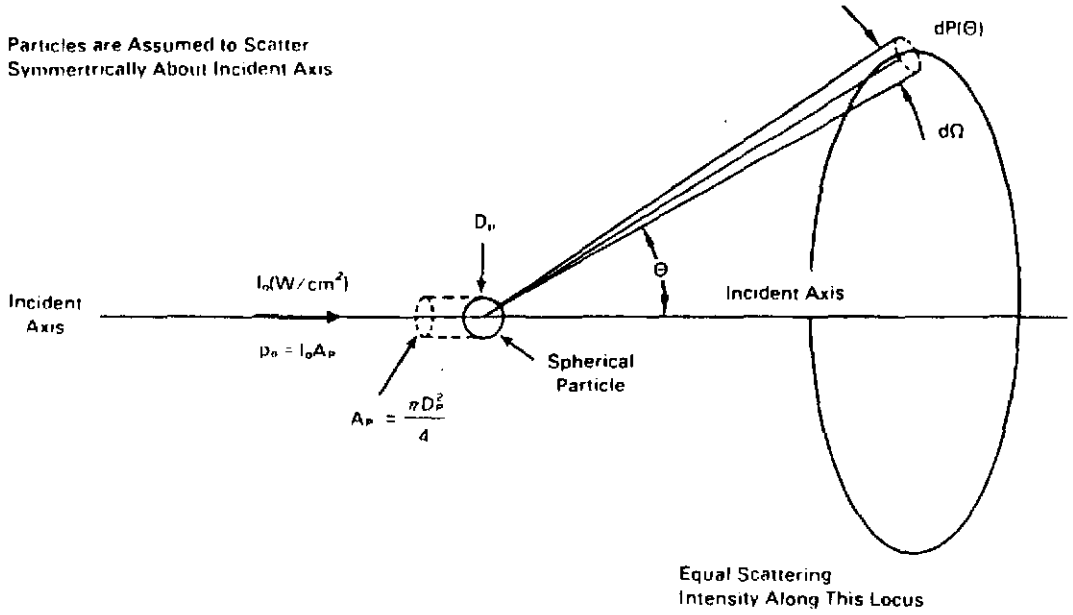

Figure 16. Diagram showing the geometry and nomenclature used to define the differential scattering cross section (DSCS)

$$\chi(\theta) = \frac{\left[\frac{dP(\theta)}{I_0}\right]}{d\Omega} = \frac{dC_{Sca}}{d\Omega} \qquad (8)$$

where I_0 is the optical intensity (watts/cm^2) incident upon the particle (assumed uniform across the particle), $dP(\theta)$ is the optical power (watts) scattered into the θ direction within solid angle $d\Omega$. The fractional power scattered into $d\Omega$ is denoted by $dC_{Sca}(\theta)$. Another quantity used to describe the angular distribution of particulate-scattered light is the phase function, $p(\theta)$. It is related to the DSCS by

$$p(\theta) = \frac{1}{C_{Sca}} \left[\frac{dC_{Sca}(\theta)}{d\Omega}\right] \qquad (9)$$

where C_{Sca} is the total scattering cross section given by

$$C_{Sca} = \int_{4\pi} \left[\frac{dC_{Sca}(\theta)}{d\Omega}\right] d\Omega \qquad (10)$$

Experimentally, determination of $\chi(\theta)$ requires a collection of scattering intensity measurements over some range of scattering angles whereas determination of C_{Sca} requires an integral measurement of light scattered over all angles (4π steradians), which can be accomplished using, for example, an integrating sphere. Further discussion in this section will be confined to the DSCS.

Angular Scattering Measurement Technique

As a practical matter, single-particle differential scattering cross sections are difficult to measure for three reasons. First, for the

particles of current interest (Norton Master Beads^{R}, $D_p \approx 325\ \mu m$) the scattered power is very low. Second, it is extremely difficult to mount a single particle of this size so that one is assured of a single scattering interaction with minimal interferences. Third, because of the non-uniform shape of the particles, the DSCS will vary both from particle to particle and for the same particle depending upon its orientation with respect to the incident radiation. A partial solution to these two problems is the free falling curtain measurement geometry previously described. In this geometry, the scattering contributions from numerous particles add to produce a detectable signal level and the nominal one-particle curtain thickness assures a single scattering interaction along the illumination source direction. This signal enhancement measurement procedure results in a determination of the differential scattering cross section for a collection of particles with a known size distribution. This cross section can be scaled to give an average DSCS for a single particle, $\bar{\chi}(\theta)$. The experimental arrangement is schematically depicted in Figure 17a.

In this measurement configuration the curtain is illuminated by a radially-symmetric collimated beam of laser radiation with cross sectional intensity distribution I(r) (watts/cm^2) The total beam power, W_0 (watts), is given by

$$W_0 = \int_0^{D_B/2} I(r)\ 2\pi r\ dr \qquad (11)$$

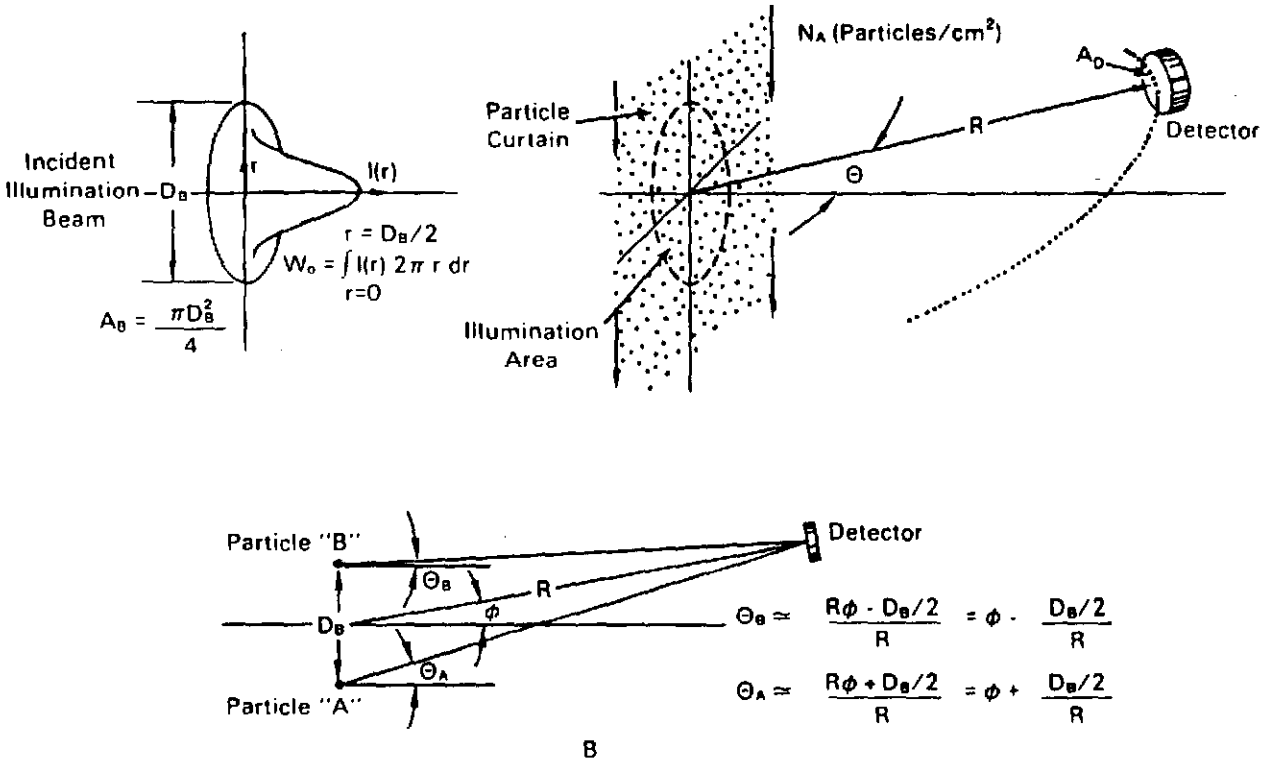

Figure 17. Diagram showing the geometry used for the angular scattering measurements.

where D_B is the effective beam diameter (i.e., the diameter beyond which no intensity is detectable). This beam illuminates an area A_B of the curtain. The curtain area particle density is denoted by N_A (particles/cm^2) and is assumed constant over the illuminated area. The scattered intensity measurements are made in a single plane with a detector of area A_D at a distance R from the center of the curtain-beam intersection. The angle between the detector and the incident beam direction is designated θ. Since the objective of the measurements is to determine the single-particle DSCS, it is necessary to establish the relationship between the many-particle measurements and the desired single-particle value. The power incident upon the detector, W_D, is simply the sum of scattering contributions from the individual illuminated particles. This sum is given by

$$W_D(\phi) = \frac{A_D}{R^2} \int_0^{D_B/2} I(r)\ \bar{\chi}(\phi)\ 2\pi r\ N_A\ dr \qquad (12)$$

A brief discussion of this expression is appropriate. Note that the incident power per particle (P_0 in Figure 16) is $I(r)A_p$. The light scattered per particle into the θ direction is $I(r)\ A_p\bar{\chi}(\theta)$ where $\bar{\chi}(\theta)$ is the average single-particle differential scattering cross section. The partial sum of contributions to the power scattered into the θ direction from the curtain areal increment ($2\pi rdr$) is $I(r)A_p\bar{\chi}(\theta)(2\pi rdr)N_A$. Note that the integral gives the total optical power per unit solid angle scattered into the θ direction, and that the factor A_D/R^2 is the solid angle subtended by the detector.

Finally, it is necessary to establish the relationship between θ and ϕ. The relationship between these angles is depicted schematically in Figure 17b. In this figure a comparison is made between the scattering angles, θ_A and θ_B for particles "A" and "B" located at the extremities of the illuminated region (where the maximum deviation from ϕ will occur) and the instrumental measurement angle ϕ. Note that θ_A and θ_B differ from ϕ by $+D_B/2R$ and $-D_B/2R$, respectively (see Figure 17b). For the actual experimental system, this maximum differential angle is approximately 5.3° (D_B= 8.1 mm and R = 43.2 mm). This inherent angular error can be reduced by either increasing the measurement radius, R, or by decreasing the curtain illumination spot diameter. It is important to note that in the actual experimental arrangement there were restrictions on the range of these two variables. For the angular scattering measurements, the range of particle areal densities varied from 5 to 100 particles/cm^2 and was limited by the curtain generator apparatus. The minimum illumination area requirement is constrained by the need to illuminate a reasonable number of particles at a given instant. This is desirable in order to provide sufficient scattering intensity for detection and to improve the quality of the computed average single-particle DSCS since the particles are characterized by a range of diameters (and shapes). Likewise, since the energy intercepted by the detector falls as $1/R^2$ it was found that stand-off distances in the range 3.8 cm to 5.1 cm (1.5" - 2.0") were required for an acceptable signal/noise level for the dark Master Beads^R particles. The use of a photodiode was dictated by the requirement of good linearity over several decades of signal level. The trade-off for this linearity is reduced

sensitivity as compared to a photo-multiplier tube. In further discussions it will be assumed that

$$\theta_A \approx \theta_B \qquad \text{and} \qquad \bar{\chi}(\theta) \approx \bar{\chi}(\phi) \tag{13}$$

and it is recognized that the accuracy of these approximations could be improved by changes to the experimental apparatus (e.g., higher power laser, using a photomultiplier tube detectors) and/or measurement geometry (e.g., smaller curtain illumination spot, larger stand-off distance).

It can be seen from Eq. 12 that it is a straightforward matter to determine the average single-particle differential scattering cross section, $\bar{\chi}(\theta)$, from a measurement of the angular scattering intensity for a collection of particles. Eq. 12 can be re-written as

$$W_D(\theta) = \bar{\chi}(\theta)\, N_A \, \frac{A_D}{R^2} \int_0^{D_B/2} I(r)\, 2\pi r \, dr \; . \tag{14}$$

The integral is just the total power in the beam, W_0, so

$$\bar{\chi}(\theta) = \frac{1}{N_A} \, \frac{1}{(A_D/R^2)} \left[\frac{W_D(\theta)}{W_0}\right] \; . \tag{15}$$

This equation is valid except for θ in the vicinity of $\pm$ 90° where the curtain is effectively many particles thick and more than one scattering interaction is likely to occur. Notice that it is not necessary to measure absolute optical intensities since the DSCS is computed as a ratio. Consequently, a signal linearly proportional to

intensity from the silicon detector is sufficient for these measurements. In practice, since the detector aperture is smaller than the incident illumination beam diameter, D_B, it is necessary to focus this light onto the detector with an auxiliary positive lens to determine W_0. The measured voltage is then corrected for lens transmission loss which is largely due to reflections at the two lens surfaces ($\approx$ 7%).

Angular Scattering Measurement Instrumentation

The angular scattering instrument which has been developed consists of two distinct components: the curtain generator and the angular positioning and detecting system. The curtain generator was designed and fabricated by G. H. Prescott and B. R. Steele, both of Sandia National Laboratory, Livermore. A detailed description of the curtain generator can be found in the report by Prescott and Steele,[7] so only a brief description will be given here. Referring to Figures 18 and 19, the bulk particulate sample is held in a hopper located at the top of the curtain generator. Particle flow from the hopper is controlled by a course-feed shovel connected to a loudspeaker coil which is driven by a signal generator-amplifier combination operating at low frequency (5 to 20 Hz) and low amplitude (about 1.7 volts peak-to-peak). The coarse-feed frequency and amplitude can be adjusted to give a range of particle mass flow rates from as low as 3 or 4 grams/minute to as high as 22 or 23 grams/minute. For a particular sample, mass flow rates are determined by particle size, weight, and shape (see the photos of Master Beads^R and Jaygo glass beads, Figures 20 and 21). The course-feed shovel delivers the particles to the fine-feed shovel below. The fine-feed shovel is also connected to a loudspeaker coil which is driven at higher

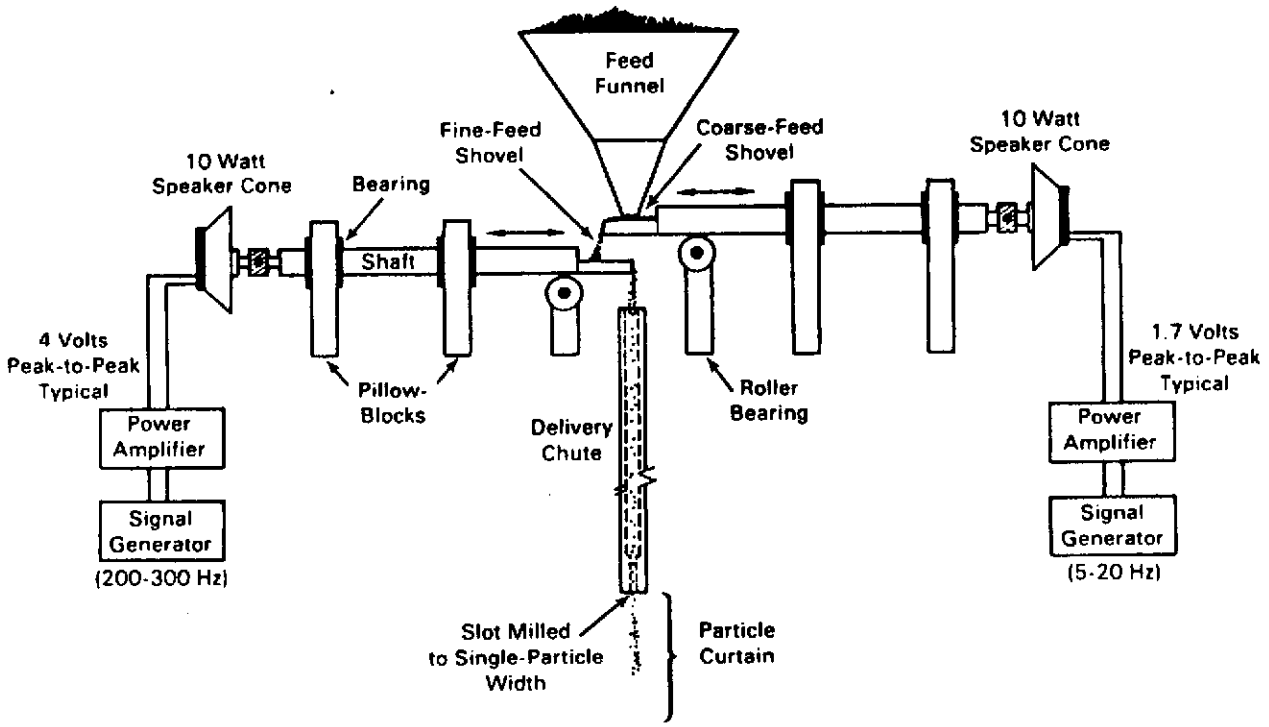

Figure 18. Diagram showing the coarse and fine feed system used to produce the particle curtain for the scattering measurements.

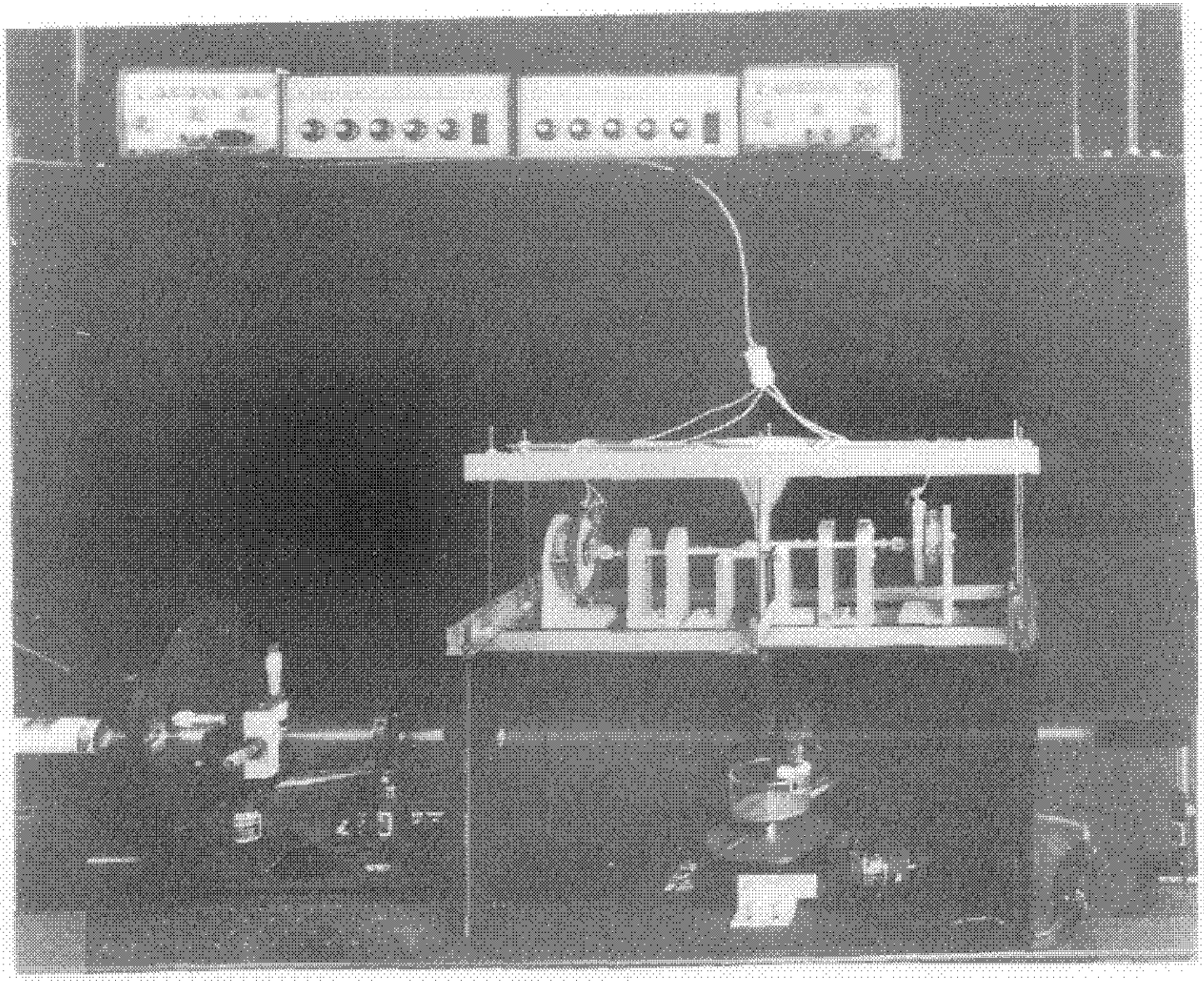

Figure 19. Picture of particle curtain generator and measurement compartment.

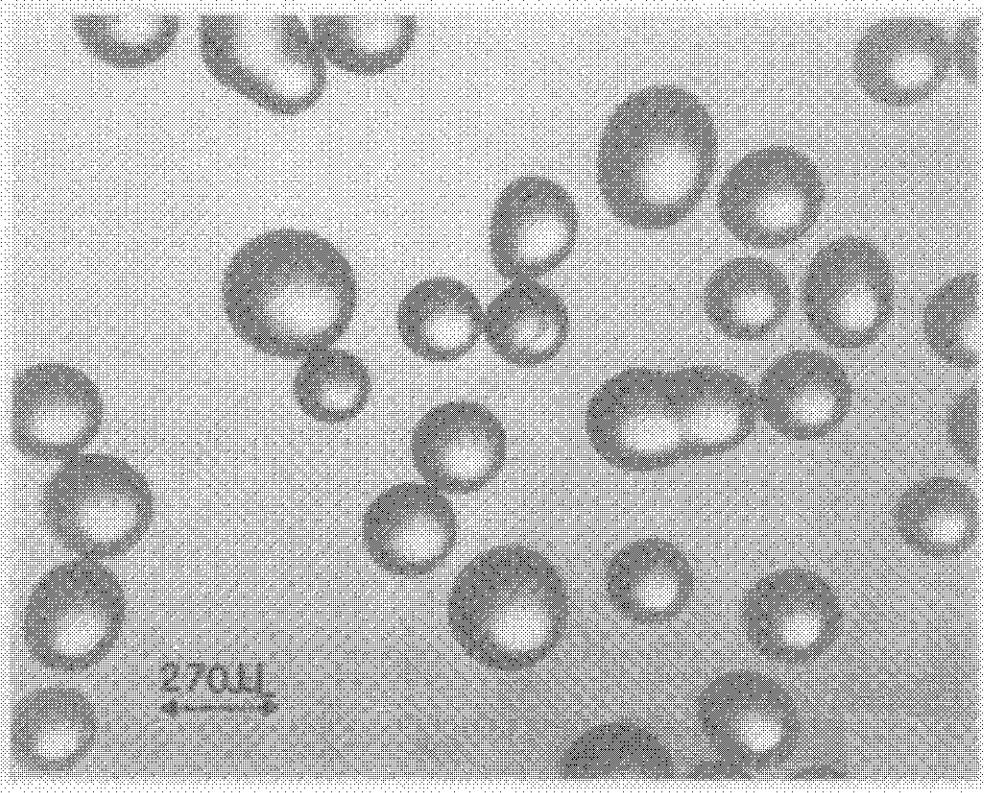

Figure 20. Optical photograph of the Jaygo glass particles.

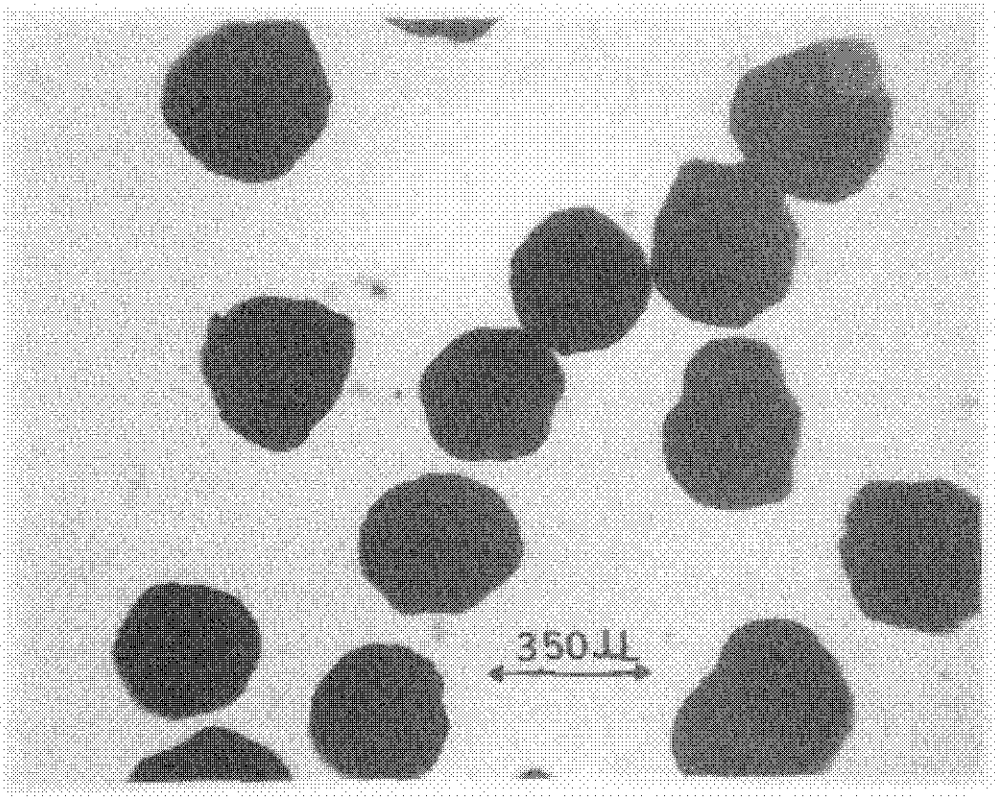

Figure 21. Optical photograph of the Master Bead® particles.

frequencies (200 to 300 Hz) and higher amplitudes (about 4 volts peak-to-peak) and serves to spread the particle flow to single-particle thickness and vibrate the particles into a delivery chute. The delivery chute was carefully machined to a width which is sufficiently large for the passage of a single particle, but too small for two particles, thereby maintaining the single-particle thickness of the falling curtain. The delivery chute released the particle curtain at a point just above the region where the illuminating laser light passed. In this way, the laser beam interacted with the particle curtain before the curtain had undergone an unacceptable amount of spread due to air resistance and turbulence. After passing through the illuminating beam, the particle curtain is collected in a catch glass below.

The remainder of the system is comprised of the electronics and optics necessary to generate, detect, and log the data. Referring to Figure 22, a 4 mW helium-neon laser beam (Spectra-Physics #102) was spatially filtered (NRC #900 with 10 X objective and 25 ξm pinhole), recollimated, and stopped down to give an illuminating beam of about 8.5 mm diameter. The beam was chopped by a rotary chopper (PARC #192) operating at about 90 Hz so that synchronous detection could be employed. Figure 23 shows a diagram of the data acquisition and detector positioning system. A silicon detector (Labsphere #SDA-1) with associated amplifying electronics was used to detect the laser light which was scattered from the particle curtain. The pre-amplifier used for the Jaygo glass bead experimentation was of a simple single-stage design utilizing a general purpose operational-amplifier, feedback resistor, and capacitor. For the Master Bead^{R} experimentation, a precision two-stage circuit is used.[8] The amplified detector signal was

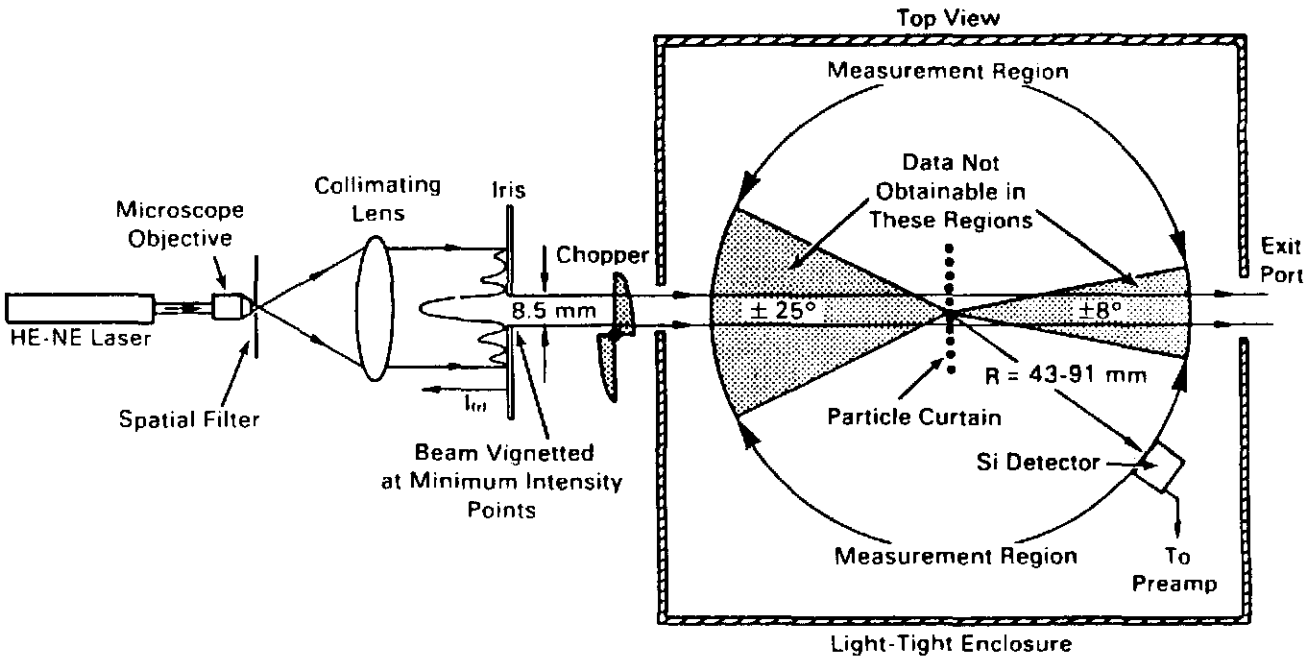

Figure 22. Schematic diagram of the optical arrangement used for the angular scattering measurements.

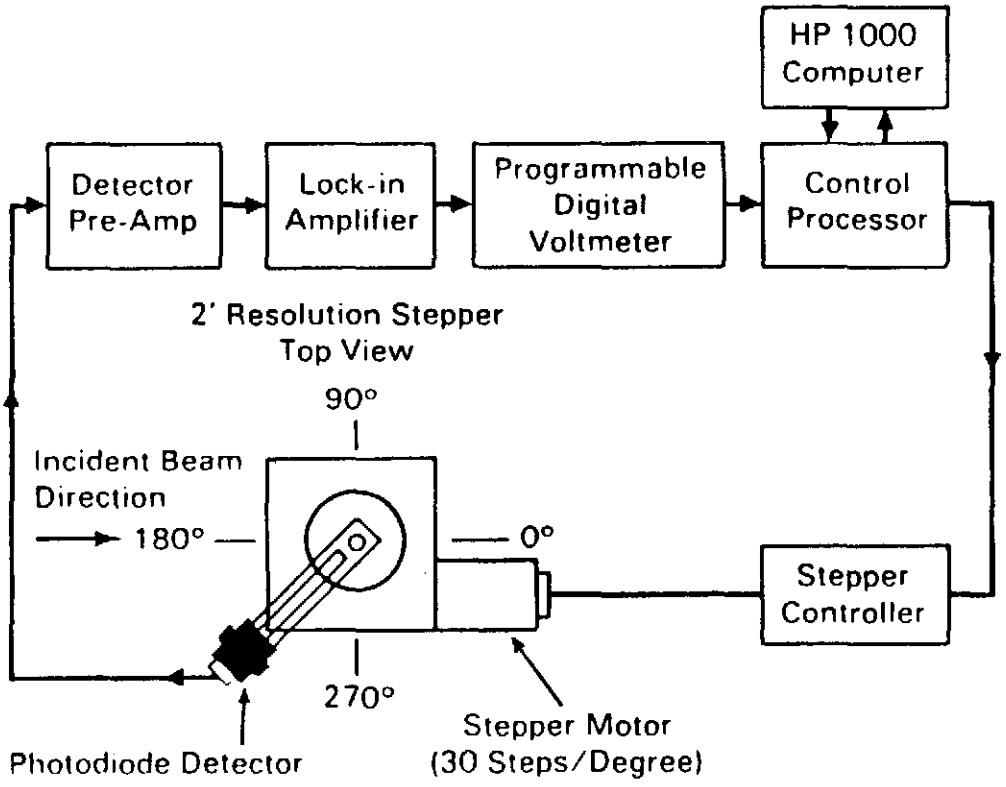

Figure 23. Diagram of the electronics components used for the angular scattering system.

sent to the lock-in amplifier (Ithaco #397 E0) which was in turn read by a programmable voltmeter. The detector is mounted on a radial arm which was adjustable over a small range of radial curtain-to-detector distances of 43 mm to 91 mm (1.7" to 3.6"). This radial arm was then mounted to a stepping-motor-driven 2' resolution rotary stage (Aerotech #ARS-304) which is capable of scanning the detector through a full 360° circle. Data acquisition and detector positioning are under the control of an HP 1000 computer.

The geometry of the system resulted in two angular regions in which data could not be gathered, as shown in Figure 24. In the backscatter direction, the detector housing eclipses all or part of the incoming beam, resulting in the loss of backscattered data in a 25° region on each side of the reverse specular direction. In the forward direction, the detector housing size is not a problem; however, the finite diameter of the illuminating beam in combination with the finite length of the radial scan arm causes the loss of forward-scattered data lying in an area roughly 8° region on each side of the specular direction.

Data Collection Algorithm

The data collection algorithm employed by the angular scatter system is of sufficient complexity to warrant a detailed discussion. Immediately preceding each data run, a background scan is made without the curtain generator running. The signals recorded during this run account for any stray light, geometry effects, and instrument artifacts that are present. A log-polar plot of a typical background scan-data scan pair is shown in Figure 25. The background data file is then subtracted from the subsequent data run to correct for such effects.

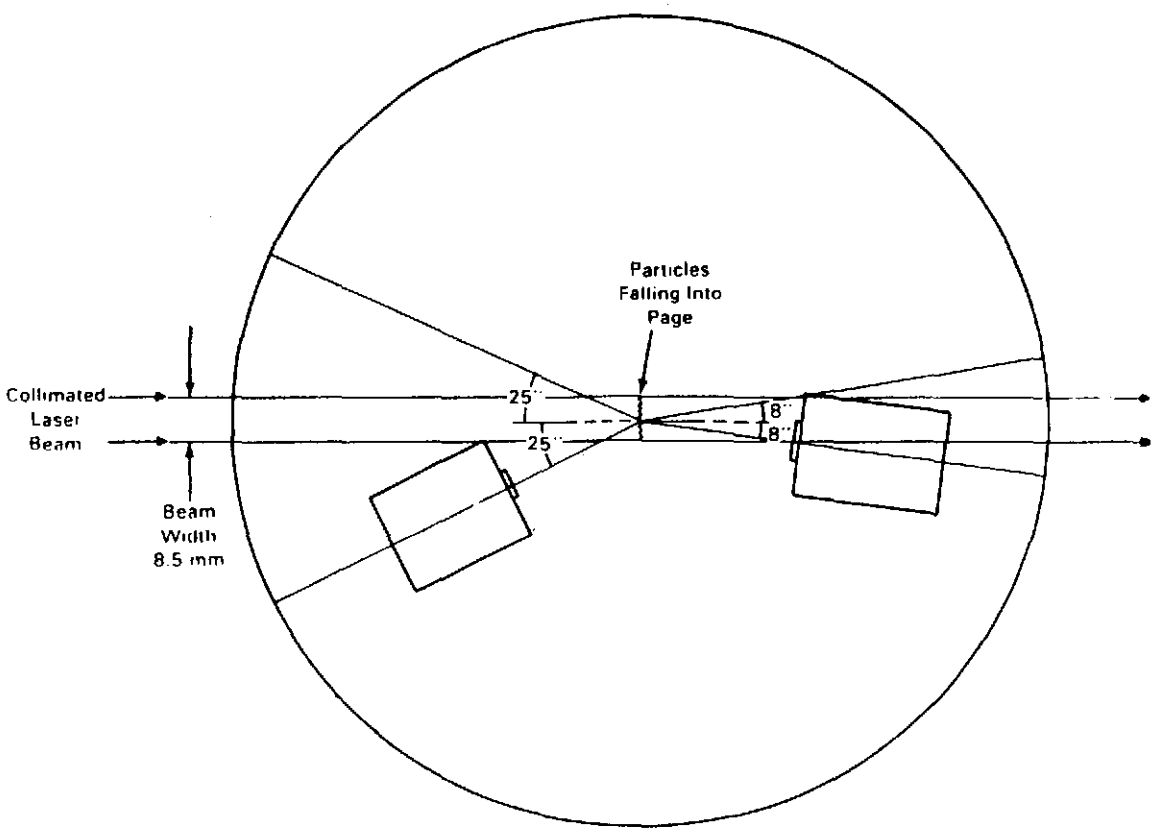

Figure 24. Diagram showing the unavailable regions in the forward direction ($\pm$ 8°) and the backscatter direction ($\pm$ 25°)

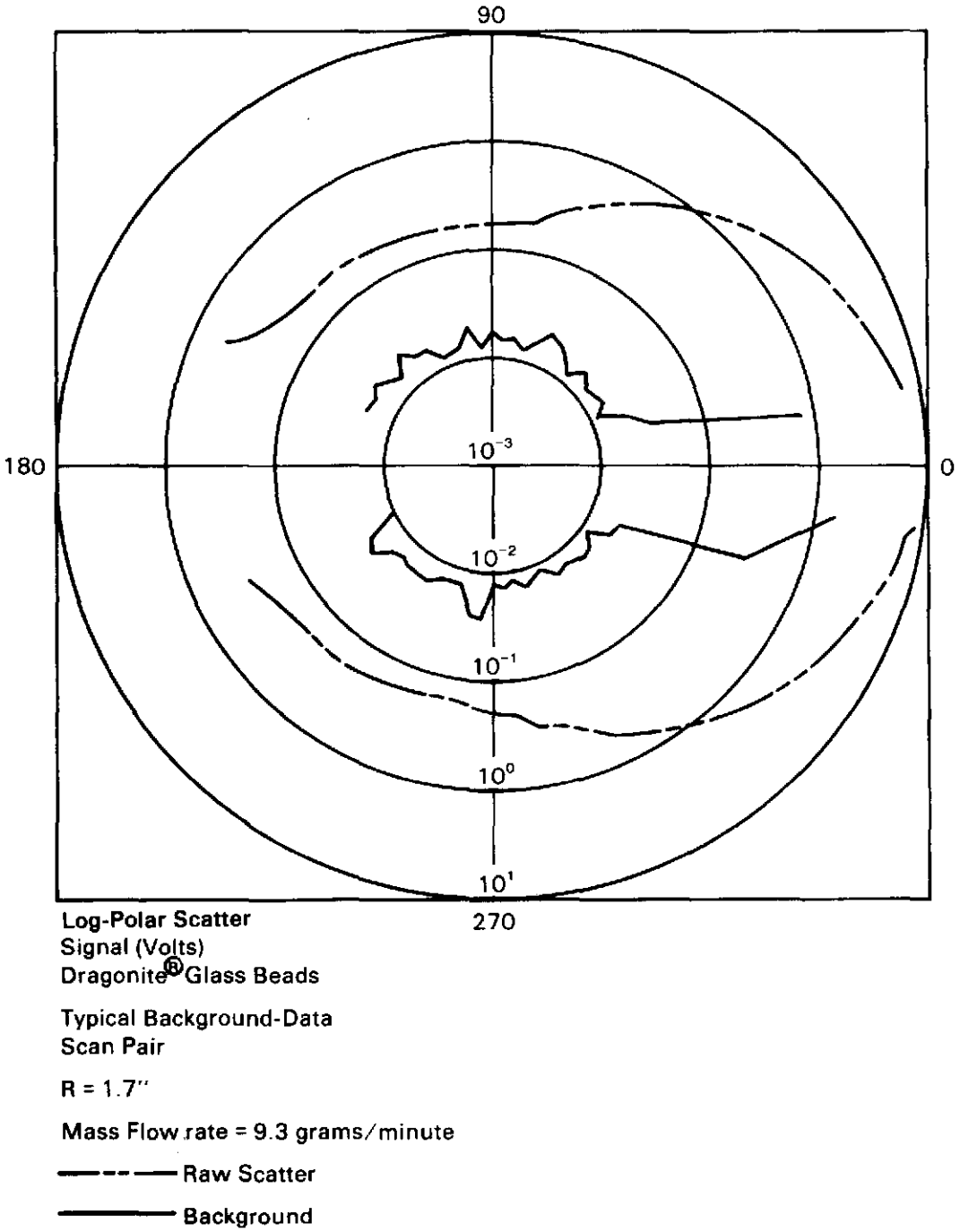

Figure 25. Log-polar plot of typical raw scattering data and background data obtained for Jaygo glass beads.

Measurements are taken at five-degree increments unless the detector is in the near specular region (10 degrees each side of the specular direction), at which point the increment size is reduced to one degree. At each measurement point the scatter signal voltage is read 50 times at 0.1 second intervals. If the standard deviation of the 50 readings is greater than an operator-input percent of the mean of the readings, the data-logging program rejects these readings and the process is repeated. This procedure results in an on-line "stability" test of the scattered light signal level. This stability test is not included in the data collection routine as a means of measuring only "quiet" signals for a given detector position. Rather, the test provides the controlling program with a means of determining whether or not the detector-lock-in combination has settled after the detector has moved to a new position and thus to a new signal level. For this reason, operator-input allowable percent variation is usually in the range of five to ten percent. Stabilities greater than this are not attainable due to the rapidly fluctuating scattered light levels caused by the varying number of particles falling through the illuminating beam.

The expression for the single-particle DSCS (Eq. 15) contains the variable N_A which is defined as the curtain areal particle density. To find N_A, strobe photography was used. Typical strobe photographs of the particle curtain for a range of flow rates appear in Figure 26. In the photos, the end of the curtain delivery chute appears at the top and the particle curtain can be seen dropping into the catch glass below. Superimposed on the particle curtain is the laser beam illumination spot which was traced out by the falling particles over a period of three to four seconds. Using this strobe technique, the number of particles

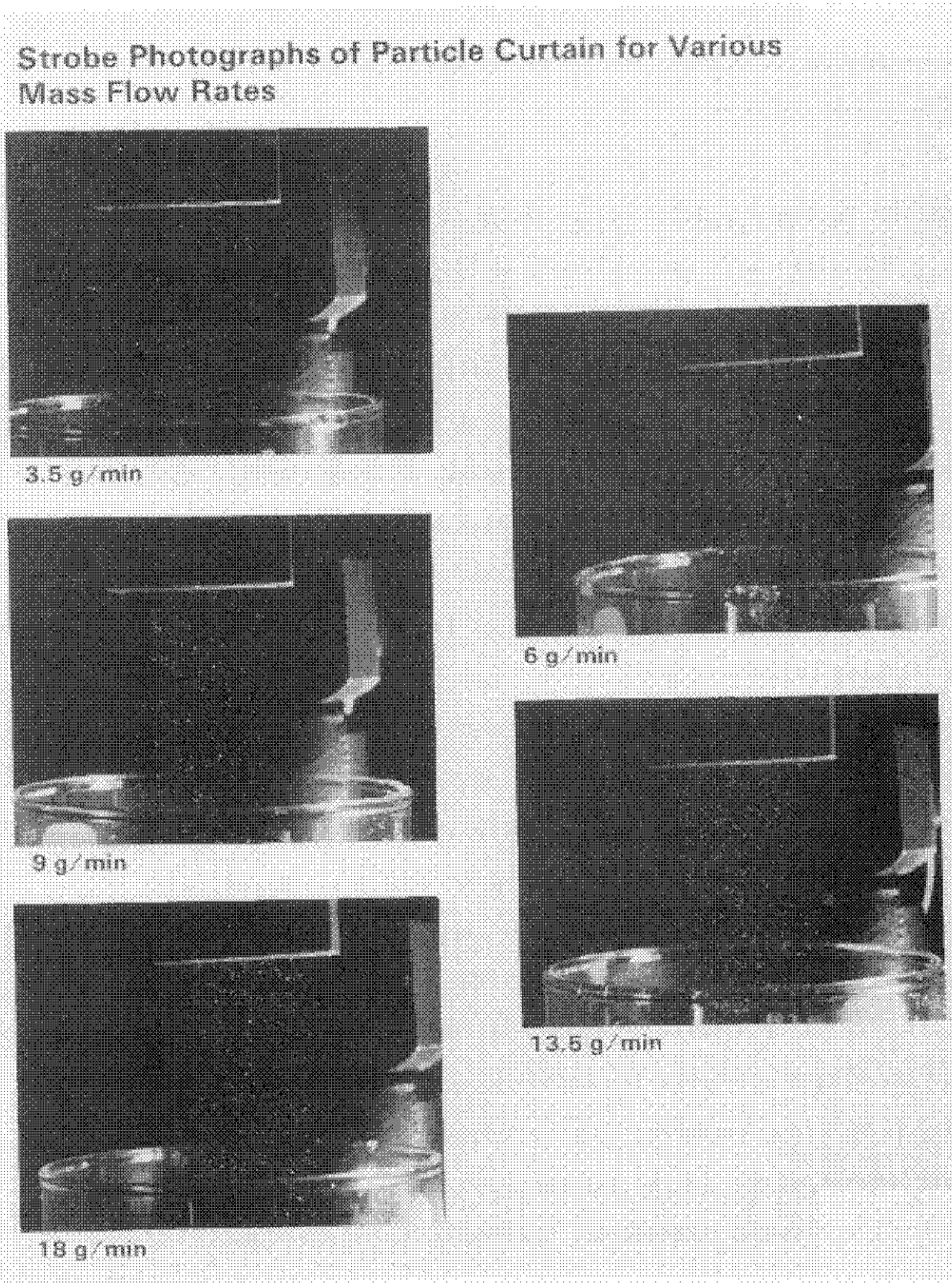

Figure 26. Strobe photographs of Jaygo glass bead curtain for mass flow rates from 3.5 g/min to 13.5 g/min.

contributing to the scatter signal at any time can be determined to a close approximation.

Angular Scattering Data - Glass Beads

The first material evaluated with the angular scatter instrument was 300 μm (nominal) diameter glass beads from Jaygo, Inc. The size distribution of a random sample of the glass beads is shown in Figure 27. These glass particles are a translucent and highly-spherical grinding media, and are composed primarily of SiO_2 with appreciable quantities of PbO, K_2O, Na_2O, and B_2O_3. The material was at no time considered a candidate for use in the solid particle receiver, but it served as a convenient and plentiful test material for initial trials of the angular scattering instrument and for testing predictive scattering codes contained in the radiative transfer model.

Since this work represents the only known experimental effort to obtain scattering properties for particles in this size range, there is no data base available in the literature with which to compare experimental results. Therefore, one must look for internal consistencies and reasonable physical results to build confidence in the data. First, since the particle curtain has a thickness of only one particle, there should be no multi-particle scattering effects except in the sidescatter direction, where scattered light reaching the detector must traverse numerous particles. Since the particle curtain undergoes some spreading in the front-to-rear direction, the region where sidescatter effects occur is uncertain, but is thought to be about three to five degrees on each side of the direct sidescatter direction ($\pm$ 90°). When multiple scattering does not occur, each particle in the illuminating beam should

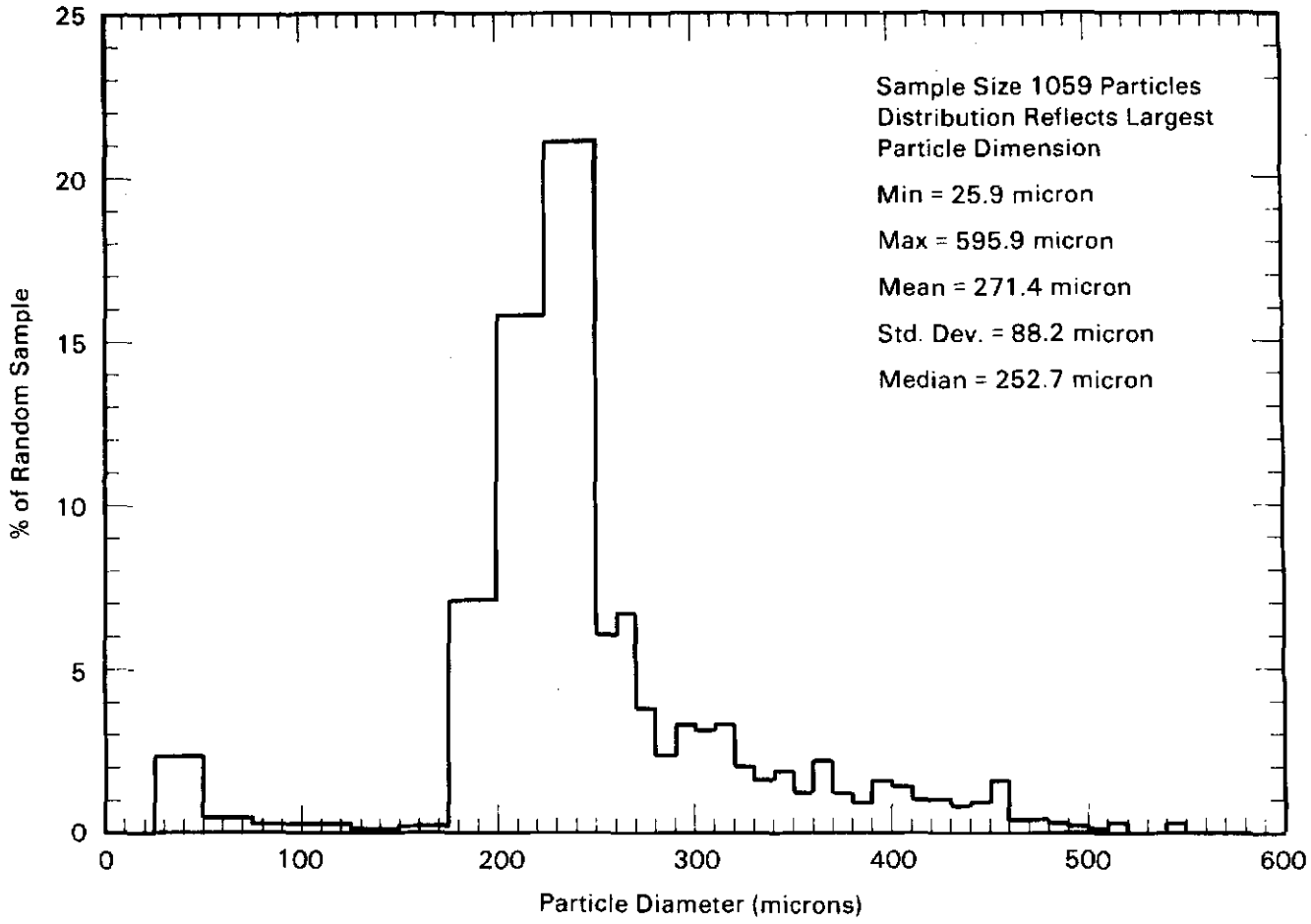

Figure 27. Particle size distribution measured for Jaygo glass beads.

act as a point scatterer, i.e., a point source. The intensity of light incident upon a detector at a distance R from a point source falls as the inverse of the square of the distance from the source to the detector so one expects the scattered light signal from the curtain at any angle (except those comprising the sidescatter region) to drop off as $1/R^2$. Figure 28 is a log-polar plot of three raw angular scatter data sets for glass particles, each having the same mass flow rate of approximately nine grams/minute (approximately 18 particles in the beam at any given time) but each with a different curtain-to-detector distance. The data show that the signals increase as R (curtain-to-detector distance) decreases. Since the DSCS includes the term $1/R^2$ (by definition $d\Omega$ = Area/R^2) and since the point source intensity falls as $1/R^2$, the DSCS for all three data sets should be independent of R. Figure 29 is a plot demonstrating that for all values of R, the DSCS is indeed virtually constant, confirming the expected point source behavior.

A second type of behavior one expects is that the angular scatter signal will scale linearly with mass flow rate since the number of particles in the illuminating beam is directly proportional to flow rate. Figure 30 shows three angular scatter data sets for the glass particles, each having the same R, but each with a different mass flow rate. The data show that the scatter signal increases with increasing mass flow rate. If one considers the DSCS for these data sets, the DSCS divided by the number of particles in the beam in each case should again ideally be identical. Figure 31 shows curtain DSCS divided by the number of particles in the beam (to give the single-particle DSCS) for each flow rate. The fact that all three data sets are virtually equal indicates that the experiment has again yielded physically reasonable results in

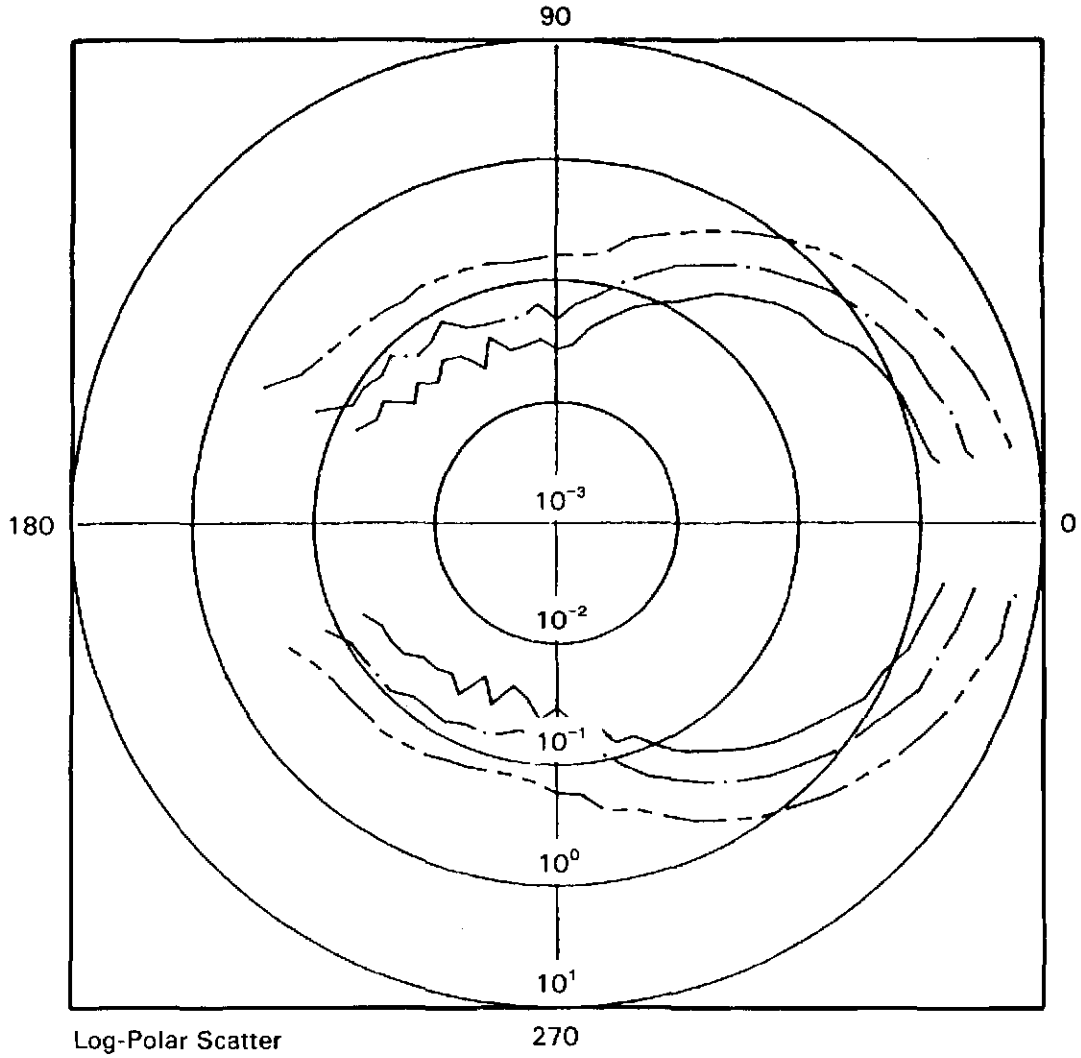

Figure 28. Log-polar plot of scattering data measured for Jaygo glass beads at a mass flow rate of 9.3 g/min and detector-particle distances of 43, 66, and 91 mm.

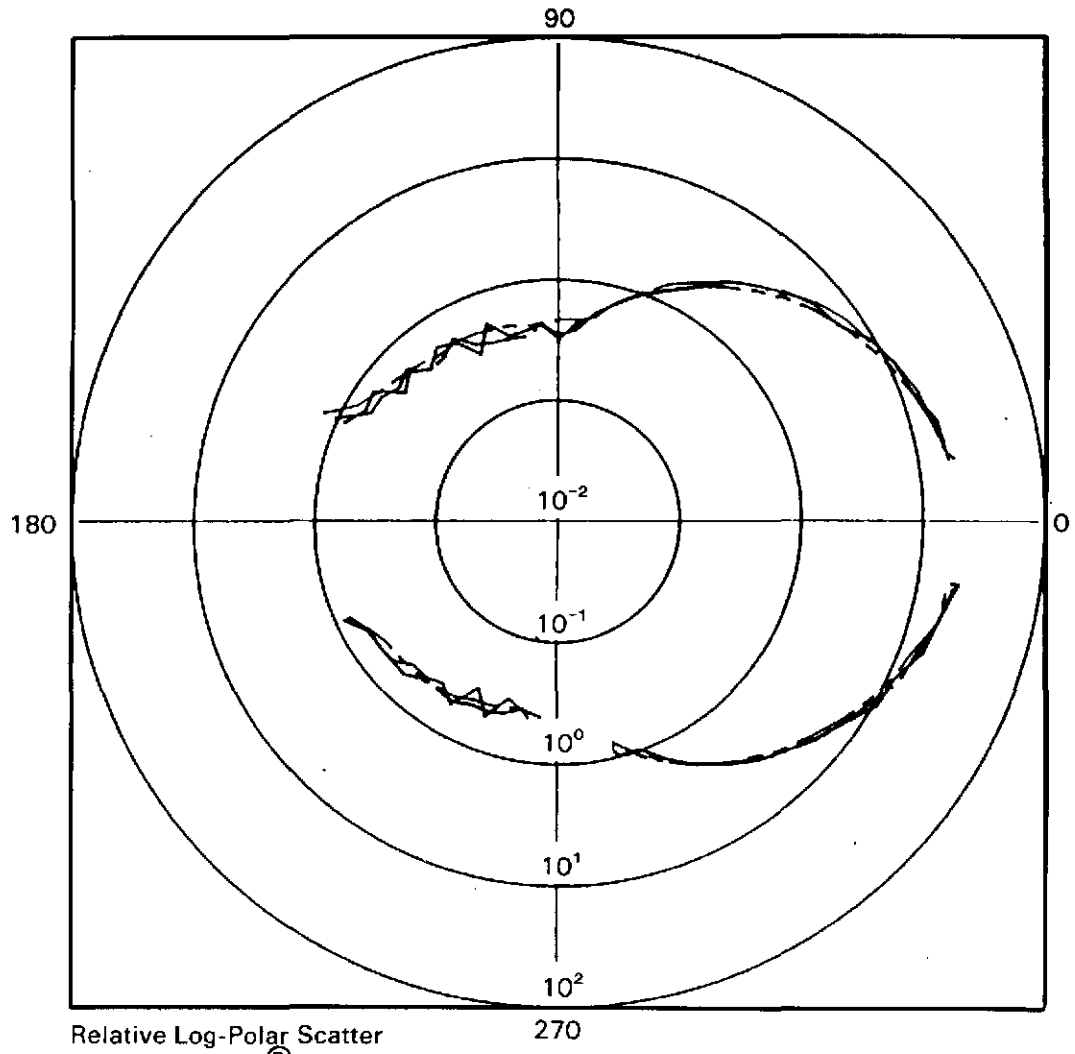

Figure 29. Log-polar plot of single-particle DSCS measured for Jaygo glass beads at a mass flow rate of 9.3 g/min and three different detector-particle distances.

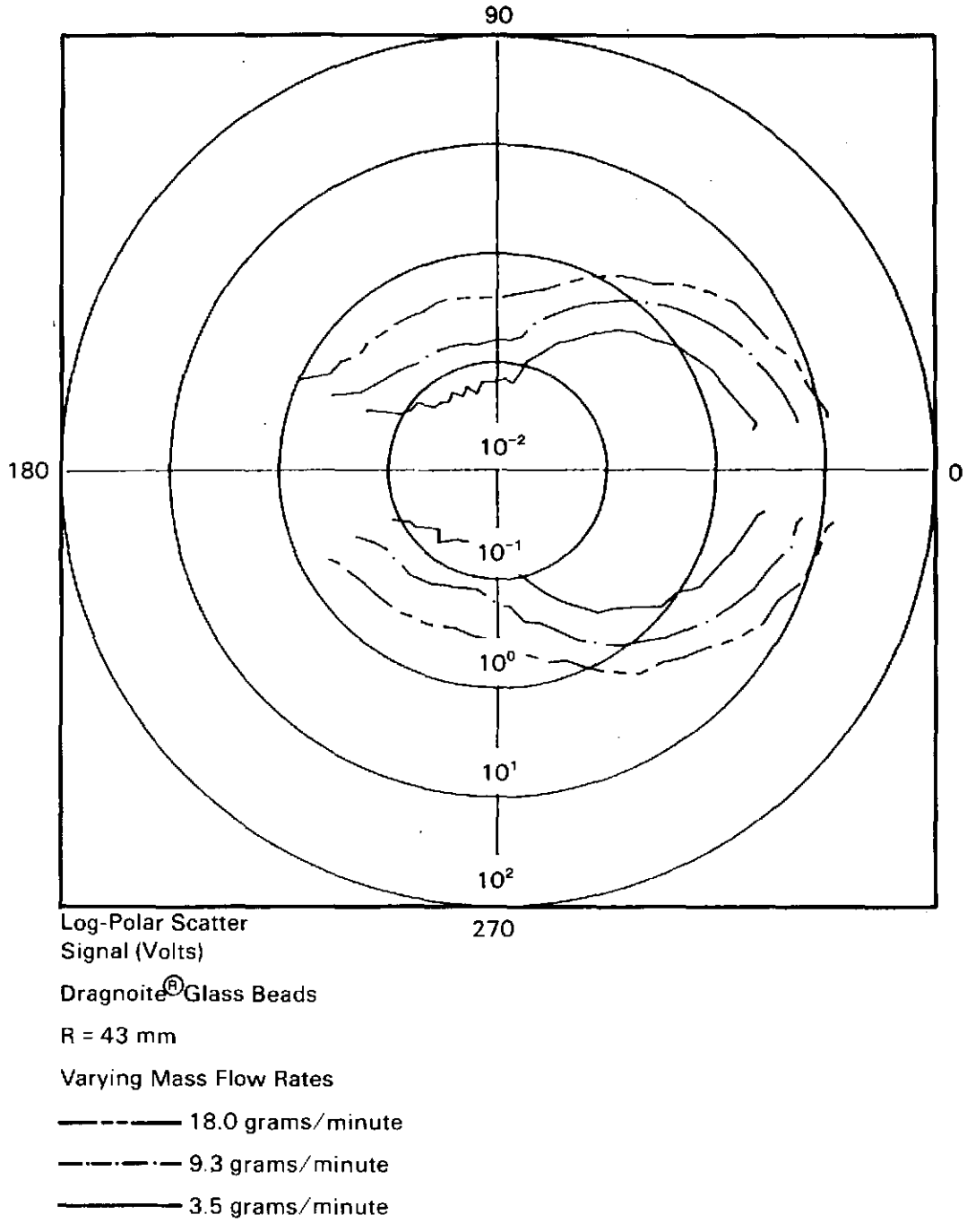

Figure 30. Log-polar plot of scattering data measured for Jaygo glass beads at mass flow rates of 18.0, 9.3 and 3.5 g/min at a detector-particle distance of 43 mm.

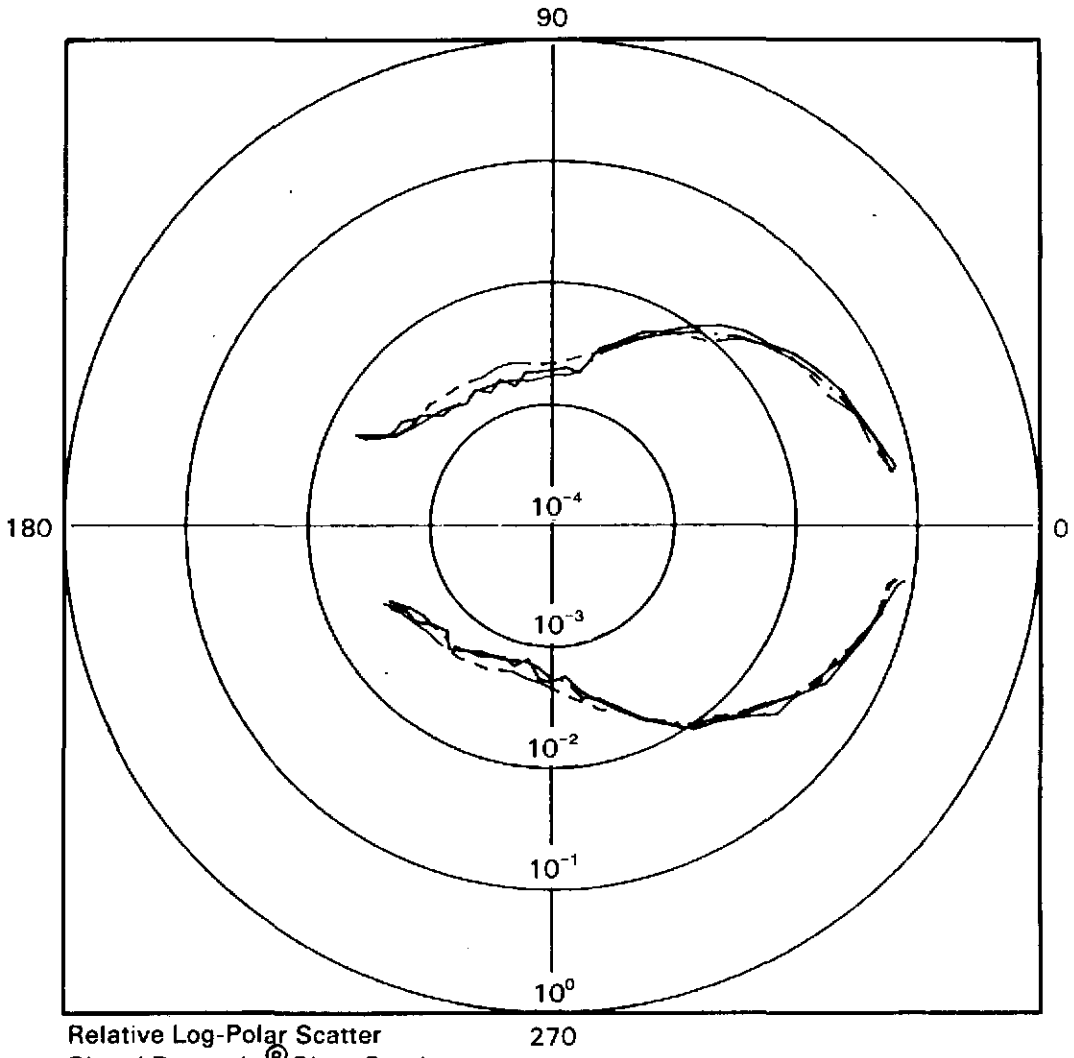

Figure 31. Log-polar plot of single-particle DSCS measured for Jaygo glass beads for three mass flow rates and a detector-particle distance of 43 mm.

that the scattered light scales linearly with mass flow rate. Having shown that the experimental angular scattering instrument yields consistent data, it can be utilized in the evaluation of the optical behavior of actual candidate solid particles.

Angular Scattering Data - Master Beads^{R}

Data have been obtained with the angular scatter system for the most promising solid particle receiver material, Master Beads^{R}. Nominal diameter of these particles is about 325 μm. The size distribution for a random sample of these Master Beads^{R} is shown in Figure 32. The measurements were performed in the same manner as that for the Jaygo glass beads. Figure 33 shows log-polar plots for Master Beads^{R} at three different flow rates and a fixed R. As in the case of the glass particles, the scattered light signal increases with increasing mass flow rates. Figure 34 shows the log-polar plot of single-particle DSCS for each of the three flow rates. Again the data for each mass flow rate are nearly equal. The data show an increased amount of randomness as compared to the glass bead scattering data. This can be attributed to the fact that the Master Beads^{R} are opaque and dark in color, which gives a much greater absorption and, therefore, much lower scattered light levels. For the very low flow rates, such as four grams/minute, the scatter signal levels are quite close to the background signal levels.

The most striking feature in these data can be emphasized through a comparison between the Master Bead^{R} data and the glass bead data. Figure 35 shows single-particle DSCS for both of these materials with the same R (43.2 mm) and very nearly the same mass flow rate (approximately 18

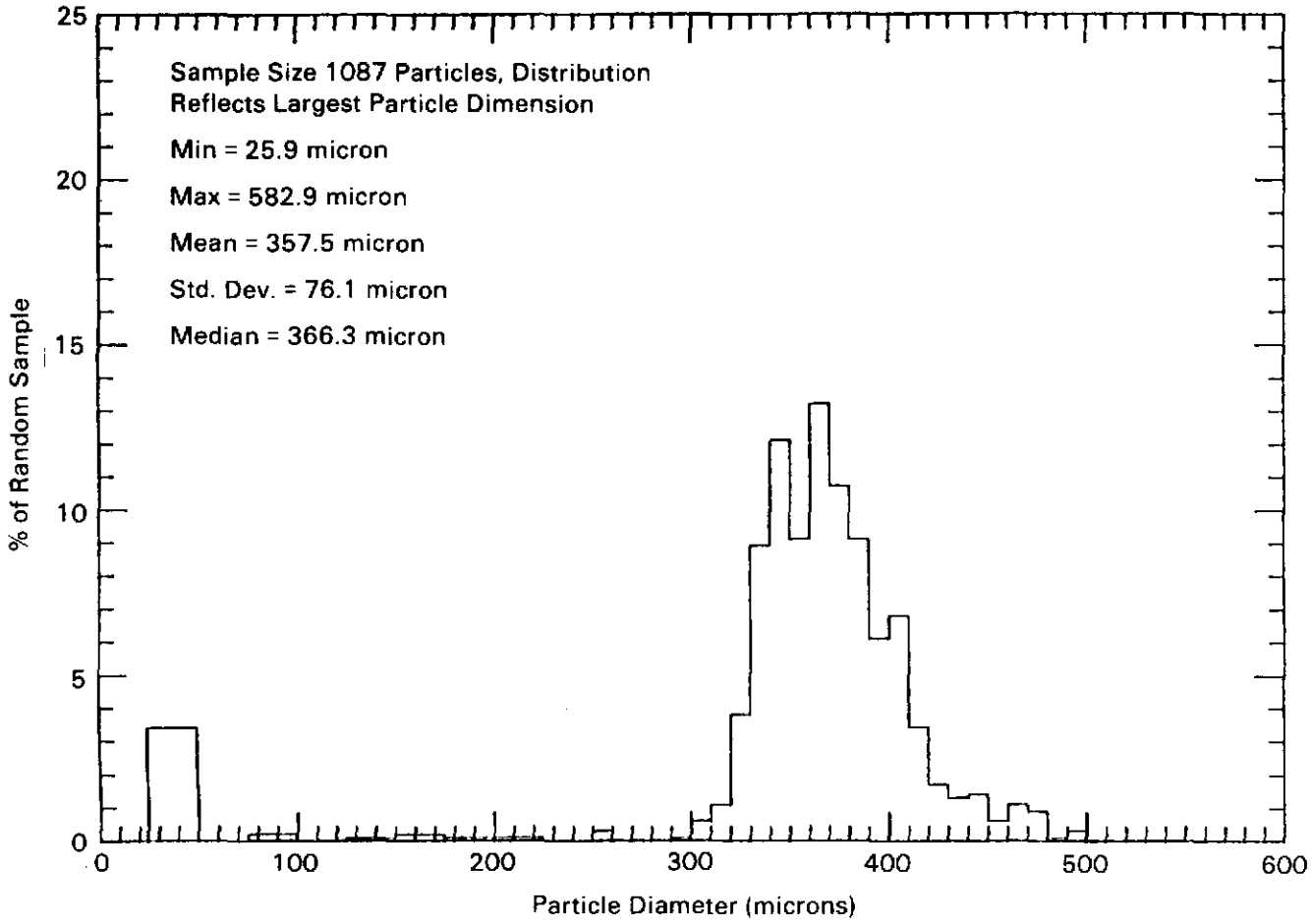

Figure 32. Particle size distribution measured for Master Beads[R].

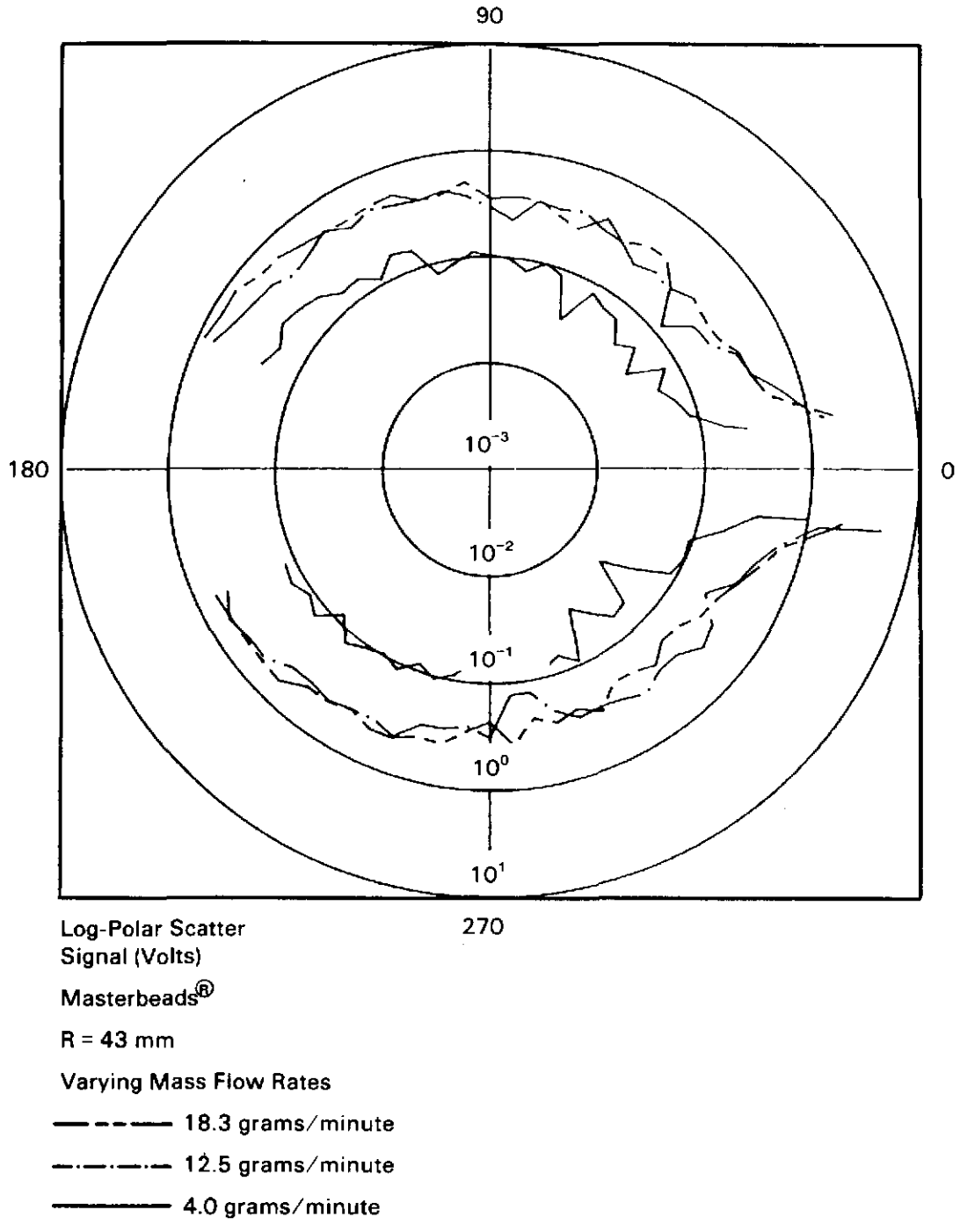

Figure 33. Log-polar plot of scattering data measured for Master Beads^{R} at mass flow rates of 18.3, 12.5, and 4.0 g/min and a detector-particle distance of 43 mm.

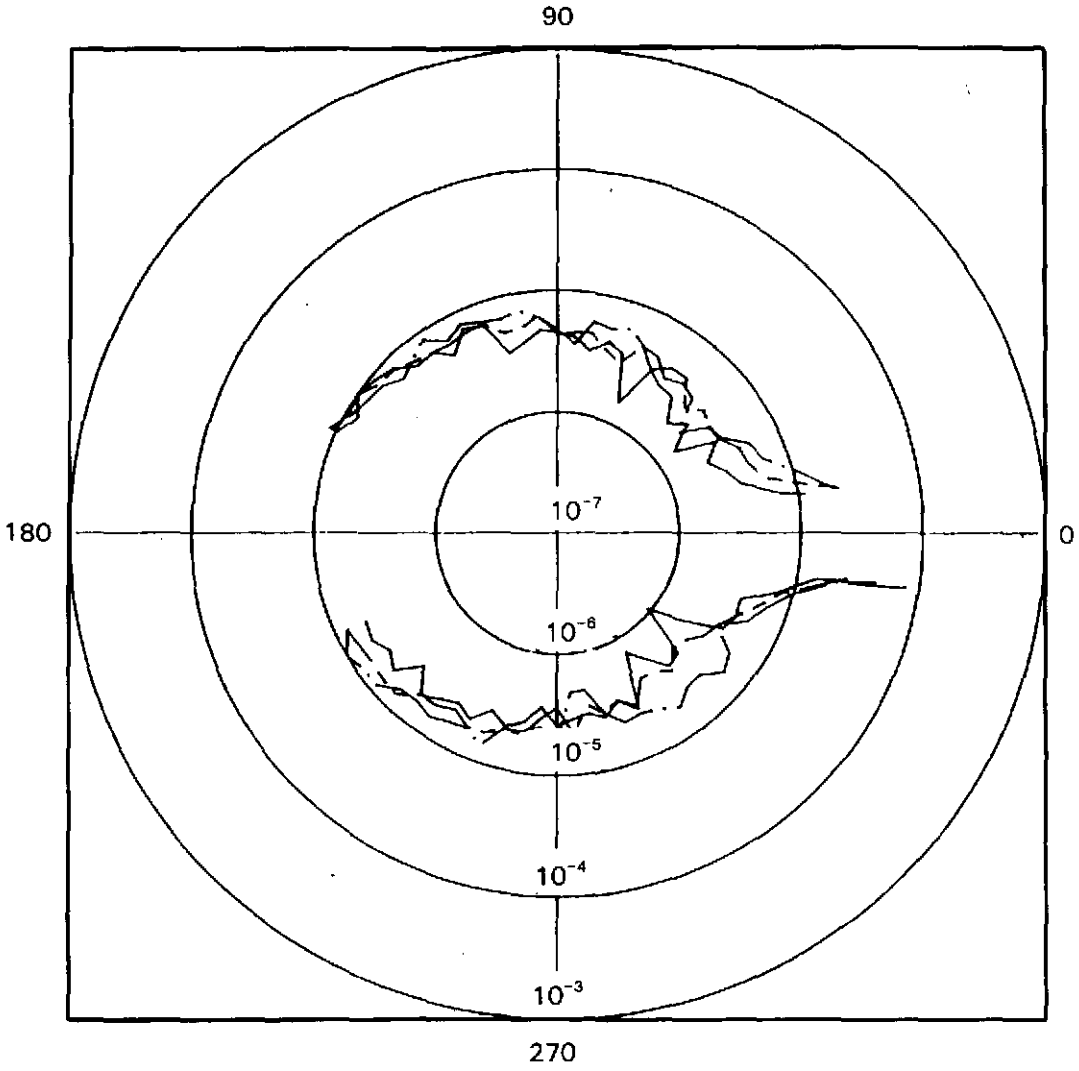

$$X(\Theta) = \frac{1}{N_A} \frac{W_D(\Theta)}{W_o} \frac{1}{A_D/R^2}$$

Average Single-Particle Differential Scattering Cross Section for Masterbeads® (cm^2)

R = 43 mm

Varying Mass Flow Rates

——— 18.3 grams/minute

·—·—· 12.5 grams/minute

——— 4.0 grams/minute

Figure 34. Log-polar plot of single-particle DSCS measured for Master Beads^R for three mass flow rates and a detector-particle distance of 43 mm.

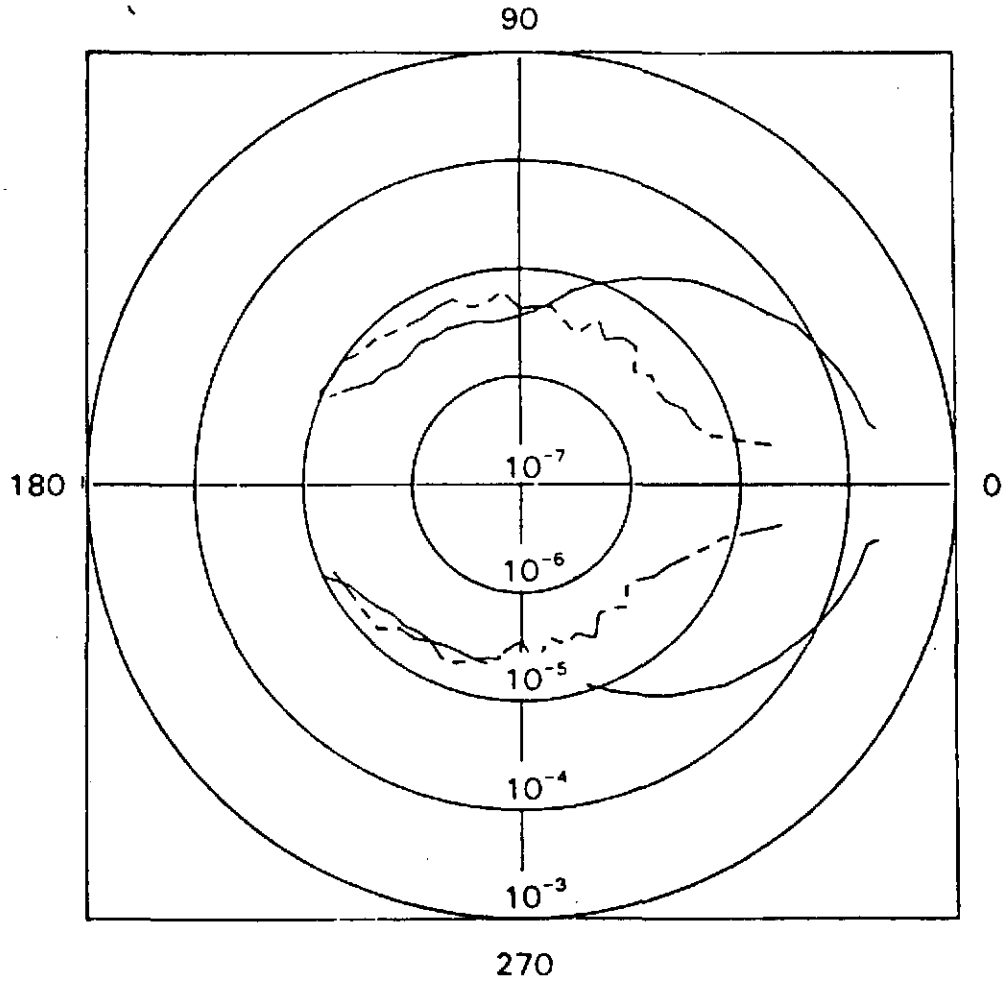

Figure 35. Log-polar plot of single-particle DSCS for Master Beads® and Jaygo glass beads.

grams/minute or approximately 30 particles/cm^2). Note that the single-particle DSCS is independent of R and mass flow rate, so the R and flow rate used to make this comparison is actually inconsequential. The magnitude of the forward-scattered light is much greater for the glass beads than for the Master Beads^R. This can be expected on physical grounds since the glass particles are highly transparent. That is, a large portion of the light incident upon the glass particles will be transmitted through the particle and detected as forward-scattered light. The highly absorbing Master Beads^R allow no transmission of incident light and therefore have no transmitted light contribution to forward scatter. This comparison conveys the dramatic effect that particulate optical absorptance can have on the scattered flux profile within the solid particle receiver absorbing curtain volume.

V. MEASUREMENT OF OPTICAL EXTINCTION

In the previously described angular scattering measurements, the concern was with the angular disposition of particle-scattered radiation. In this discussion, the contributions of optical absorption and optical scattering to the extinction of light propagating through a curtain of falling particles will be addressed.

Motivation of Extinction Measurement

The model of Houf et al. [4] for prediction of the performance of a solid particle receiver accounts for the optical properties of the particulate material via a term designated as the single-particle scattering albedo given by

$$w_\lambda = \frac{\sigma_\lambda}{\sigma_\lambda + \kappa_\lambda} = \frac{\sigma_\lambda}{\beta_\lambda} \tag{16}$$

where κ_λ is the spectral absorption coefficient (cm^{-1}), σ_λ is the spectral scattering coefficient (cm^{-1}) and β_λ is termed the spectral extinction coefficient (cm^{-1}). Note that the scattering albedo, w, assumes a value of unity for a purely scattering particle and a value of zero for purely absorbing particles and that it is wavelength dependent. This formalism assumes that monochromatic light propagation in a slab of particles can be described by

$$I(x) = I_0 \, e^{-\beta x} \tag{17}$$

where I_0 is the incident intensity at the front boundary of the slab and I(x) is the intensity measured at depth x into the curtain (both of wavelength λ). The geometry is illustrated in Figure 36. The optical extinction coefficient is a relatively easy variable to measure experimentally. One measures I_0 and I(x) at some position in (or preferably on the other side of) the curtain with detectors of equal sensitivity and surface area (preferably the same detector). Care must be taken in this measurement as discussed in reference 9. The extinction coefficient is then given by

$$\beta = \frac{-1}{x} \ln \left[\frac{I(x)}{I_0} \right] \tag{18}$$

The shortcoming of this straight-forward measurement is that it gives no information as to the disposition of the lost optical energy, i.e., was

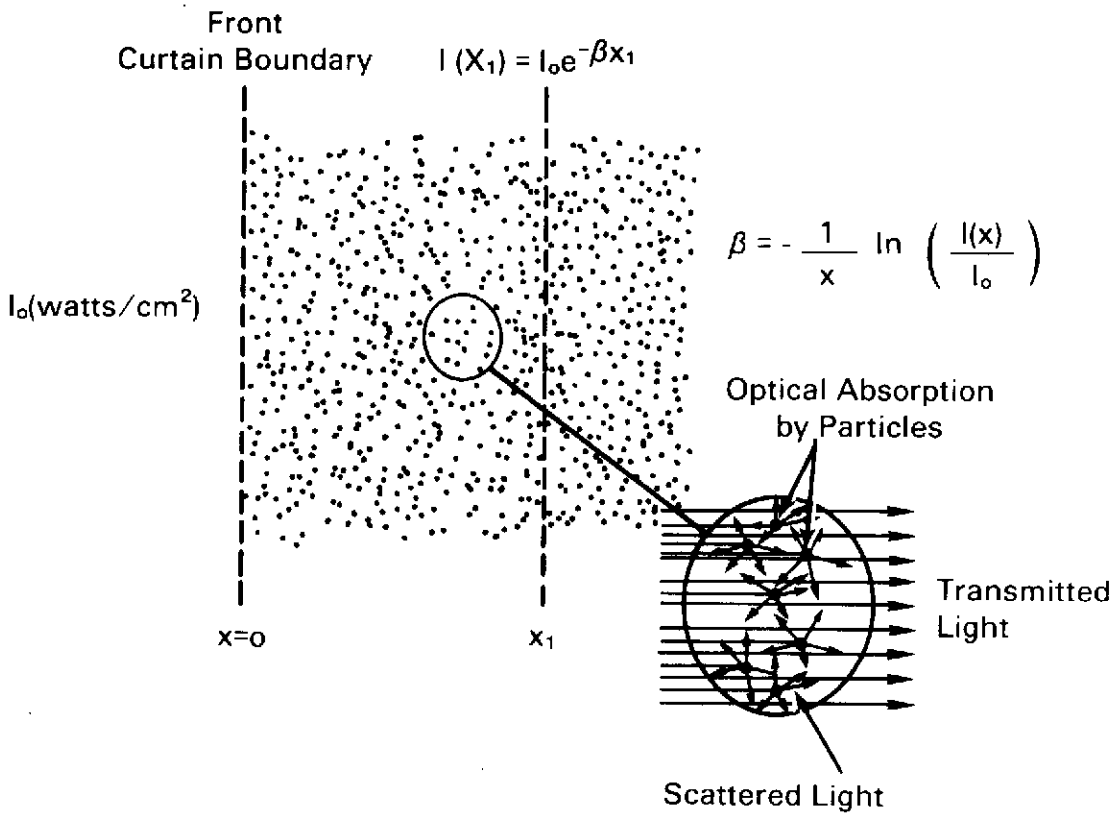

Figure 36. Schematic diagram showing the nomenclature used to defin the optical extinction coefficient (β) of a particle curtain.

it scattered out of the detector field of view or absorbed? Since the ultimate objective of the solid particle receiver is to perform efficient conversion of solar radiation to thermal energy, the contribution of optical absorption to the total extinction coefficient is especially important. Likewise, the degree of optical scattering indicated by the scattering part of the extinction coefficient is crucial for determination of available optical energy density (over all angular directions) within the curtain volume.

The objective of the experimental extinction measurements performed to date has been to identify the relative contributions of the scattering and absorption mechanisms to the total extinction coefficient to enable calculation of the scattering albedo, w. The nomenclature for the following discussion is presented in Figure 37. Once again, the power incident on the particle is denoted P_0. After the interaction the scattered, absorbed, and transmitted portions of the optical radiation are designated P_S, P_A, and P_T respectively. Since the particles of current interest are optically opaque, P_T is essentially zero. The single-particle scattering cross section is defined as P_S/P_0 (note that P_S is the sum of optical power scattered into all directions) and is designated C_{Sca}. Likewise, the single-particle absorption cross section will be defined as P_A/P_0 and designated C_{Abs}.

Since the procedure used to acquire the extinction data is specific to the experimental apparatus, a brief discussion of the measurement system is in order. The extinction apparatus is depicted schematically in Figure 38. In the integrating sphere geometry, the total incident power is measured without particle flow (i.e., no curtain) by placing a

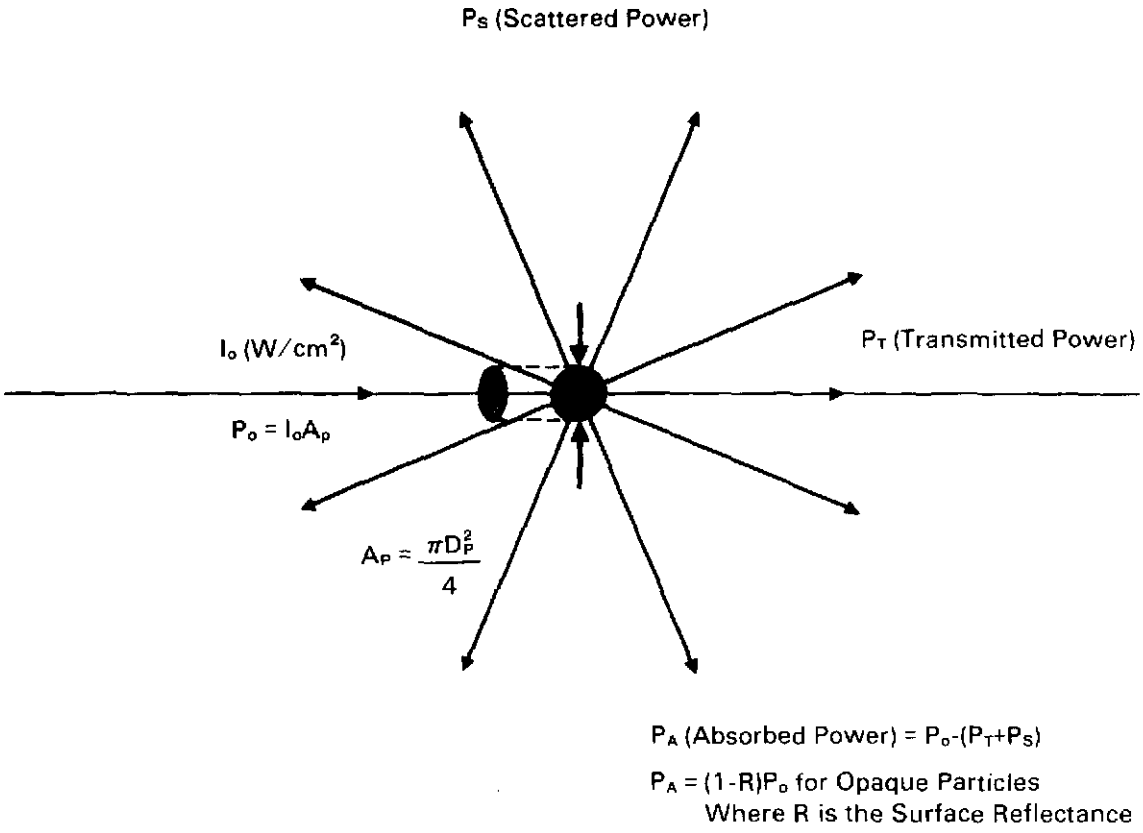

Figure 37. Diagram showing the nomenclature used for the single-particle scattering albedo.

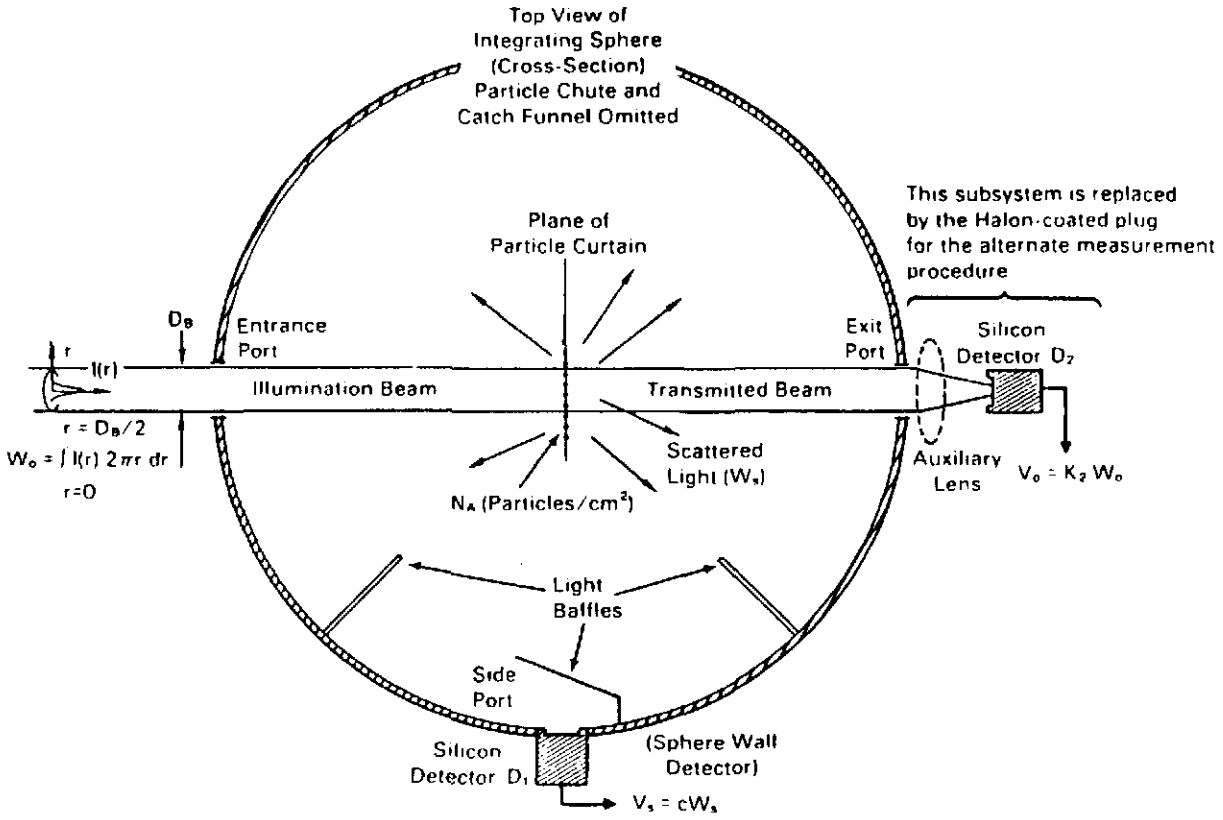

Figure 38. Schematic diagram of the integrating sphere used for the albedo measurements showing the location of the illumination beam, particle curtain, and silicon detectors D_1 and D_2.

detector outside of the exit port which intercepts the entire beam. The voltage signal of this detector is proportional to W_0 which is given by

$$W_0 = \int_0^{D_B/2} I(r)\ 2\pi r\ dr \tag{19}$$

where D_B is the beam diameter. The total scattered power, W_S, for the entire illuminated curtain area is given by

$$W_S = \int_0^{D_B/2} I(r)\ \bar{C}_{Sca}\ N_A\ 2\pi r\ dr = \bar{C}_{Sca}\ N_A\ W_0 \tag{20}$$

where $\bar{C}_{Sca}$ is the average single-particle scattering cross section. A silicon detector mounted in the integrating sphere wall will give a signal proportional to W_S, i.e.,

$$V_S = c\ W_S \tag{21}$$

where V_S is the detector/pre-amplifier voltage output and the constant, c (integrating sphere efficiency), accounts for the fraction of scattered radiation that is collected by the sphere and detected. Likewise, the total absorbed power is given by

$$W_A = \int_0^{D_B/2} I(r)\ \bar{C}_{Abs}\ N_A\ 2\pi r\ dr = \bar{C}_{Abs}\ N_A\ W_0 \tag{22}$$

It is important to note here that the illumination beam geometry is not important since the magnitudes of both the scattering and absorption signals are dependent upon the total beam power.

The average single-particle scattering cross section can be calculated from the ratio

$$\frac{W_S}{W_0} = \bar{C}_{Sca} N_A \tag{23}$$

or

$$\bar{C}_{Sca} = \frac{1}{N_A} \left[\frac{W_S}{W_0}\right] \tag{24}$$

There is an experimental difficulty encountered in forming this ratio which warrants discussion. Consider the voltages produced by the sphere wall detector, V_S, and the beam power monitor detector, V_0. They are related to the actual optical power, W_S and W_0, by

$$V_S = c W_S \tag{25}$$

and

$$V_0 = k_2 W_0 \tag{26}$$

where c has been previously defined. The monochromatic detector responsivity for the beam power monitor detector/pre-amplifier is denoted

by k_2 (volts/watt). Determination of k_2 is straightforward using an absolute power meter to measure the true illumination beam power. Likewise, c can be determined by placing a highly scattering, non-absorbing material (e.g., transparent glass beads) in the beam path (beam power, W_0 measured a priori) at the same position that the particle curtain will occupy. This is a crucial point since, for this complex integrating sphere geometry (Figure 39), the responsivity is likely to be a strong function of source position. It is also important that the scattering standard produce complete beam extinction (i.e., no beam transmission to the exit port) so that all of the illumination power can be accounted for. Since all that is required for the calculation of $\bar{C}_{Sca}$ from Eq. 24 is the following ratio (if N_A is known)

$$\frac{W_S}{W_0} = \frac{V_S/c}{V_0/k_2} = \frac{k_2}{c} \quad \frac{V_S}{V_0} \tag{27}$$

then the calibration procedure only needs to calculate the ratio k_2/c. This can be performed in a very straightforward manner by using the same beam power W_0 and measuring the respective detector voltages with (V'_{Ref}) and without (V'_0) the reference scatterer in the beam path. Then

$$V'_{Ref} = c\, W_0 \tag{28}$$

and

$$V'_0 = k_2\, W_0 \tag{29}$$

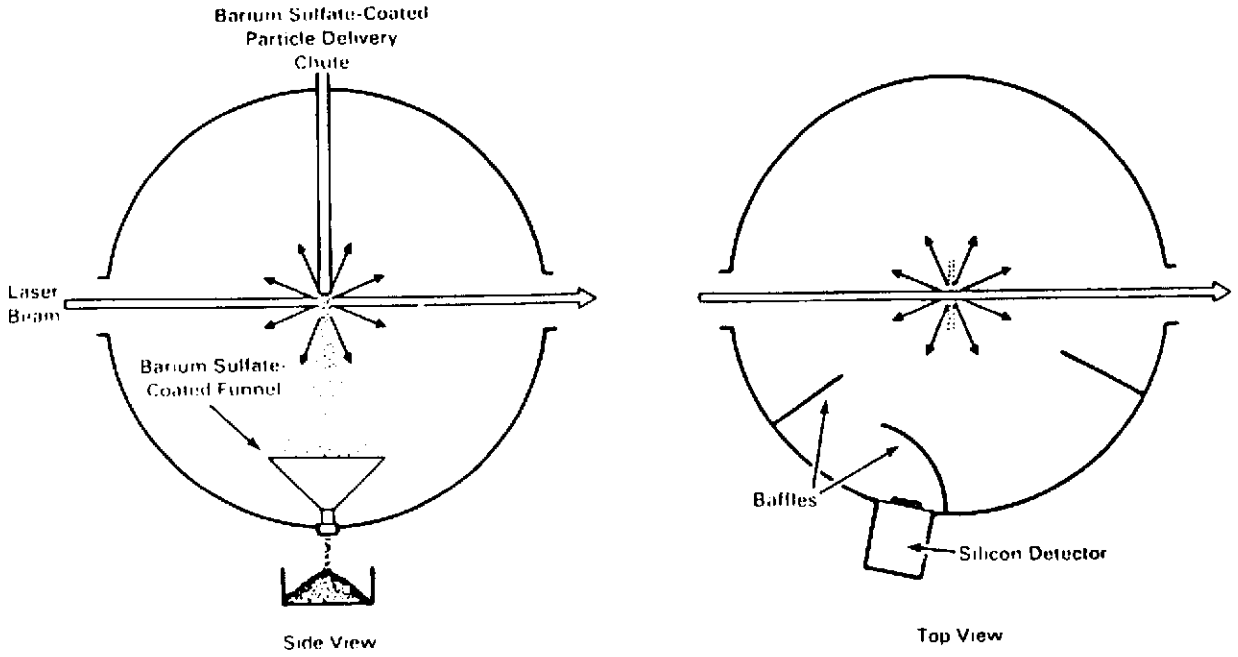

Figure 39. Schematic diagram showing the location of the collection funnel and detector baffles within the integrating sphere.

so that

$$\frac{k_2}{c} = \frac{V_0'}{V_{Ref}'} \quad . \tag{30}$$

Once this calibration factor is established, actual measurements may be performed on the particle curtain. All that remains for the determination of $\bar{C}_{Sca}$ is a photographic measurement of the curtain particle density, N_A (number of particles/cm^2).

Extinction Measurement Technique

The measurement of the average single-particle absorption cross section can be accomplished in two ways. These two data acquisition algorithms are sufficiently different to warrant detailed discussions. The first method assumes that a measurement of W_S has previously been made or that $\bar{C}_{Sca}$ is already known (note that W_S, $\bar{C}_{Sca}$, and W_A measurements should be made for identical curtain geometry, flow rate, and particle density). Assuming that the particles are opaque (e.g., Master Beads^R), the transmitted beam power W_T will be

$$W_T = W_0 - (W_S + W_A) \tag{31}$$

or dividing by W_0 and rearranging, we have

$$\frac{W_A}{W_0} = 1 - \left[\frac{W_T}{W_0}\right] - \left[\frac{W_S}{W_0}\right] \quad . \tag{32}$$

Recalling

$$\frac{W_A}{W_0} = \bar{C}_{Abs} N_A \tag{33}$$

then

$$\bar{C}_{Abs} = \frac{1}{N_A} \frac{W_A}{W_0} . \tag{34}$$

So, assuming W_S/W_0 (or $\bar{C}_{Sca}$, A_P, and N_A) has already been determined, then the average single-particle absorption cross section can be obtained from Eq. 32 and 34 by measuring the ratio of transmitted to illumination beam power at the output port. This is easily done by simply measuring the detector voltage first with no curtain flow and then again with curtain flow. Since the same detector is used, the absolute monochromatic responsivity need not be determined.

Assuming that the single-particle scattering albedo (Eq. 16) can be expressed as

$$w = \frac{\bar{C}_{Sca}}{\bar{C}_{Sca} + \bar{C}_{Abs}} \tag{35}$$

where the subscript λ has been dropped since all variables are understood to be monochromatic. Then combining Eq. 24 and 34, we have

$$w = \frac{W_S}{W_A + W_S} . \tag{36}$$

But from Eq. 31 we have

$$W_A = W_0 - W_T - W_S \quad . \tag{37}$$

So Eq. 36 can be rewritten as

$$w = \frac{W_S}{W_0 - W_T} \quad . \tag{38}$$

The numerator in the above expression is the optical power scattered by the curtain and is measured by the sphere wall-mounted detector. Recall that the voltage output of this detector as a function of scattered power is given by

$$V_S = c \; W_S \quad . \tag{39}$$

The optical power in the denominator of Eq. 38, W_0 and W_T, is determined by the same detector and the corresponding voltages are respectively

$$V_0 = k_2 \; W_0 \quad \text{and} \tag{40}$$

$$V_T = k_2 \; W_T \quad . \tag{41}$$

Eq. 38 can now be written as

$$w = \left[\frac{k_2}{c}\right] \left[\frac{V_S}{V_0 - V_T}\right] \tag{42}$$

so that w can be calculated from readily measurable voltages. Note that it is assumed that all voltages used are corrected for signals resulting from background noise and detector dark voltages. The multiplication

factor (k_2/c) can be determined from the calibration procedure described earlier. The advantage to this method is that it provides experimental values for the desired variable, the single-particle scattering albedo, without requiring detailed information pertaining to the curtain geometry (e.g., particle density and particle size).

Alternative Method for Absorption Cross Section

An alternative method exists for determination of the average single-particle absorption cross section. While the technique appears to be very sensitive to integrating sphere geometry, it warrants discussion here because it may prove useful for some types of particles. In this method, the sphere wall detector is used to measure both W_0 and W_S in order to determine W_A and subsequently $\bar{C}_{Abs}$. If the output port detector in Figure 38 is replaced by a high diffuse reflectance plug (e.g., a metal disk coated with Halon or $BaSO_4$), the sphere wall detector will output a voltage (no curtain flow) V_{W_o} given by

$$V_{W_o} = c' W_0 \tag{43}$$

where c' is a constant which accounts for integrating sphere optical and geometry effects and detector monochromatic responsivity. Note that this voltage signal arises from intense optical scattering at the back wall of the sphere (i.e., on the plug). If the particle curtain is flowing, the detector will register a new voltage $V_{Curtain}$. This voltage will be proportional to the sum of scattering intensity contributions from the back wall plug, V'_{W_o}, and the particle curtain, V_S, or

$$V_{Curtain} = \underbrace{c\ W_S}_{V_S} + \underbrace{c'\ W_0'}_{V_{Wo}'} \qquad (44)$$

where W_0' is the modified optical power on the plug due to curtain attenuation. But

$$W_0' = W_0 - (W_S + W_A) \qquad (45)$$

so

$$\frac{V_{Curtain}}{V_{Wo}} = \frac{c\ W_S}{c'W_0} + \frac{c'\ [\ W_0 - W_S - W_A]}{c'\ W_0} \qquad (46)$$

or

$$\frac{V_{Curtain}}{V_{Wo}} = \frac{c\ W_S}{c'W_0} + \left[\ 1 - \left(\frac{W_S}{W_0} + \frac{W_A}{W_0}\right)\right] . \qquad (47)$$

Rearranging, we have

$$\frac{W_A}{W_0} = \frac{c\ W_S}{c'W_0} + \left[\ 1 - \left(\frac{W_S}{W_0} - \frac{V_{Curtain}}{V_{Wo}}\right)\right] . \qquad (48)$$

Recalling that

$$\frac{W_A}{W_0} = \bar{C}_{Abs}\ N_A \qquad (49)$$

we have, finally,

$$\bar{C}_{Abs} = \frac{1}{N_A}\left[\left(\frac{c}{c'} - 1\right)\frac{W_S}{W_0} - \frac{V_{Curtain}}{V_{Wo}} + 1\right] \qquad (50)$$

where W_S/W_0 is presumed known from a previous measurement.

The difficulty with this method lies in the determination of the term c/c'. Recall that this term is essentially the ratio of integrating sphere efficiencies at two positions in the sphere -- the back wall (coated plug) and the sphere center (where the illumination beam intersects the particle curtain). Efficiency in this context refers to the optical intensity at the wall-mounted detector per unit of optical energy scattered by 1) the output port plug, or 2) the particle curtain. In the first case, the intense illumination beam illuminates a small area on the sphere wall (the plug) and scatters essentially all of the light (diffuse reflectance ≈ 0.98) isotropically over 2π steradians. In the latter case, there is still a very large contribution from the back wall but there is also a significant scattering contribution from the falling particles at the sphere center which is not isotropic over the 4π steradian scattering angle. Since the sphere geometry is significantly encumbered by the particle chute and collection funnel, it is anticipated that equal optical power scattered from these two regions in the sphere will not result in equal intensities at the detector. Consequently, there is a need to perform a calibration to determine the ratio of sphere efficiencies at these two positions. This can be accomplished in the following manner.

A non-absorbing scattering standard should be prepared with a geometry similar to the actual particle curtain (i.e., a slab). This

scattering reference should be of sufficient thickness so as to prevent any portion of the illumination beam from reaching the back plug. This standard could be most easily prepared by filling a high-grade quartz curvette with transparent glass beads. With the standard removed from the sphere, record the signal level (from the wall-mounted detector) with the illumination beam incident on the Halon-coated plug. Designate this voltage signal V_0. Next, with the scattering reference inserted in the sphere at the curtain position, record the corresponding detector voltage, designated V_1. If the two voltage values differ, it is indicative of geometry effects contributing to the sphere efficiency. If there is no signal variation, a calibration is not necessary and the ratio c/c' in Eq. 50 equals unity in which case

$$\bar{C}_{Abs} = \frac{1}{N_A}\left[\, 1 - \frac{V_{Curtain}}{V_{Wo}} \,\right] . \qquad (51)$$

If a variation in detected signal levels is present, then the ratio c/c' is not unity and is given by

$$\frac{c}{c'} = \frac{V_1}{V_0} . \qquad (52)$$

Eq. 50 can then be used to calculate $\bar{C}_{Abs}$.

Extinction Measurement Instrumentation

The experimental system assembled for these measurements appears in Figures 40 and 41. The system consists of a particle curtain generator provided by Prescott and Steele,[7] an integrating sphere, and the necessary optics and associated electronics. In this experiment, the

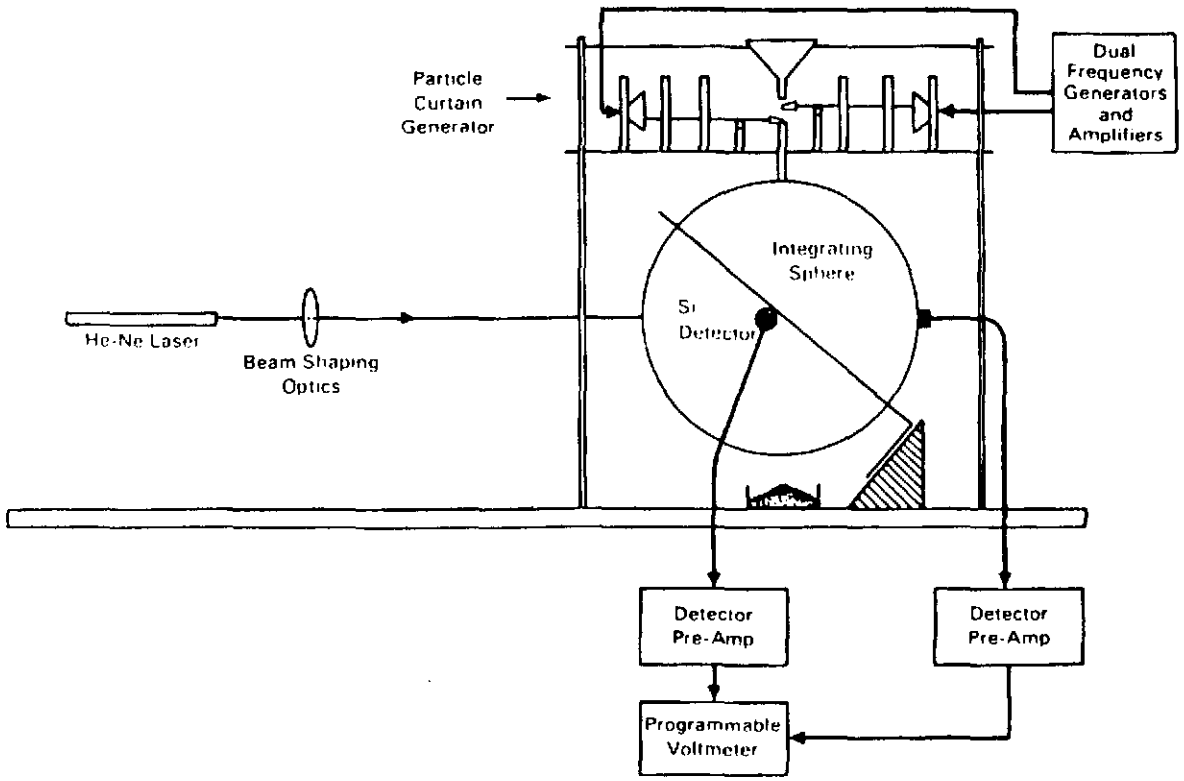

Figure 40. Schematic diagram of the single-particle extinction measurement equipment showing the incident beam, integrating sphere, particle curtain generator, and silicon detector.

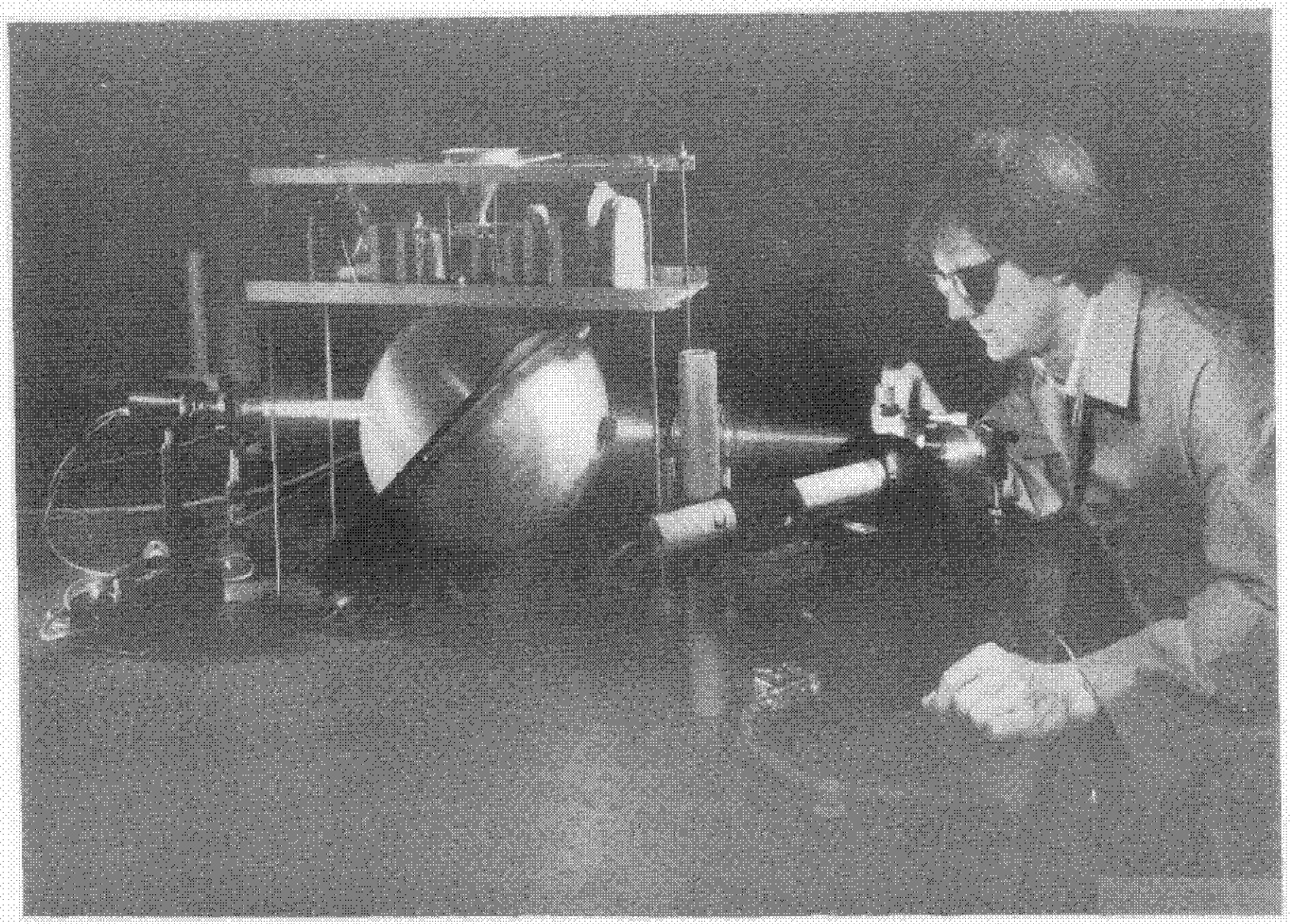

Figure 41. Photograph of the single-particle extinction measurement equipment.

illuminating laser beam impinges upon the single-particle-thick particle curtain, scattering light in all directions. The geometry of the system is such that the interactions between laser beam and particle curtain occur in the interior of the 30.5 cm (12 inch) diameter integrating sphere. The integrating sphere captures and distributes all light uniformly upon its interior regardless of the direction from which the light originates. The light intensity at the sphere wall may then be measured with a detector placed in the side of the sphere. A detector may also be placed at the sphere beam exit port to measure transmitted beam intensity directly. The particle curtain generator is essentially an exact copy of the generator used for the angular scattering system and will therefore not be described further. Referring to Figure 41, the curtain generator delivery chute releases the particle curtain at a point just above the illuminating laser beam, which passes through the center of the integrating sphere. The curtain is collected by a funnel mounted on the interior of the sphere, and then flows out to a catch glass below. In an attempt to preserve the optical integration property of the integrating sphere, the funnel and delivery chute are coated with barium sulfate. Barium sulfate-coated baffles are strategically placed in the sphere so that the detector may not look directly at the particle curtain or laser beam entrance/exit ports. In the absence of these baffles, the detector would not sample the average intensity at the sphere wall, but would instead measure the average wall intensity plus some scattered light coming directly from the particle curtain and/or the entrance/exit ports, giving erroneous results.

A diagram of the optical system and detection system is shown in Figure 42. The illuminating source was a 4 mW He/Ne laser (Spectra-Physics #102) which is chopped by a rotary chopper (PARC #192) operating at about 1 kHz. The chopped beam is spatially filtered (NRC #400 10X25 ξm filter) and recollimated before insertion into the integrating sphere. The final laser beam diameter was about 8 mm. The detectors used were silicon photodetectors (EG&G #UV444) amplified by a precision two-stage pre-amplifier [8]. The signals from the detector pre-amplifier are demodulated by a lock-in amplifier (PARC #186A). The lock-in output is read by a programmable voltmeter and displayed for data logging and analysis by the operator.

Extinction Calibration Procedure

It is required that the two detectors used in the experimental system be calibrated in terms of detector output voltage versus the absolute power falling on the detector face. Calibration of D_2, the detector monitoring the beam after it passes through the integrating sphere, is straightforward. An optical power meter (NRC #815) is placed in the laser beam at a point just in front of the detector. The reading obtained gives the optical power incident upon the detector and takes into account the beam attenuation caused by the neutral density filter and reflections from the condensing lens. Then, by removing the power meter and noting the detector output voltage, the ratio, k_2, of detector output voltage to absolute incident optical power can be formed. The linearity of the detector was confirmed by calculating k_2 for several optical power levels over the range of interest (achieved by placing filters with various optical density values in the beam). Calibration of D_1, the detector mounted on the integrating sphere wall, was accomplished

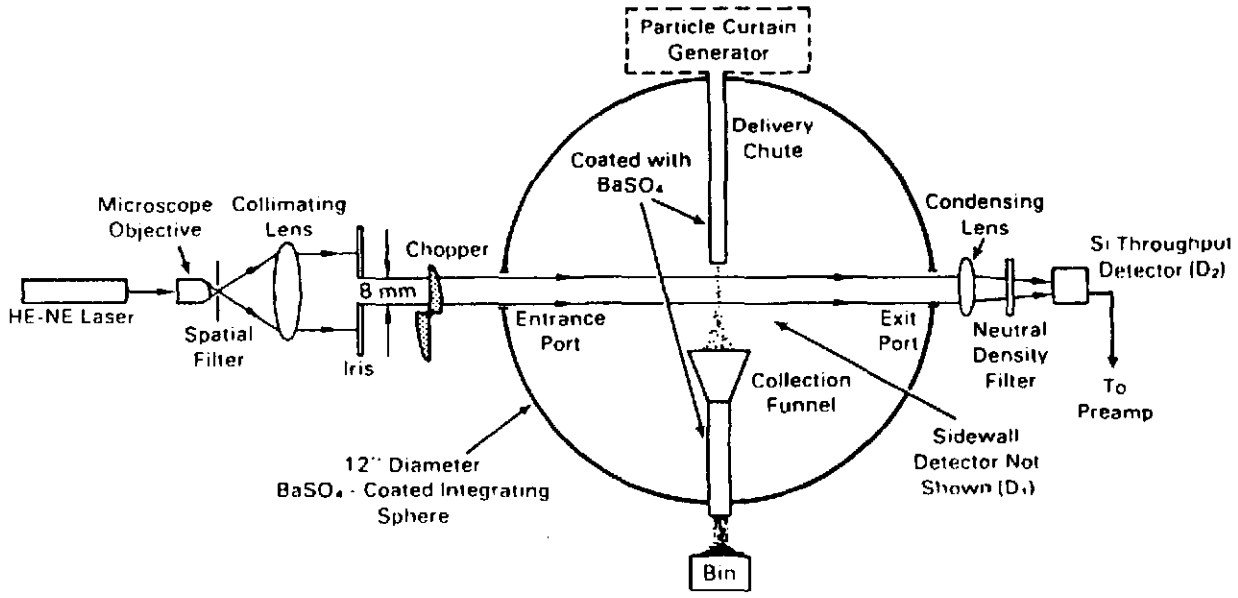

Figure 42. Schematic diagram of the optical system and detection system used for the single-particle extinction measurement experiment.

with the use of a reference scatterer as previously mentioned. The referenced scatterer, as diagrammed in Figure 43, was created by attaching a number of the Jaygo 300 ξm diameter glass beads (chosen for their good isotropic non-absorbing scattering characteristics) to a microscope slide. The reference scatterer was mounted on a support rod and was positioned in the center of the integrating sphere in the region where the particle curtain normally intersects the illuminating beam. With the reference scatterer in position, the power meter was aligned to intercept the beam before the beam entered the integrating sphere, thus giving the optical power incident on the scattering reference. The power meter was then removed, allowing the laser beam to strike the reference scatterer, and the resulting detector (D_1) output voltage was recorded. The ratio, c, of detector D_1 voltage to absolute incident optical power was then calculated. Again, the detector linearity was confirmed by calculating c for a series of optical power levels.

Collection of data from the extinction system involved two readings from each of the two detectors. First, V_{Scb}, the background signal resulting from any stray laser light scattered into the integrating sphere, was measured with detector D_1 (the sphere wall-mounted detector). Next, detector D_2 (the detector monitoring the beam after it has passed through the integrating sphere) was read for a measure of V_0, the incident illumination signal. Measurement of the incident illumination at the sphere exit port assumes no optical loss as the beam traverses the sphere volume (with no curtain flow). Once these two signals had been established, the particle curtain generator was turned on and several seconds were allowed for the curtain flow to stabilize. With the curtain flow stabilized, V_S (the signal corresponding to the amount of scattered

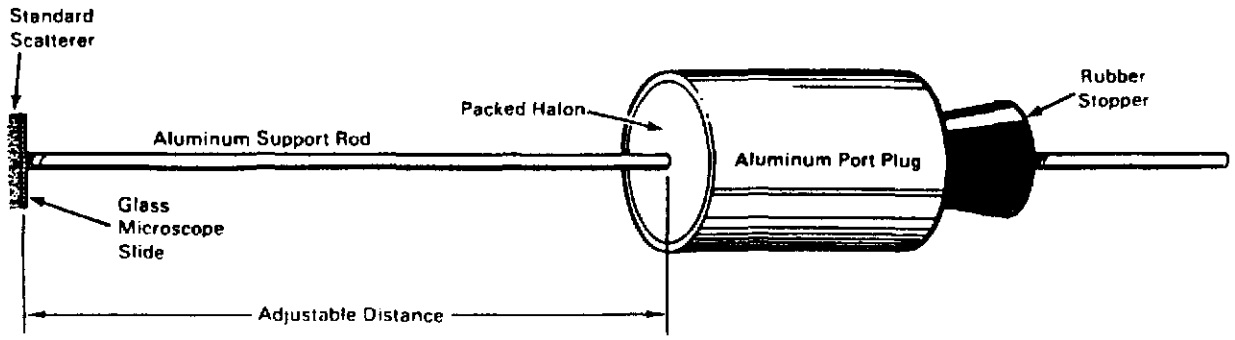

Figure 43. Schematic diagram of the diffuse reflectance standard used to calibrate detector D_1 in the integrating sphere.

light within the integrating sphere) and V_T (the signal resulting from light transmitted by the particle curtain) were measured. From Eq. 42, the single-particle scattering albedo was calculated by

$$w = \frac{k_2}{c} \cdot \frac{V_S - V_{Scb}}{V_0 - V_T} \quad . \tag{53}$$

All signals were measured with a digital voltmeter (HP3456A) programmed to take 15 readings per second. The signals were sampled over a 30 second interval. Thus, the resulting voltages are the average of 450 readings. The voltmeter also calculates the standard deviation of the 450 readings for use in the uncertainty analysis of the data.

Extinction Data

Table 1 shows a set of extinction data for 325 μm diameter Master Beads^R at several different mass flow rates as determined at 632.8 nm. Column three shows the single-particle scattering albedo, w_λ, for each flow rate, as well as the average w_λ for all flow rates combined.

It is possible to estimate the single-particle scattering albedo from the diffuse spectral reflectance of a bulk sample of Master Beads^R to validate the measurements. Recall that the single-particle scattering albedo is given by

$$w_\lambda = \frac{\sigma_\lambda}{\sigma_\lambda + \kappa_\lambda} \quad . \tag{54}$$

Note that $\sigma_\lambda \propto R_\lambda(2\pi)$ where $R_\lambda(2\pi)$ is the Master Bead^R hemispherical reflectance at the corresponding wavelength (632.8 nm). Consequently,

Table 1. Summary of the single-particle scattering albedo, w, measured for Master Beads® at 632.8 nm for a range of mass flow rates.

Mass Flow Rate (g/min)	Scattering Albedo w
4.28	0.096
4.30	0.090
4.39	0.119
4.47	0.091
7.62	0.100
7.65	0.104
7.34	0.097
9.68	0.095
10.03	0.107
10.26	0.092
14.86	0.096
15.03	0.106
15.29	0.109
18.71	0.086
19.56	0.091
19.57	0.094
22.64	0.102
23.82	0.085
24.14	0.111
24.83	0.112
Average	0.10 ± 0.01

$\kappa_\lambda \propto [1-R_\lambda(2\pi)]$ for the non-transmitting Master Beads^R. So, w_λ can be estimated as

$$w_\lambda \approx \frac{R_\lambda(2\pi)}{R_\lambda(2\pi) + [1-R_\lambda(2\pi)]} = R_\lambda(2\pi) \quad . \tag{55}$$

Thus, the predicted value for w_λ should be approximately equal to the bulk hemispherical reflectance $[R_\lambda(2\pi)]$ of the sample. Figure 12 shows that the bulk reflectance of the Master Beads^R at λ = 632.8 nm is 0.07. Therefore, the predicted and actual values for w_λ shows reasonable agreement. In addition to the agreement between bulk reflectance and w_λ, w_λ should be independent of flow rate. This is expected since the derivation of w_λ takes into account the particle size and particle number density. The consistency of the results with respect to mass flow rate shows good agreement with this expected behavior as well.

Improvements to the system could yield a third significant digit of accuracy for w_λ. Because of detector and laser intensity drift during the time over which the measurements are made (about four minutes), the signals may vary by several percent. The calibrations of D_1 and D_2 would also be improved by elimination of laser drift. To account for the laser intensity fluctuation, a third detector monitoring the beam power could be used to normalize the readings from D_1 and D_2.

VI. MEASUREMENT OF ELEVATED TEMPERATURE BULK REFLECTANCE

The fourth area of investigation is concerned with the optical properties of bulk particulates at elevated temperatures. In particular,

the reflectance of the particles at temperatures as high as 1000°C is of interest since such temperatures are likely to be experienced in an operating solar receiver. Using conventional spectrophotometric techniques, the reflectance of particles which have been heated to high temperatures for some time and then cooled to room temperature can be measured. However, measuring the reflectance of the candidate particles at temperature is a more difficult matter. After attempting, unsuccessfully, to adapt a commercial Beckman spectrophotometer to the high-temperature task, a custom diffuse reflectance measurement system was designed and implemented.

High-Temperature Measurement Instrumentation

The system designed for the high temperature reflectance measurements is illustrated schematically and photographically in Figures 44 and 45, respectively. A 1-kilowatt xenon arc lamp (Schoeffel #LH 151 lamp housing and #LPS 255 power supply, ORC #XB1600 xenon bulb) is used to illuminate the bulk particulate sample. A sample cup assembly is inserted into a modified cylindrical ceramic fiber heater. The illuminating xenon light is chopped (EG&G #192 rotary chopper operating at 40 Hz) in order to sidestep a major problem present in any such high-temperature spectrometer, namely the decoupling of the sample-reflected spectrum and the sample thermal emission spectrum. As the temperature of a material rises, the material's emission spectrum shifts to shorter and shorter wavelengths. If the emission spectrum begins to overlap the illumination spectrum, the two will become indistinguishable and accurate reflectance values will not be attainable. By chopping the illumination light, one may use synchronous detection to discriminate between the

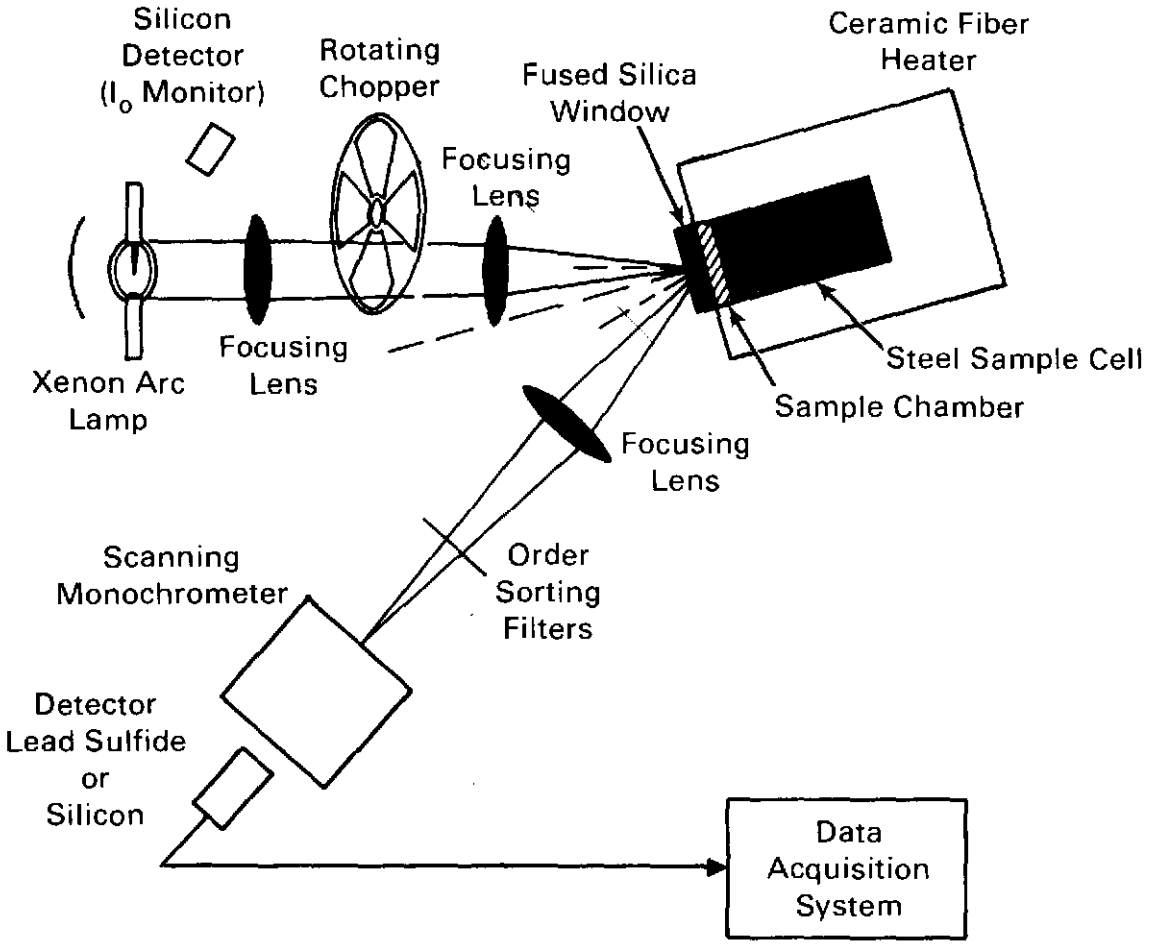

Figure 44. Schematic diagram of the optical system and sample chamber used for the high temperature diffuse reflectance measurements.

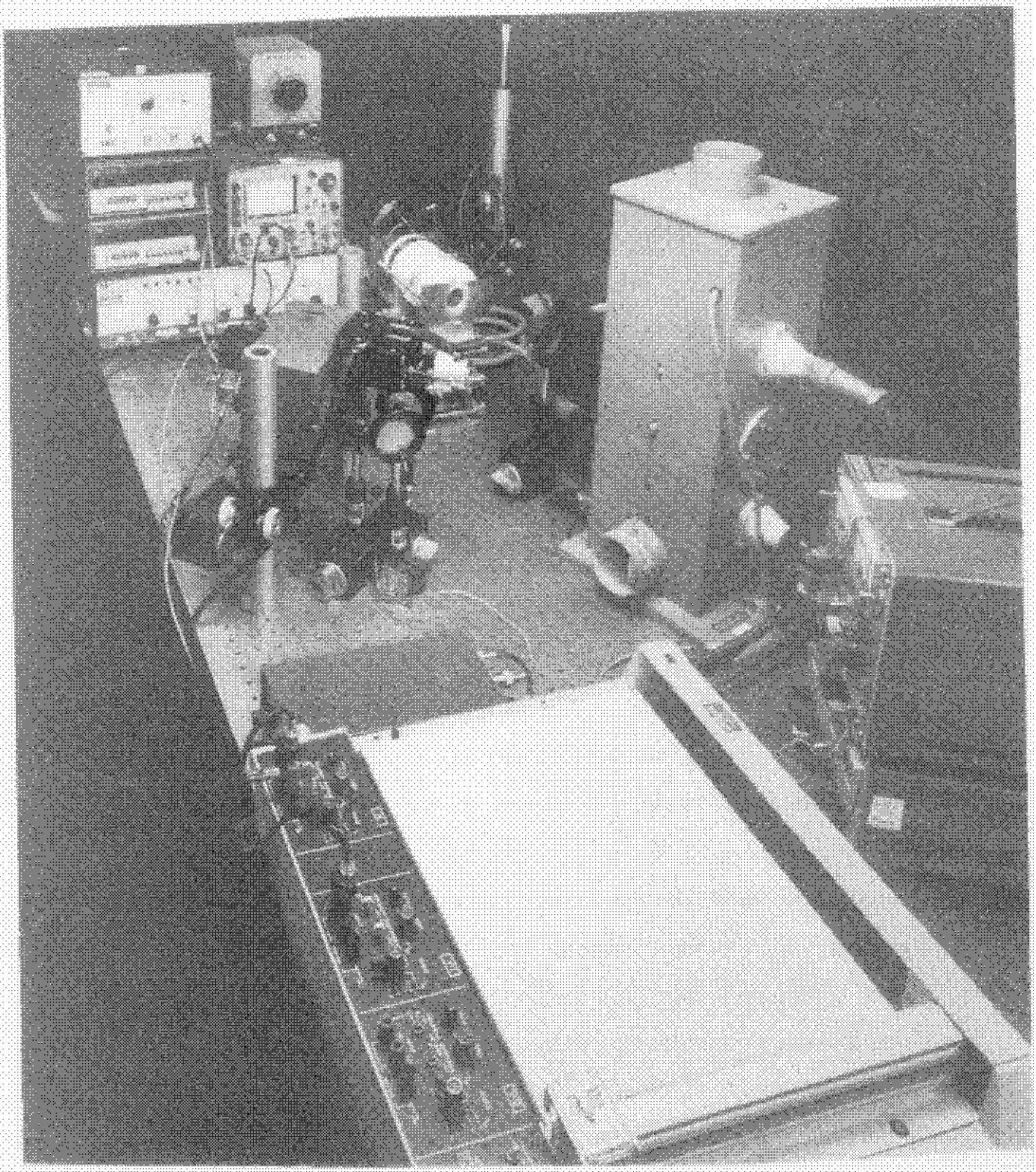

Figure 45. Photograph of the high temperature diffuse reflectance measurement system.

reflected light (which will be modulated by the chopper) and the emitted light (which will be unmodulated). A collecting lens focuses diffusely reflected light from the sample onto the monochromator (Oriel #7240) entrance slit. Order sorting filters are placed before the monochromator as required to eliminate erroneous results caused by overlap of higher diffracted orders within the monochromator. At the 600 nm monochromator position, a 550 nm cut-off filter is inserted; at the 1000 nm position, a 850 nm cut-off filter is inserted; at the 1600 nm position, a 1400 nm cut-off filter is used. One of a set of diffraction gratings is installed in the monochromator as necessary to allow a scan of the full solar spectral range of 300 nm to 2500 nm. A 1200 lines/mm grating is used for 300 nm to 700 nm; a 600 lines/mm grating is used for 700 nm to 1600 nm; a 300 lines/mm grating is used for 1600 nm to 2500 nm. The monochromator exit slit width is 2 mm which, for the 1200 lines/mm grating gives a bandwidth of about 13 nm; for the 600 lines/mm grating the bandwidth is about 26 nm; for the 300 lines/mm grating the bandwidth is about 52 nm.

A block diagram of the electronics system is shown in Figure 46. A detector placed at the monochromator exit slit measures the dispersed spectrum of reflected light from the sample. The detector is silicon (EG&G #UV444 with precision amplification)[8] for the 300 nm to 700 nm range and lead sulfide (Infrared Industries #IR2309 with amplifier circuit of Figure 47) for the 700 nm to 2500 nm range. The detector voltages are sent to a lock-in amplifier (PARC #5204). The illumination light intensity is also monitored for signal normalization purposes by a silicon detector (EG&G #UV444 with precision amplifier).[8] The sample signal voltages from the lock-in, as well as the illuminating source

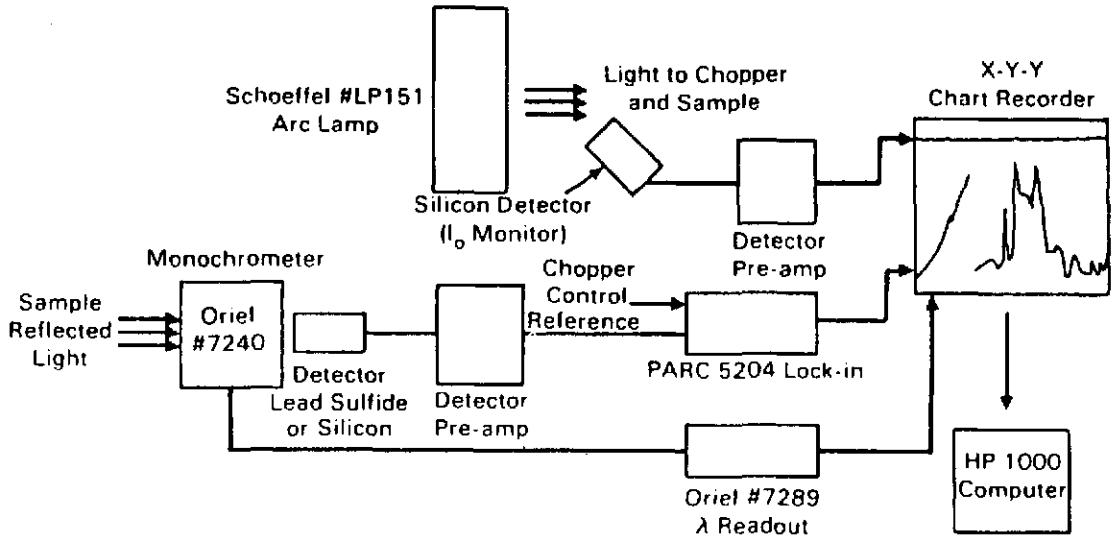

Figure 46. Diagram of the electronics system used with the high temperature diffuse reflectance system.

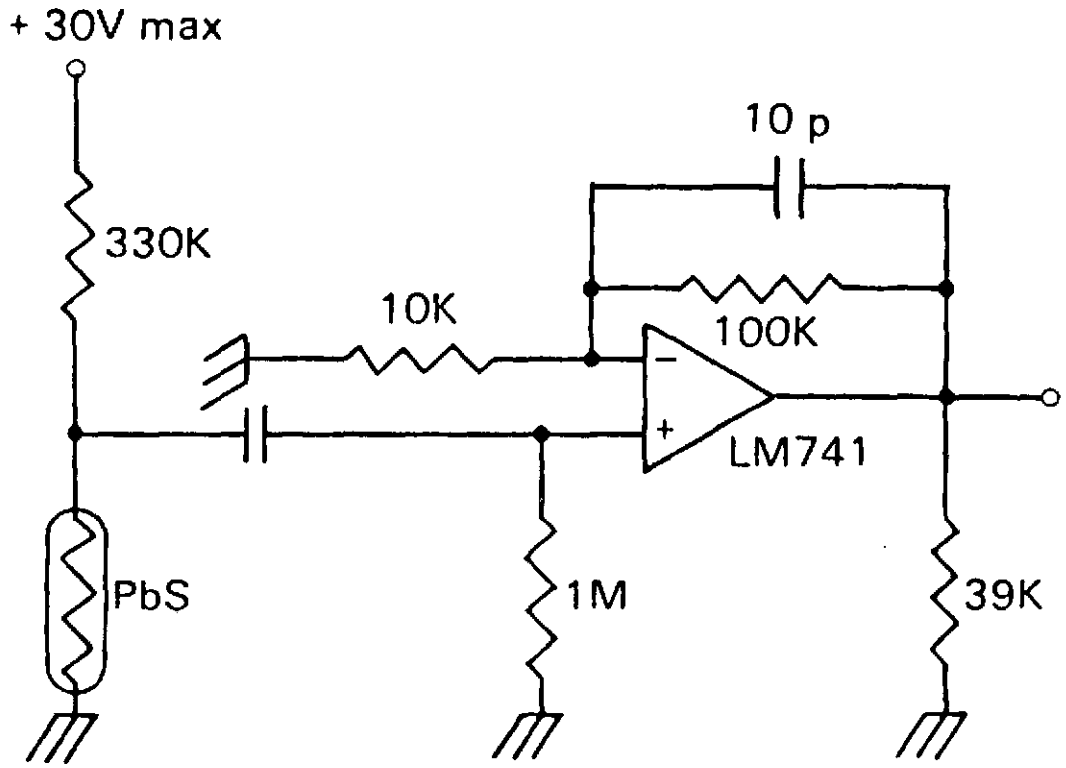

Figure 47. Diagram of the PbS detector pre-amplifier circuit used with the high temperature diffuse reflectance system.

signals, are recorded on the Y-axes of an X-Y-Y plotter. The X-axis of the plotter is driven by a monochromator wavelength readout (Oriel #7289). The resulting data curves are then digitized and manipulated on the HP 1000 computer.

To obtain corrected reflectance data, the output of the measurement system was calibrated using a diffuse reflectance standard. For these experiments, a Halon standard was used. The Halon was compacted in a holder to the density recommended by the NBS in reference.[5] The measurement process consisted of first recording the detector response for the Halon standard $[H_s(\lambda)]$ as a function of wavelength λ. At the same time, the broadband arc lamp output signal $[H_x(\lambda)]$ is measured. Next, the particle sample of interest was mounted and its temperature stabilized. Measurement of the sample signal $[V_s(\lambda)]$ and the corresponding lamp signal $[V_x(\lambda)]$ were obtained. Using the hemispherical reflectance values for the Halon standard $[R_{NBS}(\lambda)]$ as determined by NBS[5] the corrected sample reflectance $[R_s(\lambda)]$ at each wavelength was calculated using the equation

$$R_s(\lambda) = \left[\frac{V_s(\lambda)}{V_x(\lambda)}\right] \cdot \left[\frac{H_x(\lambda)}{H_s(\lambda)}\right] \cdot R_{NBS}(\lambda) \qquad (56)$$

The oven used to achieve these rather high sample temperatures is detailed in Figure 48. The commercially-available ceramic fiber heater (Watlow #VC401E060A) is capable of attaining temperatures in excess of 1000°C, but the unit does not heat uniformly over its full extent. Since the sample must be located near the front end of the heater to allow for illumination and imaging of the particles, heat must be transferred from

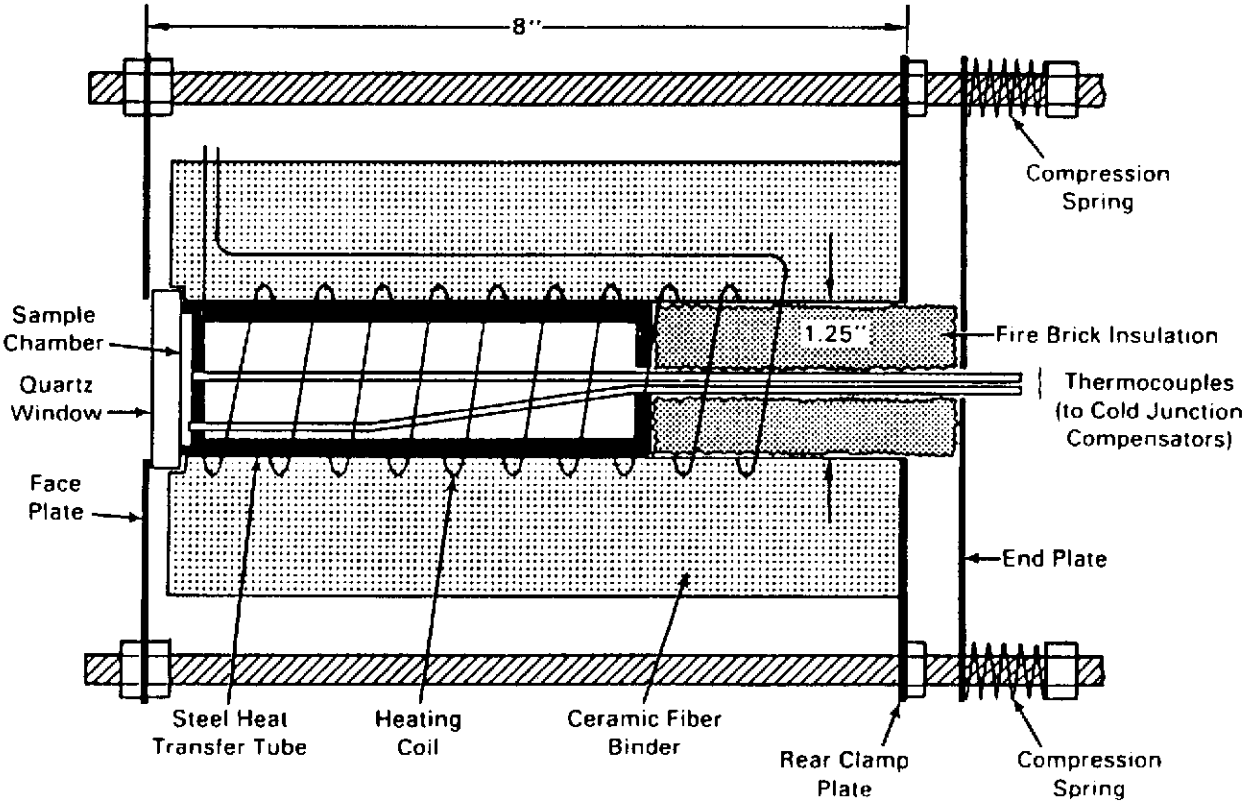

Figure 48. Detailed diagram of the high temperature oven used to heat samples for the diffuse reflectance measurements.

the more central region of the heater out to the sample chamber. This was achieved through the use of a steel tube which extends into the central, hottest part of the oven. In this way, the sample can be heated and still remain at the outer limits of the heater. The sample chamber was formed by machining a cup into the end of this steel heat transfer tube. Since the sample was to be mounted vertically, the sample cup was covered by a quartz window. The sample cup was about 1.3 mm deep, providing an optically opaque sample which was still thin enough to minimize any large thermal gradients within the sample volume. Two thermocouples were buried in the sample -- one in the center rear of the sample cup and one toward the outer portion of the cup and about mid-depth into the sample. Using this oven configuration, the thermocouples buried in the sample indicated that sample temperatures from 150°C to about 950°C are obtained. Thermocouple indications for temperatures in the 900°C range have also been confirmed by optical pyrometry. Temperatures lower than 150°C are not available due to sample heating by the 1 kilowatt xenon illumination flux. The rear end of the ceramic fiber heating unit was plugged with fire brick inserts to help insulate the oven. The fire brick, heat transfer tube, and quartz window are held firmly in contact by a spring-loaded clamp device. The primary purpose of the clamp device was to keep the sample cell components (consisting of the heat transfer tube and the quartz window) in contact as they undergo thermal expansion and contraction.

High-Temperature Reflectance Data

High temperature diffuse reflectance data for the 325 ξm diameter Master Beads^{R} is shown in Figure 49. The data show a marked decrease in

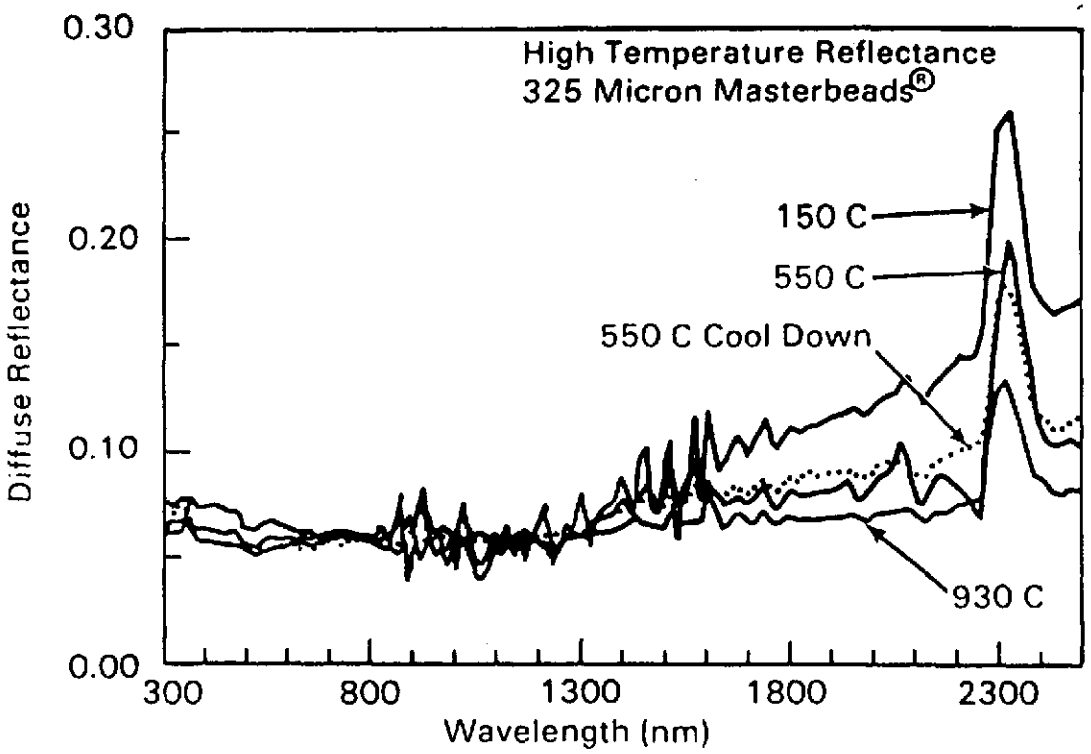

Figure 49. Plot of the diffuse reflectane as a function of wavelength measured for Master Beads® at 150°C, 550°C, and 930°C. Also shown is the reflectance measured at 550°C during cool down.

reflectance, particularly at the longer wavelengths, as sample temperature increases from 150°C to 930°C. Note, however, that the general shape of the reflectance curve persists over the entire temperature range. Figure 50 shows the spectrophotometric bulk hemispherical reflectance for Master Beads^{R} which have been evaluated prior to and after heat treatment (measurements made at room temperature). The heat-treated Master Beads^{R} were raised to a temperature of 1000°C for approximately three hours in air. This treatment was of sufficient severity to cause discoloration of the Master Beads^{R}, giving them a distinct green hue. The data show an increase in the reflectance of the heat-treated Master Beads^{R} beginning in the green portion of the spectrum and continuing through the remainder of the wavelengths scanned, to 2500 nm. The solar averaged absorptance decreased from an initial value of 0.93 to a value of 0.89 after the heat treatment. The high temperature and room temperature data therefore indicate that when the Master Beads^{R} are subjected to elevated temperatures, both permanent and temperature-dependent changes in their optical reflectance properties occur.[10]

Future work with the high temperature reflectance system should focus on the identification and testing of a standard high-temperature material which could be used an an experimental reference. The standard would preferably be in a particulate form resembling the Master Beads^{R} in size and shape but could also be a paint or a solid disk of material. The important feature of such a standard would be that its reflectance would not change over the temperature range at which the high-temperature system operates. At present no such standard has been identified.

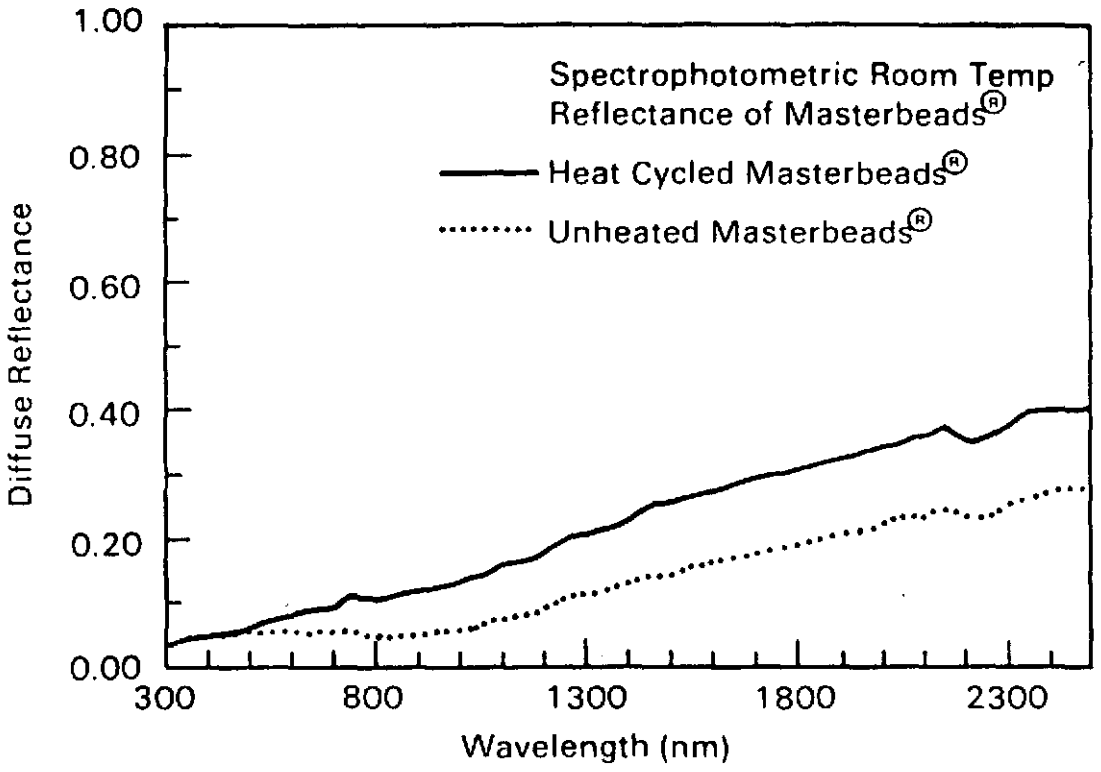

Figure 50. The hemispherical reflectance of Master Beads® measured both before and after heating to 1000°C in air for three hours.

VII. SUMMARY

Measurement techniques and instrumentation have been developed for determining the optical scattering and extinction properties of particulates of interest as carriers in the solid particle solar central receiver. This instrumentation allows rapid screening of carrier candidates for suitability from an optical standpoint. Estimation of material optical scattering and extinction properties at wavelengths other than 632.8 nm appears feasible using measurements of bulk diffuse reflectance properties.

An experimental system designed to measure the diffuse reflectance of candidate particulate solar absorbers as a function of temperature has been designed and constructed. Diffuse reflectance data for Norton Master Beads^{R} up to 930°C show no change in solar absorptance as compared to room temperature data. However, after only 3 hours at 1000°C in air, the solar absorptance decreased from 0.93 to 0.89.

VIII. ACKNOWLEDGMENTS

We, the authors, thank G. H. Prescott and B. R. Steele, Sandia National Laboratory Livermore, for providing the particle curtain generators; A. Duncan, Pantex plant, Amarillo, Texas, for performing the Quantimet particle sizing studies; D. A. Nelson, Pacific Northwest Laboratory, for technical assistance; and W. G. Houf, Sandia National Laboratory Livermore; R. Greif, University of California, Berkeley; and B. B. Brenden, Pacific Northwest Laboratory, for informative technical discussions. This work was supported in part by the U.S. Department of Energy under contract number DE-AC04-76-DP00789.

IX. REFERENCES

1. P. K. Falcone, J. E. Norning and J. M. Hruby, "Assessment of a Solid Particle Receiver for a High Temperature Solar Central Receiver System," Sandia National Laboratories Report SAND 85-8208 (1985)*; C. A. LaJeunesse, "Thermal Performance and Design of a Solid Particle Cavity Receiver," Sandia National Laboratories Report SAND 85-8206 (1985)*; and V. P. Burolla, J. M. Hruby, and B. R. Steele, "High Temperature Solar Thermal Energy Absorption With Solid Particles," Proceedings of the 19th Intersociety Energy Conversion Engineering Conference, Vol. 3, 1984.

2. J. W. Griffin, K. A. Stahl, and R. B. Pettit, "Optical Properties of Solid Particle Receiver Materials I: Angular Scattering and Extinction Characteristics of Norton Master Beads®", SPIE Vol. 562 Optical Materials Technology for Energy and Solar Energy Conversion IV, (Aug, 1985) pgs. 223-237.

3. K. A. Stahl, J. W. Griffin, and R. B. Pettit, "Optical Properties of Solid Particle Receiver Materials II: Diffuse Reflectance of Norton Master Beads® at Elevated Temperatures", SPIE Vol. 562 Optical Materials Technology for Energy and Solar Energy Conversion IV, (Aug, 1985) pgs. 238-242.

4. W. G. Houf and R. Grief, "Radiative Transfer in a Solar-Absorbing Particle-Laden Flow", Presented at the 1985 National Heat Transfer Conference, Denver, CO.

5. V. R. Weidner and J. J. Hsia, "Reflectance Properties of Pressed Polytetrafluoroethylene Powder," J. Opt. Soc. Amer. 71 (1981) 856.

6. "Terrestrial Photovoltaic Measurement Procedures", ERDA/NASA/1022-77/16, NASA-TM-73702, June 1977.

7. G. H. Prescott and B. R. Steele, "A Particle Curtain Generator for Optical Property Measurements of Solid Particles", Sandia National Laboratories Report, SAND 84-8255, 1985.*

8. M. A. Lind, E. F. Zalewski and J. B. Fowler, "The NBS Detector Response Transfer and Intercomparison Package: The Instrumentation." NBS Technical Note 950, U.S. Department of Commerce, Washington, D.C., July 1977.

9. C. Bohren and D. R. Huffman, Absorption and Scattering of Light By Small Particles, (Wiley, New York, 1983) Section 11.7.

10. J. R. Hellmann, "Evaluation of Spherical Refractory Aggregates for Solar Thermal Transfer Media," Sandia National Laboratories Report (to be published).*

---

* Available from NTIS, U. S. Department of Commerce, 5285 Port Royal Road, Springfield, Virginia 22161.

UNLIMITED RELEASE UC - 62d

INITIAL DISTRIBUTION

U. S. Department of Energy (5)
Forrestall Building, Room 5H021
Code CE-314
1000 Independence Avenue, S.W.
Washington, D.C. 20585
Attn: H. Coleman
C. Mangold
F. Morse
M. Scheve
F. Wilkens

U. S. Department of Energy
Albuquerque Operations Office
P. O. Box 5400
Albuquerque, NM 87115
Attn: J. Weisiger

U. S. Department of Energy
San Francisco Operations Office
1333 Broadway
Oakland, CA 94612
Attn: R. Hughey

University of California
Department of Mechanical Engineering
6167 Etcheverry Hall
Berkeley, CA 94720
Attn: Prof. R. Greif

Georgia Institute of Technology
Atlanta, GA 30332
Attn: C. Thomas Brown

University of Houston
Solar Energy Laboratory
4800 Calhoun
Houston, TX 77704
Attn: Prof. A. F. Hildebrandt

University of Lowell
1 University Avenue
Lowell, MA 01854
Attn: Prof. J. Martin

Centre National De La Recherche Scientifique (2)
Laboratorie d'Energetique Solarie
Odiello, B. P. 5, 66120 Font-Romeu
France
Attn: G. Flamant
C. Royere

Battelle Pacific Northwest Laboratory (2)
Battelle Boulevard
P. O. Box 999
Richland, WA 99352
Attn: K. A. Stahl
B. S. Matson

Electric Power Research Institute
P. O. Box 10,412
Palo Alto, CA 94303
Attn: E. DeMeo

Pacific Gas and Electric Company
3400 Crow Canyon Road
San Ramon, CA 94526
Attn: G. Braun

Solar Energy Research Institute (2)
1617 Cole Boulevard
Golden, CO 80401
Attn: B. Gupta
D. H. Johnson

Southern California Edison
P. O. Box 800
Rosemead, CA 92807
Attn: J. N. Reeves

Lawrence Berkeley Laboratory 90-2024
University of California
Berkeley, CA 94720
Attn: A. J. Hunt

United Technologies Research Center
Optics and Applied Tech. Lab.
P. O. Drawer 4181
West Palm Beach, FL 33402
Attn: J. W. Griffin

Norton Research Corporation
8001 Daly St.
Niagara Falls, Ontario
Canada L2G6S2
Attn: Dr. J. Patchett

R. L. Schwoebel, 1800; Attn: R. J. Eagan, 1840
M. J. Davis, 1830
R. E. Whan, 1820
J. N. Sweet, 1824
R. B. Pettit, 1824 (10)
A. R. Mahoney, 1824
F. P. Gerstle, 1845
J. R. Hellmann, 1845
C. Nelson, 1845
E. H. Beckner, 6000; Attn: V. Dugan, 6200
D. G. Schueler, 6220
J. V. Otts, 6222
J. T. Holmes, 6226
J. A. Leonard, 6227
R. W. Rhode, 8310
R. L. Rinne, 8470
J. C. Swearengen, 8473
J. M. Hruby, 8473 (3)
W. G. Houf, 8245

Technical Library, 3141
S. A. Landenberger, 3141 (5)
W. L. Garner, 3151 (3)
C. H. Dalin, 3154-3 for DOE/OSTI (28)
P. W. Dean, 8024 (1)
Technical Library, 8214
D. Ottesen, 8313
D. Lindner, 8313